UNIVERSITY OF GRONINGEN

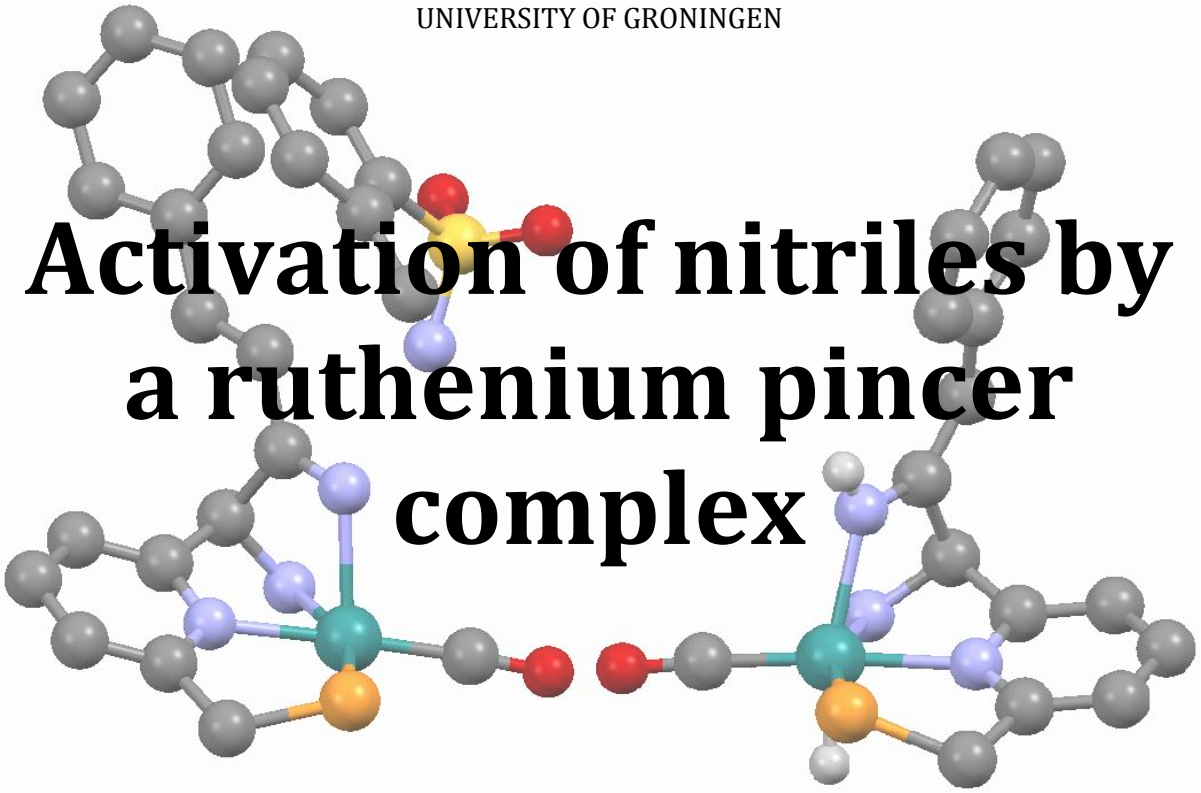

Activation of nitriles by a ruthenium pincer complex

Linda E. Eijsink
Molecular inorganic chemistry
Supervised by prof. Edwin Otten

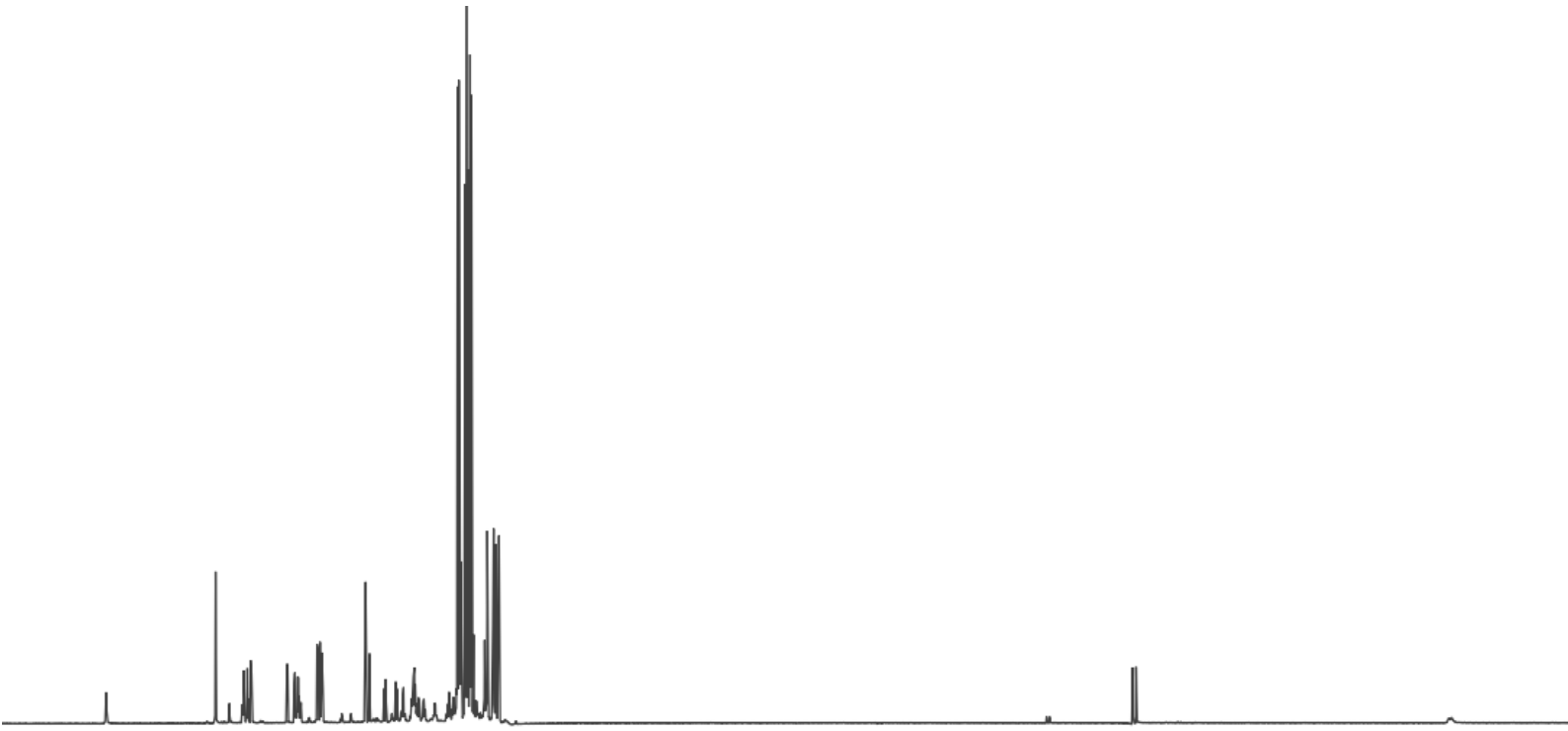

Contents

1 Summary

In this report, the activation of nitriles by a [Ru]PNN pincer complex is described. Pincer complexes consist of a metal centre and a pincer ligand, which is a sturdy, tridentate, neutral or anionic ligand. Pincer ligands have a large variety of modification sites, which makes it relatively easy to change the electronic and structural properties of the ligand, and hence of the metalorganic complex.

Here, the metal used is ruthenium, and the pincer ligand consists of a pyridine centre, one methylene-bridged di-*tert*-butylphosphine arm and one methylene-bridged diethylamine arm. The PNN ligand is neutral, but can be deprotonated, upon which the pyridine loses its aromaticity. This dearomatised complex **1** is capable of small molecule activation, such as H_2 and CO_2, as well as activation of several double bonds. This is shown in the left side of Figure 1.

Complex **1** is also known to activate vinylic and allylic nitriles, which then undergo oxa-Michael addition of nucleophiles such as isopropanol or octanethiol on the 3-position.

This report focusses on the activation of various other nitrile substrates by **1**. As is shown in Figure 1, several different complexes were observed. Often, several complexes were present in the solution simultaneously. This is also in agreement with the DFT calculations, which show the observed complexes are close in energy. The energy difference between the observed complexes is often less than 1 kcal/mol.

In the case of 4-pentenenitrile, the observed equilibria between **1**, $\mathbf{1}^{4PN}$**A**, $\mathbf{1}^{4PN}$**B**, and $\mathbf{1}^{4PN}$**C** were studied in more detail. The equilibrium between **1** and **1A** is fast on the NMR time scale, and an average is observed. The other two complexes, **1B** and **1C** do give distinct NMR signals. The equilibrium constants and the change in enthalpy and entropy were calculated using the relative integrals, as well as the chemical shift of **1** ⇄ $\mathbf{1}^{4PN}$**A** in the ^{1}H-NMR spectrum, and are shown in Table 1.

Although vinylic and allylic nitriles undergo oxa-Michael addition via an intermediate closely related to **1B**, the complexes reported here do not seem to undergo any of the tested reactions. Adding octanethiol to the reaction mixture resulted in replacement of

	K_1	K_2	K_3	
K	41 (±20)%	0.5	6	M^{-1}
ΔH	-50	-17	-0.82	kJ mol^{-1}
ΔS	-143	-63	-12	J K^{-1} mol^{-1}

Table 1: Calculated values for *K*. ΔH, and ΔS of equilibria K_1, K_2, and K_3.

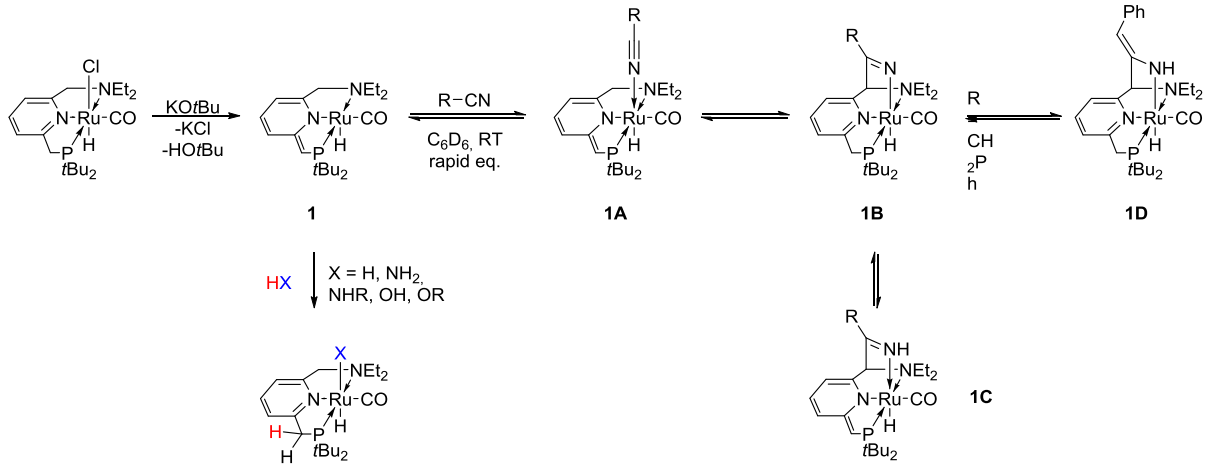

Figure 1: Generation of complex 1 from its precursor (left), activation of HX substrates (bottom left), and the different complexes formed upon activation of a nitrile substrate.

the nitrile by the thiol. Hydrogenation of the nitrile to an imine or amine did not succeed, although this reaction has been reported previously using an [Fe]PNP or a [Co]PNNH complex. Other substrates such as diethylamine and triethylsilane did not yield any reaction. The reaction with *o*-toluenesulfonamide resulted in protonation and rearomatisation of complex $\mathbf{1}^{\mathbf{CN}}\mathbf{C}$, but the expected addition reaction did not occur.

During the high-temperature NMR studies on a 4-pentenenitrile/**1** mixture, the formation of ethylene was observed. This ethylene is presumably generated from the diethylamine ligand arm. The resulting complex was, however, not characterised.

2 Introduction

Pincer complexes are organometallic complexes composed of a metal centre and a multidentate "pincer" ligand. The chemistry of pincer complexes started about 40 years ago with the synthesis of 1,3-bis[(di-*tert*-butylphosphino)methyl]benzene (PCP) and its nickel, rhodium, iridium, palladium and platinum complexes by Moulton and Shaw.[1] From there, the field of pincer complexes emerged.

2.1 Pincer complexes

Pincer ligands have a general structure shown in Figure 2, where E is a neutral σ-donating atom such as phosphorus, nitrogen, sulfur, oxygen, or an N-heterocyclic carbene. X is generally an aromatic or aliphatic carbon or nitrogen, which can be either neutral or anionic. The metal centre can be a platinum group metal (Ru, Rh, Pd, Os, Ir, Pt) or base metals such as iron, cobalt or nickel. These metals generally have low oxidation states and bind to soft σ-donating ligands such as nitrogen or phosphorus.

Pincer ligands are sturdy, tridentate neutral or mono-anionic ligands. Coordination of the metal centre yields two five-membered metallacycles. The planarity of the ligand is suited for square-planar, trigonal bipyramidal, square pyramidal and octahedral coordination geometries. The d^6-metals such as Rh^{I}, Pd^{II}, and Ni^{II} generally prefer square-planar geometry, whereas d^8-metals such as Ru^{II} and Rh^{III} prefer a square pyramidal geometry. Due to the chelate effect, pincer complexes are remarkably (thermally) stable, with decomposition temperatures generally above 100°C.[2]

The properties of the pincer complex can be greatly varied. The introduction of a pyridine backbone instead of an aryl eliminates the otherwise necessary aryl metalation step and changes the ligand from an anionic to a neutral ligand. Adjusting the donor atom (E) alters the electron density on the metal centre. Electron-withdrawing or donating substituents can also alter the electronic properties of the metal centre. Substituents on the aryl have only a small effect on the electron density, as was demonstrated with various *para*-substituents on an (R-$^{t\mathrm{Bu}}$POCOP)Ir(CO) complex. Changing R from the electron-donating MeO to the electron-withdrawing C_6F_5 resulted in a change in ν(CO) of 8 cm^{-1}.[3] This in contrast to changing the methylene CH_2 to oxygen, which shifts the ν(CO) by approximately 25 cm^{-1}. The size of the substituents on donor atoms E influences the binding affinity of the metal centre by steric effects.[2] The different influences of the ligand are summarised in Figure 3.[4]

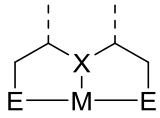

Figure 2: General design of a pincer-type complex.

2.1.1 Metal-ligand cooperation

In most organometallic reactions, the actual reaction takes place at the metal centre. The ligand functions to control solubility, sterics and electron-density on the metal centre, but is not involved in the actual reactions. This in contrast to non-innocent ligands, which actively participate in substrate activation. Non-innocent ligands can be either redox-active or chemically active. Redox-active ligands are ligands that can undergo a redox-process and often form radical intermediates. Common organometallic transformations are

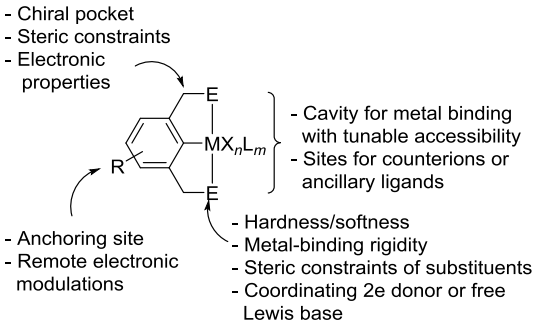

Figure 3: Modification sites for ECE pincer ligands.[4]

oxidative addition and reductive elimination, both of which are two-electron processes. Redox-active ligands can account for one electron in these transformations.[5]

Chemically active ligands are involved by making and breaking bonds with the substrate. An example of chemical metal-ligand cooperativity is shown in the nitrile hydrogenation by an [Fe]PNP pincer complex. The catalytic cycle of this hydrogenation can be seen in Figure 4. In the calculated transition state, the nitrile-nitrogen is coordinated to the protic hydrogen on the amine, and the nitrile-carbon is coordinated to the iron hydride. The ligand nitrogen undergoes an amino-amido transformation, and thus the oxidation state of the iron centre remains unchanged. After hydrogenation of the nitrile, reaction with hydrogen gas yields again the active catalyst, which can then hydrogenate the formed imine to the amine following a similar pathway.

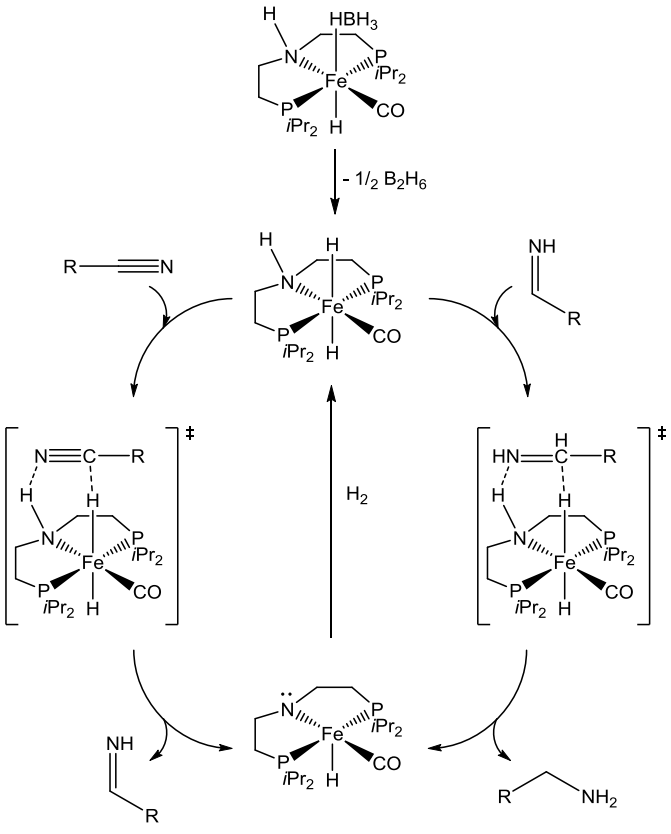

Figure 4: Nitrile hydrogenation by an aliphatic iron PNP pincer complex.[6]

Using 1 mol% of catalyst, elevated temperatures and 30 bar of H_2 gas, quantitative conversion was achieved for both aromatic and aliphatic (di)nitriles.[6]

2.1.1.1 Ligand aromatisation/dearomatisation

Some pincer complexes, and especially those with a pyridine backbone have a slightly different mode of reaction. In case of a CH_2 methylene arm on the 2- or 6-position, the ligand can be deprotonated, losing one of the methylene protons and creating an anionic pincer ligand. The pyridine loses its aromaticity, hence this process is called ligand dearomatisation. Usually, chloride is simultaneously liberated from the metal centre, thus generating HCl from the complex. The oxidation state of the metal remains unchanged. A basic reaction site in the ligand backbone is created, opening up new possibilities for metal-ligand cooperation. Figure 5 shows this process of ligand dearomatisation.

2.1.2 The Milstein [Ru]PNN complex

A special case of a dearomatised pincer complex is the Milstein [Ru]PNN complex, first reported by David Milstein and co-workers in 2005.[7] It is special because of its asymmetric ligand: the pyridine backbone has one phosphine and one amine arm, hence PNN. Its chloride precursor **1a** is synthesised from $RuHCl(CO)(PPh_3)$ and the PNN ligand (2-(di-*tert*-butylphosphinomethyl)-6-diethylaminomethyl)pyridine. Upon addition of base, the precursor loses HCl to yield the dearomatised complex (**1**), as is shown in Figure 5.

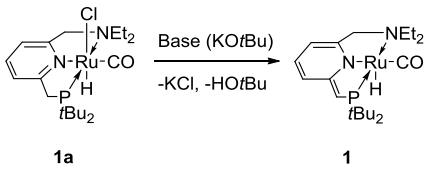

Figure 5: Synthesis of complex 1 from its precursor.[7]

Deprotonation and thus dearomatisation occurs at the phosphine arm of the ligand. Although deprotonation at the amine arm is also possible, the resulting complex is higher in energy and hence this is not observed. Its reactivity and supporting calculations however suggest both complexes (deprotonated at the phosphine arm and deprotonated at the amine arm) are in equilibrium.

2.2 Reactivity of pincer complexes

As the nitrile activation by an aliphatic [Fe]PNP complex in Figure 4 already illustrated, some pincer complexes can activate substrates using both the metal centre and a ligand site.

Apart from the [Fe]PNP complex in Figure 4, various other transition metal amino and amino hydride complexes have been employed for hydrogenations and transfer hydrogenations of (polar) multiple bonds. Examples include Noyori's ethylenediamino ruthenium arene,[8] Grützmacher's [Rh(trop$_2$N)(PPh$_2$R][9] and the Morris catalyst,[10] which has a tetradentate PNNP ligand and a ruthenium centre.

2.2.1 Bond activation by dearomatised pincer complexes

In dearomatised pincer complexes, the dearomatised methylene arm plays a crucial role in bond activation by the complex. The dearomatised pincer complex is able to perform heterolytic bond cleavage and bond activation, where the negatively polarised atom ends up on the metal centre, and the positively polarised atom, for example hydrogen, ends up on the ligand backbone,

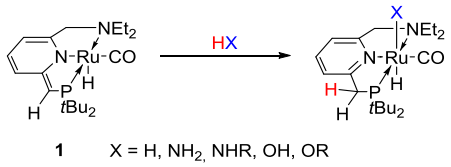

Figure 6: Heterolytic bond cleavage of various polarised bonds.

re-forming an aromatic pyridine. Figure 6 summarises this heterolytic bond cleavage by ligand rearomatisation. Deprotonation and thus dearomatisation occurs at the phosphine arm of the ligand, but the catalyst can isomerise to a form where the amine arm is deprotonated. Although this has never been observed, it is a key intermediate in many transformations, such as in the activation of CO_2. The reaction of the Milstein [Ru]PNN-complex with CO_2 is illustrated in Figure 7. At room temperature, CO_2 adds on the phosphine arm of the ligand. Upon removal of the CO_2-atmosphere, this cycloaddition product partially reverts back to **1**, suggesting the reaction is reversible. Heating the product to 70°C for 15 minutes results in the formation of a different product, in which the CO_2 has added on the amine arm of the ligand via the unobserved intermediate **1-taut**. This complex does not revert back to **1**. Thus, reaction on the phosphine arm of the ligand yields the kinetic product, whereas reaction on the amine arm of the ligand yields the thermodynamic product.[11]

Bond activation is also possible with various other double and triple bonds. Figure 4 already showed the activation and transformation of nitrile and imine by an aliphatic pincer complex. Dearomatised pincer complexes can perform this reaction as well.

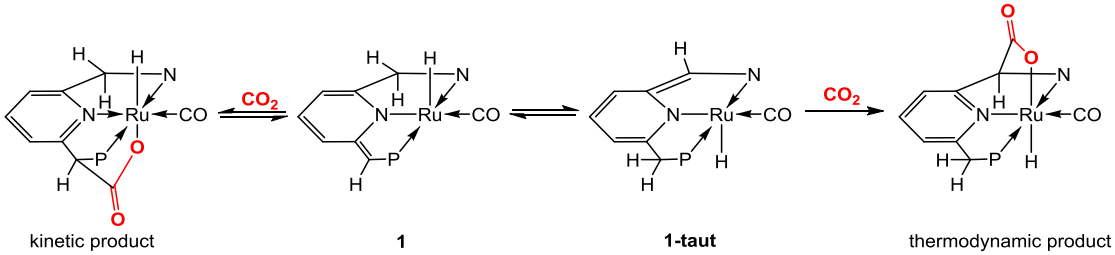

Figure 7: Reaction of the 1 with CO_2, yielding either the kinetic or the thermodynamic product.[11]

Hydrogenation of nitriles to amines has also been achieved with a [Co](PNNH) pincer complex, amongst others.[12] Dearomatised pincer complexes have been shown to activate aldehydes, ketones, carboxylic acids, CO_2 and nitriles forming C-C and M-O (or M-N) bonds reversibly. The variety of bond activations by ruthenium pincer complexes has recently been summarised by Gunanathan and Milstein in Chemical Reviews.[13]

2.2.2 Alkene isomerisation

In 2014 it was shown that **1** is able to isomerise alkenes in the presence of isopropanol.[14] Starting from pure 1-octene, a mixture of 1-, 2-, 3- and 4-octene was obtained. The use of an alcohol is essential, and the conversion is highest using isopropanol compared to ethanol and *tert*-amyl alcohol. Figure 8 shows coordination of alcohol to Milstein's [Ru]PNN complex, followed by alkene coordination. Upon addition of alcohol to the ruthenium metal centre, the pyridine is rearomatised and the labile diethylamine arm is released. This then opens a coordination site for the alkene, which first undergoes olefin insertion and subsequent hydride abstraction, by which the alkene is isomerised.

2.3 Nitrile activation

Nitriles are an important class of materials. They are components and precursors of many plastics, rubbers, glues and pharmaceuticals. Hydrolysis of nitriles results in amides or carboxylic acids, whereas reduction yields primary or tertiary amines and aldimines, which can then be hydrolysed to aldehydes.

2.3.1 Nitrile activation by frustrated Lewis pairs

As was already discussed before, nitrile activation is possible with a variety of complexes, such as the aliphatic [Fe]PNP pincer complex shown in Figure 4 or the [Co](PNNH) pincer complex described in section 2.2.1. Frustrated Lewis pairs (FLP's) have been shown to activate benzonitrile as well, as is shown in Figure 9.[15] Compound **2A** is synthesised by hydroalumination of an alkynylphosphine precursor. When benzonitrile is added, the lone pair of electrons on the nitrogen coordinates to the Lewis-acidic aluminium, forming compound **2B**. Heating compound **2B** at 50°C for 12h yields compound **2D** in 73% yield. Calculations show **2C** is an intermediate in this reaction. Thus, the nitrile undergoes cycloaddition first to **2C**, before a proton shift from phosphorus

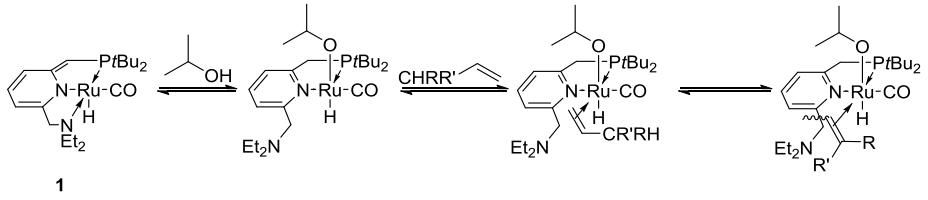

Figure 8: Alkene isomerisation by Milstein's catalyst.[14]

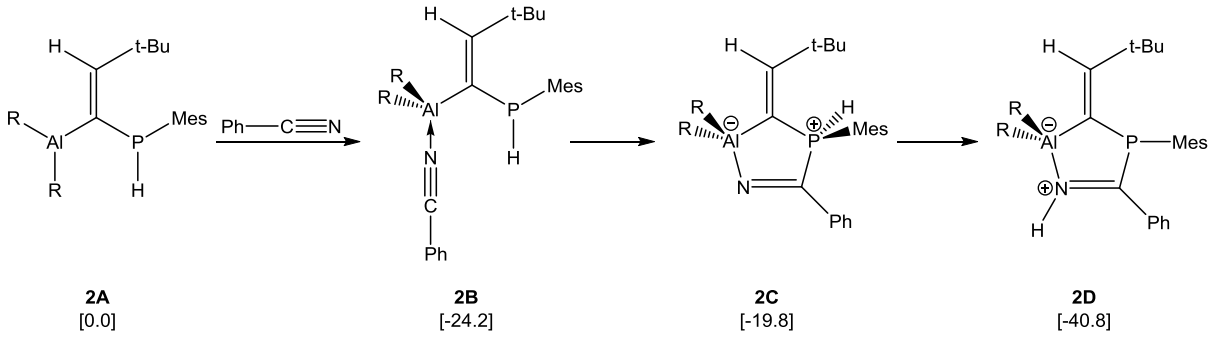

Figure 9: Nitrile activation by frustrated Lewis pairs. R = $CH(SiMe_3)_2$. Calculated energies in square brackets [kcal mol^{-1}], M062x/6-311 + G(d,p) + GD3 +ZPE.[15]

to the more basic nitrogen takes place, and compound **2D** is formed. Figure 9 also shows the calculated energies for this reaction.

2.3.2 Nitrile activation by pincer metal complexes

Dearomatised pyridine-based pincer complexes have also showed nitrile activation. An example of this is the [Re]PNP complex **3**. Nitrile activation occurs via a coordination of the nitrile-nitrogen to the metal centre, after which a C-C bond is formed between the ligand and the nitrile. In the presence of an α-proton, the formed rhenium-ketimido species can then tautomerise to a rhenium-enamido-species.[16] This bond activation sequence is summarised in Figure 10. The energy levels of the reaction course have been calculated for different nitriles. The calculated energies are shown schematically in Figure 11.[16]

2.3.3 Oxa-Michael addition to unsaturated nitriles

Besides nitrile hydrogenation, another application of nitrile activation is oxa-Michael addition. The Milstein [Ru](PNN) complex **1** has shown to catalyse this reaction in the case of unsaturated nitriles.[17,18] Ethanol, iso-propanol and other nucleophiles have been shown to add to α,β- and α,γ-unsaturated nitriles, such as 2- and 3-pentenenitrile. The catalytic cycle is shown in Figure 12, and is

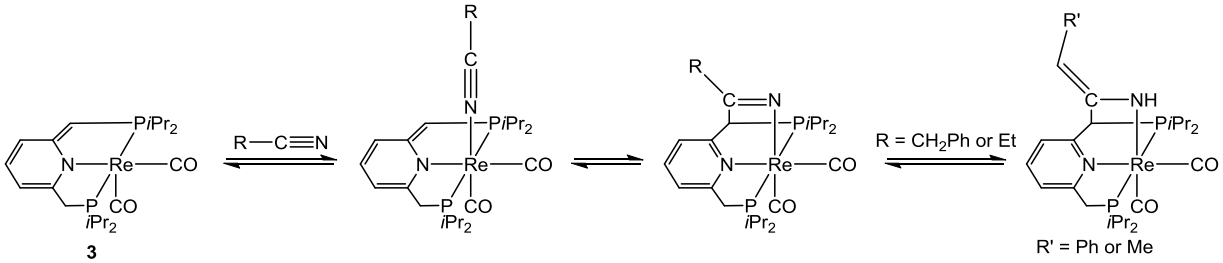

Figure 10: C≡N activation by [Re]PNP pincer complex 3. First, coordination to the metal centre, followed by cycloaddition with the ligand.[16]

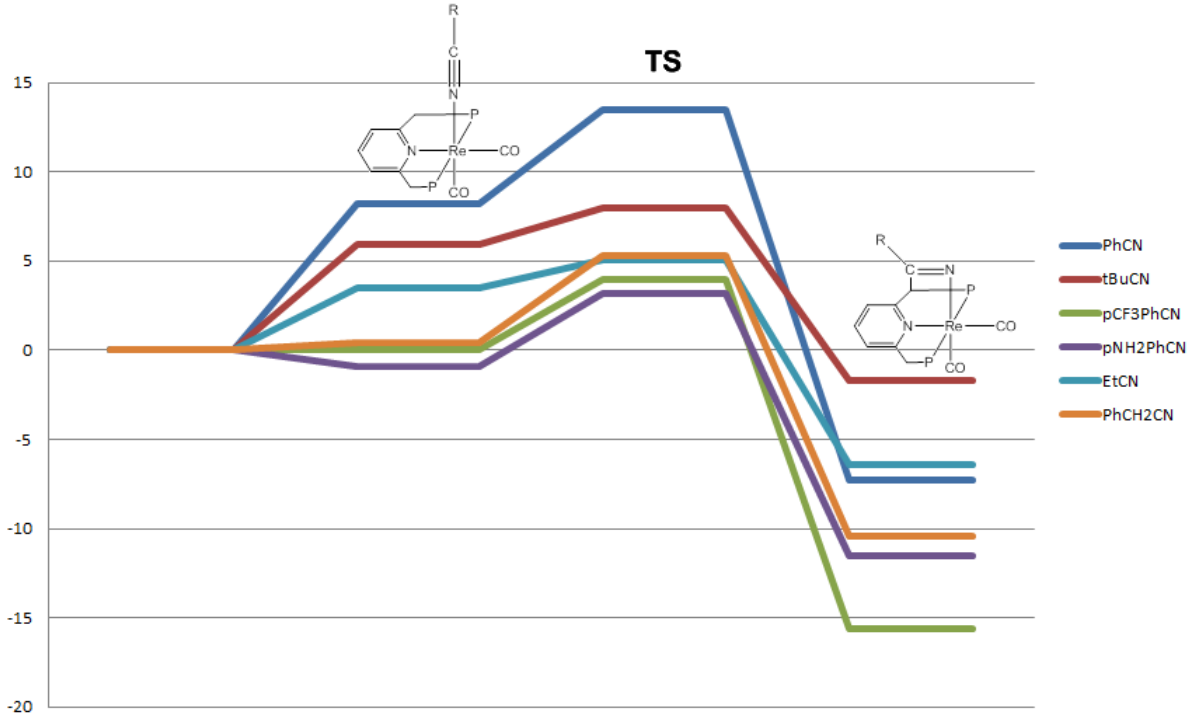

Figure 11: Reaction profiles (Δ G298,sol, kcal/mol, at the SMD(npentane)-DSD-PBEP86/cc-pV(D+d)Z//DF-PBE+dv2/SDD(d) level of theory) for the reactions of 3 with various nitriles.[16]

initiated by nitrile activation in a similar fashion as the [Re]PNP complex just described. Both 2- and 3-pentenenitrile add to the [Ru]PNN complex to form the enamido species $\mathbf{1}^{PN}$, via a ketimido intermediate. For 2-pentenenitrile this is ketimido species **A**. **A** is also the species able to coordinate the proton of, for example, isopropanol by a hydrogen-bonding interaction. Then, via the six-membered transition state **TS B/C**, the isopropanol is added to pentenenitrile to give species **C**. This can then isomerise to species **D**, before it liberates the product and regenerates the catalyst. In the presence of nitrile substrate, complex $\mathbf{1}^{PN}$ is the catalytic resting state. Several different unsaturated nitriles and nucleophiles were deployed, such as acrylonitrile, crotonitrile and allyl cyanide. Isopropanol, ethanol, benzyl alcohol, 1-octanethiol, ethylamine and benzylamine showed reasonable to good yields as nucleophiles. Addition of water to the unsaturated nitrile is also possible, as is ring-closure, which was shown with 6-hydroxy-2-hexenenitrile and 7-hydroxy-2-heptenenitrile, which could be transformed into the corresponding 5- and 6-membered heterocycles.

2.4 Imines

As shown in Figure 4, Figure 10 and Figure 12, ketimines are an important intermediate in reactions of pincer complexes with nitriles.

Imines, which can be subdivided in primary and secondary aldimines and ketimines, are well-known to both organic and inorganic chemists. Imines are generally formed by a condensation of a ketone or aldehyde with a primary amine or ammonia, like in the Strecker synthesis shown in Figure 14. Secondary amines always give iminium ions, in the case of primary amines and ammonia this depends on the reaction conditions. Imine synthesis is reversible in water, and hence imines are used to generate dynamic combinatorial libraries in supramolecular chemistry.[19] Imines are also commonly used as chelating ligands. 1,3-Diketimines (NacNac),

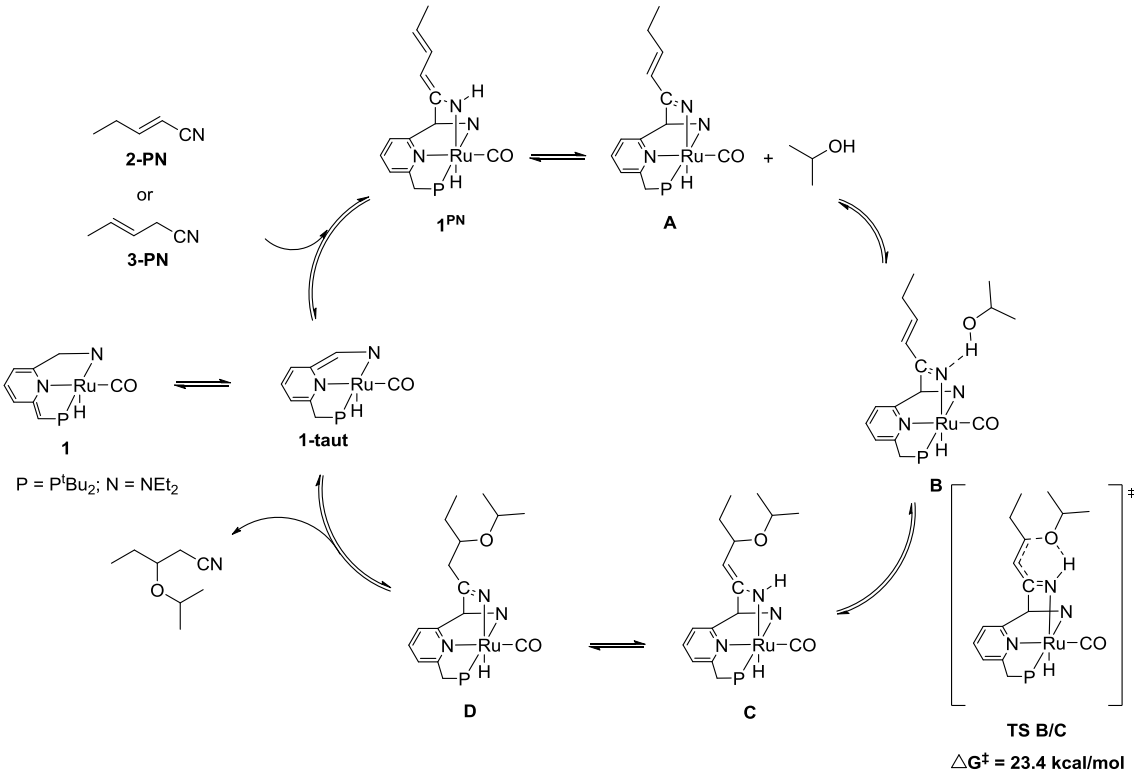

Figure 12: Catalytic cycle for oxa-Michael addition of isopropanol to 2- and 3-pentenenitrile.[18]

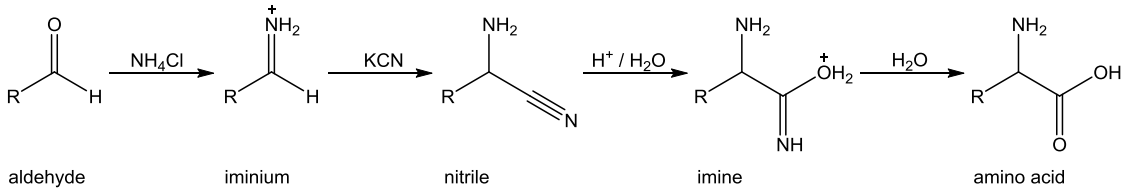

Figure 14: Strecker synthesis of amino acids. [24]

formed from α,β-diketones and primary amines, are mono-anionic, bidentate ligands, commonly used for alkali earth metals and various transition metals.[20] *N,N'*-bis(salicylidine)ethylenediamine (salen) is a tetradentate bi-anionic ligand synthesised from ethylenediamine and two equivalents of salicylaldehyde. The NacNac and salen ligands are shown in Figure 13. For both ligands, electronic and structural properties can be tuned by tuning the ligand backbone. Chirality is easily introduced in the salen ethylenediamine backbone, opening up possibilities for enantioselective catalysis.[21–23]

2.4.1 Nucleophilic addition to ketimines

After activation of a nitrile by a pincer complex, often a ketimine moiety is created. In order to further explore the opportunities of this ketimine or ketimido substrate, it is good to take a look at the conventional chemistry of ketimines and their addition products. This shows addition of a nucleophile to an imine is one of the possibilities.

2.4.1.1 The Strecker synthesis

The Strecker synthesis, shown schematically in Figure 14, is a way to synthesise amino acids from aldehydes and even ketones. Discovered in 1850 by Adolph Strecker, this synthesis involves a nitrile, imine and iminium ions as key intermediates.[24] An aldehyde is condensed with ammonia or an amine to form an iminium ion. Cyanide then adds to the carbon centre to form the α-aminonitrile intermediate. 2 equivalents of H_2O add to the nitrile to form the amino acid upon the liberation of ammonia.

2.4.1.2 Addition to a ketimine ligand

In 2015, De Bruin and co-workers synthesised a new rhodium-PNN complex (**4a** in Figure 15). The starting [Rh(CO)(PNN^{H2})PF_6] complex is deprotonated twice to create both an imine and a dearomatised pyridine moiety. This ligand then has two reaction sites: the nucleophilic imine and the electrophilic methylene arm. Indeed, compound **4a** was shown to react with *o*-toluenesulfonamide, in which the sulfonamide adds to the imine and the methylene arm is protonated to rearomatise the pyridine backbone. The oxidation state of the metal is retained. Apart

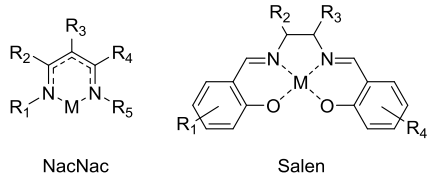

Figure 13: The 1,3-diketimine (NacNac) ligand (left) and the *N,N'*-bis(salicylidine)ethylenediamine (salen) ligand (right).

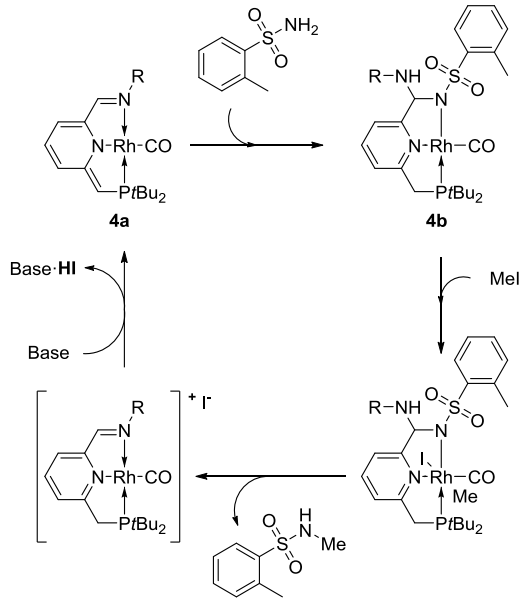

Figure 15: Aminal formation by addition of *o*-toluene-sulfonamide to an imine, and the subsequent catalytic cycle. [25]

from the addition, the formed aminal also rearranges to complex **4b** (see Figure 15), in which instead of diisopropylaniline, now the sulfonamide coordinates to the rhodium metal centre. Subsequent reaction with MeI gives *N*,2-dimethylsulfonamide. A reaction with base closes the catalytic cycle. However, due to side reactions, only one turnover was achieved.[25]

2.5 Addition of cinnamonitrile to the Milstein complex

The reaction of cinnamonitrile with isopropanol did not yield the expected 1,4-addition product. Increasing the catalyst loading from 0.5 mol% to 5 mol% and using excess isopropanol only yielded traces of the addition product, as was observed by ^{1}H-NMR. The stoichiometric reaction of **1** with cinnamonitrile gives some clues why. Figure 16 shows the addition products of **1** with either 2- or 3-pentenenitrile (**1**^{PN}) and cinnamonitrile (**1**^{CN}).[26]

1^{PN} has a rearomatised pyridine backbone and the nitrile forms an unsaturated enamido structure. Due to the phenyl ring, the cinnamonitrile adduct cannot form this enamido complex. However, the tautomer of **1**^{PN}, the ketimido complex (**A** in Figure 12), is the one activating isopropanol. This ketimido complex could also form for the cinnamonitrile adduct, but instead the ketimido-nitrogen deprotonates the ligand side arm to form the dearomatised complex **1**^{CN}.

2.6 Goal of this project

The goal of this project is to combine the alkene isomerisation described in Section 2.2.2 with the oxa-Michael addition described in Section 2.3.3, as well as to design a chiral ligand for this reaction in order to do enantioselective oxa-Michael addition. In order to study this, 4-pentenenitrile is used as a model substrate. Chirality of the ligand is to

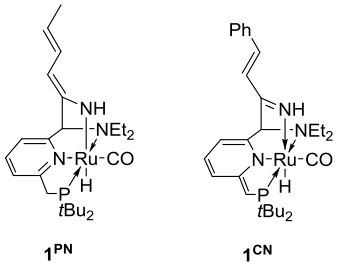

1^{PN} **1**^{CN}

Figure 16: Cycloaddition products of 2- or 3-pentenenitrile (1^{PN}, left) and cinnamonitrile (1^{CN}, right).

be introduced on the amine side-arm of the pincer ligand.

Furthermore, we would like to gain further understanding into the addition of nitriles to the dearomatised [Ru]PNN complex described in Section 2.1.2. This is studied mainly by various NMR techniques including concentration-dependent and temperature-dependent studies, combined with DFT calculations.

3 Results

One goal of this project was alkene isomerisation followed by oxa-Michael addition. Although both have been observed using complex **1** (see sections 2.2.2 and 2.3.3), these reactions do not occur consecutively, as will be discussed in in section 3.1.1. A second goal was the synthesis of a chiral ligand for enantioselective catalysis. The results of this are summarised in section 3.5. This report focusses mainly on nitrile activation by complex **1** and will give further information on the addition of nitriles to this dearomatised [Ru]PNN pincer complex, including observed and calculated relative energies and applications of this nitrile activation.

3.1 Activation of various nitriles

Crystal structures of dearomatised pincer complexes are rare. One of the very few known is the structure of [Rh(PNN)] complex **4a** shown in Figure 15 on page 11. Nevertheless, crystallisation of complex $\mathbf{1}^{CN}$ was attempted but unsuccessful. Complex $\mathbf{1}^{CN}$ can be synthesised in solution, but evaporation of the solvent leads to a loss in peak intensity on ^{1}H-NMR and probably generation of a paramagnetic species, amongst others.

3.1.1 4-pentenenitrile

As complex **1** is capable of catalysing alkene isomerisation as well as oxa-Michael addition, 4-pentenenitrile was expected to first undergo isomerisation to 3- or 2-pentenenitrile, after which subsequent oxa-Michael addition by isopropanol would yield the 1,4-addition product also obtained from 2- or 3-pentenenitrile. However, GC-MS analysis showed little to no conversion of 4-pentenenitrile. This was then further investigated by (stoichiometric) NMR spectroscopy.

Instead of the expected isomerisation followed by oxa-Michael addition, three different species were observed by ^{1}H-NMR spectroscopy, which were then characterised using various 1D and 2D NMR techniques. This showed the presence of four different species in equilibrium, of which one is complex **1**.

Complex **1** is in rapid equilibrium with complex $\mathbf{1}^{4PN}\mathbf{A}$, and on NMR timescale, an average is observed. At a 1:1 ratio of complex **1** and 4-pentenenitrile, the hydride shift is observed at -21.07 ppm. This is however dependent on **1**/nitrile ratio and temperature, as will be discussed below in Section 3.2 on page 15. Complex $\mathbf{1}^{4PN}\mathbf{B}$ is only observed in small quantities and could therefore not be characterised fully, but this complex is expected to be a rearomatised nitrile addition product. Its hydride is observed at -11.87 ppm. Compound $\mathbf{1}^{4PN}\mathbf{C}$ resembles $\mathbf{1}^{CN}$ and shows comparable ^{1}H-NMR shifts, i.e. a hydride signal at -13.88 ppm (-12.95 ppm for $\mathbf{1}^{CN}$) and an imine proton at 9.66 ppm (9.68 for $\mathbf{1}^{CN}$). Figure 17 shows the observed complexes, alongside the hydride region of the ^{1}H-NMR spectrum of the described mixture.

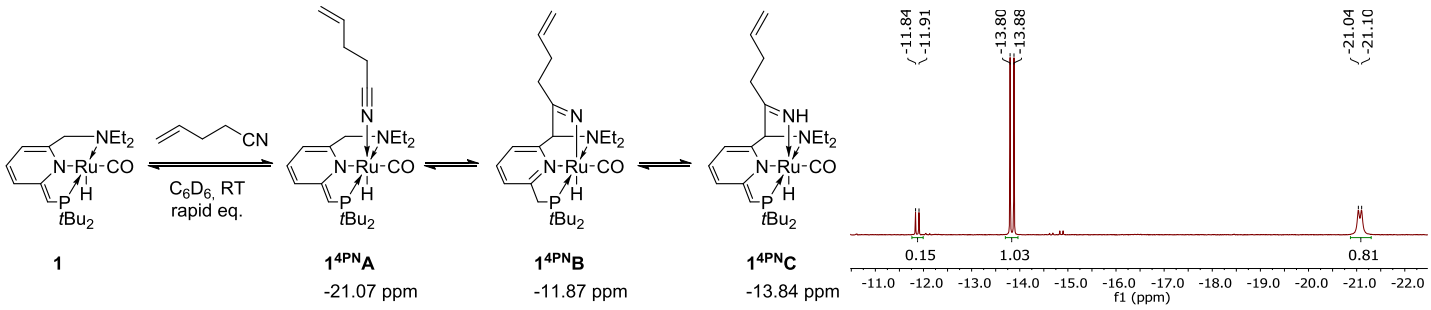

Figure 17: Equilibrium formed between 1 and 4-pentenenitrile. All species are in equilibrium with one another. The observed ruthenium-hydride shifts are noted below the complexes and shown in the ^{1}H-NMR spectrum on the right. In the case of complex 1^{4PN}A, an exchange-averaged proton-shift is observed.

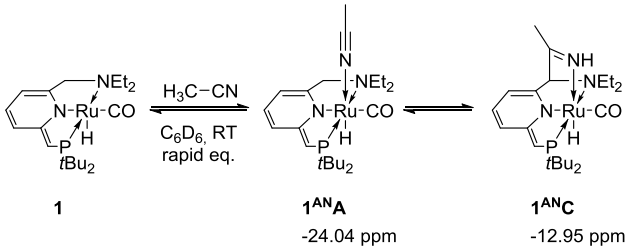

Figure 18: Equilibrium formed between 1 and acetonitrile. The observed [Ru]-H shifts are noted below the complexes.

3.1.2 Acetonitrile

Similar results were obtained for the reaction of **1** with acetonitrile, as can be seen in Figure 18. The acetonitrile-analogue of **1^{4PN}B** was however not observed by ^{1}H-NMR. Three species are formed in solution, of which the first two are in rapid equilibrium (**1** and **1^{AN}A**). The second equilibrium, between **1^{AN}A** and **1^{AN}C**, is much slower, as this shows two distinct signals in NMR. In C_6D_6, the ketimine proton is observed at 9.24 ppm and the hydride signals are observed at -12.95 (**1^{AN}C**) and -24.04 (**1/1^{AN}A**).

The big difference in hydride shift between **1/1^{AN}A** (-24.04 ppm) and **1/1^{4PN}A** (-20.94 ppm) can be explained if the equilibrium is taken into account. Both are rapid equilibria, but most probably the equilibrium between **1** and **1^{4PN}A** lies more towards the addition product, whereas the equilibrium between **1** and **1^{AN}A** lies more on the side of complex **1**. Addition of more acetonitrile to the reaction mixture shifts the equilibrium more towards **1^{AN}A** and away from **1**, which causes a downfield shift of the hydride signal. When instead of one, five equivalents of acetonitrile are added, the hydride signal for **1/1^{AN}A** can now be observed at -18.66. Complex **1** has its hydride at -26.56 ppm, typical for such a penta-coordinated 16e$^-$ ruthenium complex.[7,26] Introduction of a substituent *trans* to the hydride typically shifts the hydride signal from -25 to -15 ppm. Thus, the downfield shift of the hydride upon addition of more acetonitrile indicates a shift in the equilibrium towards complex **1^{AN}A**.

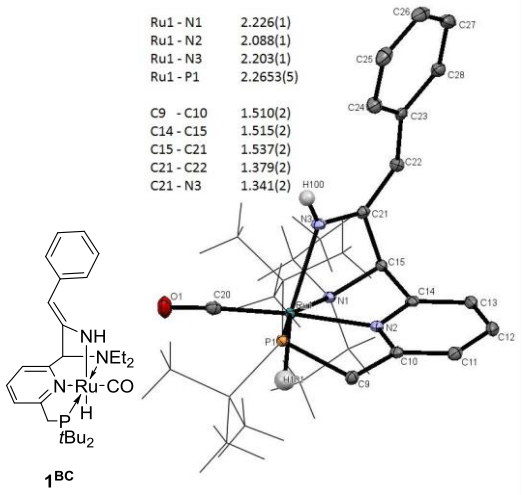

Figure 19: Molecular structure of compound 1^{BC}D. Selected bond lengths [Å] are given and thermal ellipsoids are set at 50% probability. The P^{t}Bu$_2$ and NEt$_2$ groups are drawn as wire-frame model and H-atoms (except Ru-H and N-H) are omitted for clarity.

The ratio between **1^{AN}C** and **1/1^{AN}A** is 1:1.60 when a 1:1 ratio of acetonitrile and **1** is used. Addition of 5 equivalents of acetonitrile changes the ratio between the two to 1:0.35. Thus, more acetonitrile leads to more of complex **1^{AN}A** and hence more of complex **1^{AN}C**.

3.1.3 Benzyl cyanide

Milstein's study on a [Re]PNP complex shows similar results to those we have obtained for our nitrile substrates (see Figure 11), and therefore the same substrates were also applied here. For benzyl cyanide, enamido species **3^{BC}** is reported, which, according to the calculations, is formed following the scheme in Figure 10 on page 9.

Complex **1** reacts with benzyl cyanide to give complex **1^{BC}D**, depicted in Figure 19 along with its crystal structure. The selected bond lengths, also shown in Figure 19, suggest a rearomatised backbone and an enamido-structure. This is also supported by the ^{1}H-NMR spectrum, which shows the hydride doublet at -11.98 ppm and the amido-proton at 5.10 ppm. This is significantly different from the ketimine protons of **1^{4PN}C**, **1^{CN}** and **1^{AN}C**, which are observed at roughly 10 ppm.

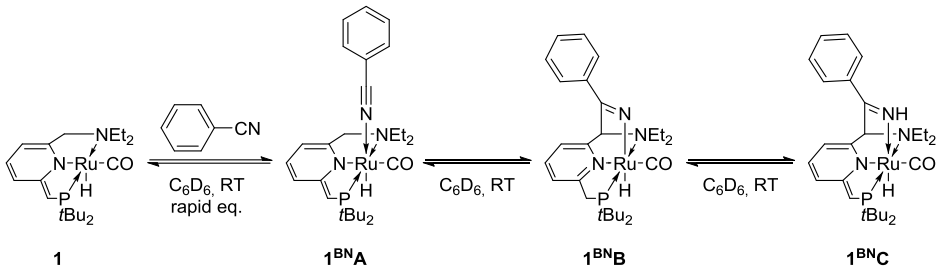

Figure 20: Observed species in a 1/benzonitrile solution.

In the first few minutes of this reaction, another compound is also observed. Due to its rapid disappearance, full characterisation was not possible, but the Ru-H resonance at -13.71 ppm, the ^{31}P-NMR resonance at 109.9 ppm and the absence of a N-H resonance around 10 ppm suggest it to be complex **1^{BC}B**.

3.1.4 Benzonitrile

Like cinnamonitrile, benzonitrile lacks the α-protons needed for the tautomerisation towards the enamido form. Thus, complexes such as **1^{AN}A** and **1^{4PN}C** are to be expected. Indeed, the reaction of **1** and benzonitrile yields complexes **1^{BN}A** and **1^{BN}C**, as was observed by ^{1}H-NMR. Again, a third species was observed on ^{1}H-NMR and ^{31}P-NMR, which could not be fully characterised. The suggested structure of this complex **1^{BN}B** is shown in Figure 20. The hydride signal is observed at -10.02 ppm, which is significantly downfield from the -13.23 ppm observed for complex **1^{BN}C**. The phosphorus signal of **1^{BN}B** is observed at 120.87 ppm, comparable to the phosphorus signal of complex **1^{BC}D** and **1^{PN}**. This indicates a rearomatised species for complex **1^{BN}B**.

3.1.5 Overview of the different observed complexes

Table 3 summarises the observed signals in ^{1}H- and ^{31}P-NMR for the complexes described above, along with complex **1** and the previously reported complex **1^{PN}**. An overview of the observed complexes is given in Figure 21.

3.2 Nitrile comparison

The activation of nitrile by **1** is similar to the nitrile activation by the aluminium-phosphorus frustrated Lewis pair described above in section 2.3.1 on page 8.[15] Coordination of the nitrile to the metal centre is followed by cycloaddition and subsequent proton transfer. Which proton is transferred depends on the nitrile used. It could be a proton from the nitrile substrate to form **1D**, of from the ligand backbone to form **1C**. Further investigations into the acidity and basicity of the intermediates as well as DFT-calculations might give some insight into which proton is transferred and hence which complexes are observed in solution.

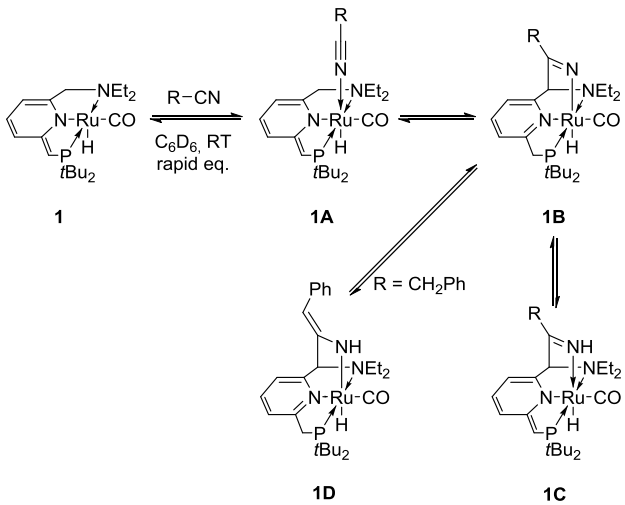

Figure 21: Overview of the formed complexes described in sections 2.3.3, 2.5 and 3.1.1 to 3.1.4.

3.2.1 Acidity of the intermediates and basicity of the formed ketimine

Different nitriles lead to different complexes: in the case of 3-pentenenitrile or benzyl cyanide, the α-proton of the nitrile is abstracted, resulting in rearomatised ruthenium enamido complex **1D**. For cinnamonitrile, acetonitrile, 4-pentenenitrile, and benzonitrile the ligand proton is abstracted, resulting in dearomatised ruthenium ketimine complex **1C**. For cinnamonitrile and benzonitrile, this is to be expected, as there is no α-proton available. For acetonitrile and 4-pentenenitrile, the α-proton is apparently less acidic than the ligand proton, and the ligand is deprotonated preferentially. To conclude, benzylic and allylic hydrogens are acidic enough to be deprotonated by the formed ketimido complex, but aliphatic hydrogens are not and the ligand is deprotonated instead.

Table 2 shows pKa-values of selected compounds. Complex $\mathbf{1^{BN}B}$ can be formed if the imido-complex is not basic enough to deprotonate the ligand. In order to reduce the basicity of the imine and thereby characterising complex $\mathbf{1^{BN}B}$, a reaction between **1** and pentafluorobenzonitrile (C_6F_5CN) was attempted. However, this did not yield any characterisable product.

Substrate		pKa (DMSO)
Acetonitrile	CH_3CN	31.3
Propionitrile	CH_3CH_2CN	32.5
Benzyl cyanide	$PhCH_2CN$	21.9
Octanethiol	$CH_3(CH_2)_7SH$	10.64
***o*-toluene-sulfonamide**	*o*-$MePhSO_2NH_2$	10.18
Isopropanol	$(CH_3)_2CHOH$	17.1

Table 2: pKa values of selected compounds. Data taken from *Acc. Chem. Res* 1988, *21* (10), 456–463.[53] For a schematic overview see: http://www.chem.wisc.edu/areas/reich/pkatable/

3.2.2 ^{1}H- and ^{31}P-NMR shifts

Table 3 shows the observed characteristic Ru-H signals, as well as the ^{31}P-NMR resonances and imine/amine resonances (when applicable) for all complexes described above in section 3.1. The ^{31}P-NMR resonances seem to be very indicative of the formed complex, although a distinction between **1B** and **1D** based only on ^{31}P-NMR is impossible, as both are hexa-coordinated $18e^-$ ruthenium complexes with a rearomatised ligand backbone. For complex **1A**, the trend in ^{1}H-NMR shift matches the trend in ^{31}P-NMR shift: $\mathbf{1<1^{AN}A<1^{BN}A<1^{PN}A}$. This indicates the observed ^{1}H- and ^{31}P-NMR chemical shifts are a result of the location of the equilibrium rather than an indication of the chemical shift of the pure complexes. Addition of 16 equivalents of 4-pentenenitrile to **1** shifts the ^{1}H-NMR signal from -20.94 to -15.38 ppm, which is to be expected as the equilibrium approaches $\mathbf{1^{4PN}A}$. The hydride signals for pure complex $\mathbf{1^{AN}A}$ and $\mathbf{1^{BN}A}$ are also expected close to -15 ppm.

3.2.3 DFT calculations

The use of DFT calculations can give an insight into the relative energies of the different complexes. The geometries of **1B**, **1C**, and **1D** were optimised by prof. Edwin Otten using DFT calculations, as described in *Dalton Trans*, **2016**, *45*, 16033-16039.[27] DFT calculations were performed at the TPSSTPSS level of theory using a LANL2DZ basis set (with effective core potential) for ruthenium and 6-21(d,p) for all other atoms. Calculations were performed in the gas phase, thus omitting any solvent effects present (see section 3.2.4). The calculated stationary points were confirmed to be local minima by subsequent frequency analyses. Single-point TPSSTPSS calculations using Ahlrichs'def2-TZVP basis set[28] and employing Grimme's D3 empirical dispersion correction[29] were used to further refine the energies of the calculated geometries. Calculated relative energies are shown in Table 4.

		1	1^{AN}	1^{4PN}	1^{CN}	1^{BN}	1^{BC}	1^{PN}
A	Hydride	-26.59	-24.04	-20.94		-21.22		
	Phosphorus	94.0	94.9	96.1		95.4		
B	Hydride			-11.88		-10.02	-13.71	
	Phosphorus			121.0		120.9	109.8	
C	Hydride		-13.95	-13.88	-12.59	-13.23		
	Imine		9.24	9.66	9.68	10.20		
	Phosphorus		106.0	106.0	105.7	106.0		
D	Hydride						-11.98	-12.03
	Amine						5.10	3.96
	Phosphorus						120.9	120.7

Table 3: Overview of the observed NMR signals at room temperature described here. The data for 1^{AN}B, 1^{4PN}B and 1^{BN}B are of the equilibria formed for a 1:1 ratio of nitrile and 1. Data for 1^{PN} were taken from *Angew. Chemie Int. Ed.* 2015, *127*, 4310–4314.[18]

	1B[a]	1B[b] (%)	1C[a]	1C[b] (%)	1D[a]	1D[b] (%)
Cinnamonitrile	1.8	0	0	100	-	-
4-pentenenitrile	0.5	9	1.0	48	0	0
Acetonitrile	0.5	0	0	49	1.0	0
Benzonitrile	0	20	0.3	76	-	-
Benzyl cyanide	7.9	0	5.7	0	0	100

Table 4: *a)* Gibbs free energies in kcal mol^{-1} relative to the lowest energy isomer.
***b)* Relative amount of each component as determined by 1H NMR integration of 1 : 1 mixture 1 + nitrile at room temperature (remainder is 1 + 1A). Data taken from *Dalton Trans.* 2016, *45* (40), 16033-16039.[27]**

For cinnamonitrile and benzyl cyanide, the synthesis converged to only one complex. The DFT calculations correspond to this. $\mathbf{1^{CN}C}$ is preferred over $\mathbf{1^{CN}B}$ with an energy difference of 1.8 kcal mol^{-1}. For benzyl cyanide $\mathbf{1^{BC}D}$ is preferred over $\mathbf{1^{BC}B}$ and $\mathbf{1^{BC}C}$ by 7.9 and 5.7 kcal mol^{-1} respectively. For 4-pentenenitrile, acetonitrile and benzonitrile the differences in calculated energy are small, and this reflects the equilibria observed in solution.

For acetonitrile, only $\mathbf{1^{AN}A}$ and $\mathbf{1^{AN}C}$ are observed, and this is reflected by the calculated energies. $\mathbf{1^{AN}C}$ is calculated to be lower in energy than $\mathbf{1^{AN}B}$ and $\mathbf{1^{AN}D}$, but only by 0.5 and 1.0 kcal mol^{-1}. For 4-pentenenitrile, $\mathbf{1^{4PN}D}$ was calculated to be the lowest in energy. However, $\mathbf{1^{4PN}B}$ and $\mathbf{1^{4PN}C}$ are the complexes observed in solution, together with $\mathbf{1^{4PN}A}$. The calculated energy differences between $\mathbf{1^{4PN}D}$ and $\mathbf{1^{4PN}B}$ and $\mathbf{1^{4PN}C}$ are however only 0.5 and 1.0 kcal mol^{-1}. The small differences in energy support the fact that these complexes are in equilibrium in solution.

The same goes for complex $\mathbf{1^{BN}}$. The more prevalent complex $\mathbf{1^{BN}C}$ was calculated to be 0.3 kcal mol^{-1} higher in energy than complex $\mathbf{1^{BN}B}$, which is also observed in solution, albeit in a lower quantity.

The DFT calculations support the observation that several different complexes are present in solution, as the energy differences between the complexes are low enough for the system not to convert to one complex only.

3.2.4 Solvent effects

The DFT calculations described above were performed in gas phase and do not take into account any solvent effects. The inconsistency between calculations and experimental data can well be caused by these solvent effects.

Most reactions were either performed in benzene-d_6 or toluene-d_8, and in the case of acetonitrile, 4-pentenenitrile and benzonitrile, there is free nitrile in solution. Aromatic rings as well as nitriles can be weak hydrogen-bond acceptors,[30–35] thus stabilising the ketimine-

complex **1C** and/or the enamido-complex **1D**. This could well explain why the calculated energies of these complexes (especially $\mathbf{1}^{4PN}\mathbf{C}$ and $\mathbf{1}^{BN}\mathbf{C}$) differ from the observed relative amounts of the different complexes in solution.

3.3 Determination of equilibrium constants

As was discussed in section 3.1.2, the amount of acetonitrile added to a solution of **1** determines the ratio between the formed complexes, as well as the observed shift of $\mathbf{1} \rightleftarrows \mathbf{1}^{AN}\mathbf{A}$. Addition of 5 equivalents of acetonitrile instead of 1 results in a ^{1}H-NMR shift of Ru-H from -24.04 to -18.66 ppm. At the same time, the ratio between $\mathbf{1}^{AN}\mathbf{C}$ and $\mathbf{1} \rightleftarrows \mathbf{1}^{AN}\mathbf{A}$ changes from 1:1.60 to 1:0.35. Addition of more acetonitrile thus leads to more of complex $\mathbf{1}^{AN}\mathbf{C}$. For $\mathbf{1}^{4PN}$, the equilibrium was studied in depth, both by varying concentration and varying temperature. This then gives, *via* a Van 't Hoff plot, more information about equilibrium constants as well as ΔH and ΔS. The obtained ^{1}H-NMR spectra are given in Figure 22.

For 4-pentenenitrile, $\mathbf{1} \rightleftarrows \mathbf{1}^{4PN}\mathbf{A}$, $\mathbf{1}^{4PN}\mathbf{B}$ and $\mathbf{1}^{4PN}\mathbf{C}$ are observed in solution, so the equilibria K_1, K_2, and K_3 (see equation 1) were taken into account.

$$1 + 4PN \underset{}{\overset{K_1}{\rightleftharpoons}} 1^{4PN}A \overset{K_2}{\rightleftharpoons} 1^{4PN}B \overset{K_3}{\rightleftharpoons} 1^{4PN}C \quad (1)$$

3.3.1 Concentration dependence

From the ratio between the different complexes in solution, the equilibrium constants can be calculated. K_3 was determined as 6 M^{-1} from the $\mathbf{1}^{4PN}\mathbf{B}/\mathbf{1}^{4PN}\mathbf{C}$ ratio. However, the concentration of **1** and $\mathbf{1}^{4PN}\mathbf{A}$ in solution cannot be determined directly by NMR integration due to the rapid exchange between the two complexes. Hence, the equilibrium constant had to be determined differently.

The exchange-averaged chemical shift of the observed equilibrium indicates the ratio between the complexes in solution. The chemical shift shifts from one extreme (pure complex **1**) to the other (pure complex $\mathbf{1}^{4PN}\mathbf{A}$), depending on the relative concentration of 4-pentenenitrile compared to complex **1**. In the case of a rapid equilibrium, a NMR titration experiment can be performed. The amount of one component is kept constant, while the amount of the other component is varied. If the chemical shifts of both extremes are known, the equilibrium constant can be determined from the observed chemical shift. A similar approach was used here, however, the amount of **1** and 4-pentenenitrile participating in equilibrium K_1 depends on the amount of $\mathbf{1}^{4PN}\mathbf{B}$ and $\mathbf{1}^{4PN}\mathbf{C}$, which in turn depend on the amount of $\mathbf{1}^{4PN}\mathbf{A}$, which depends on the relative amount of 4-pentenenitrile. The concentration of complex

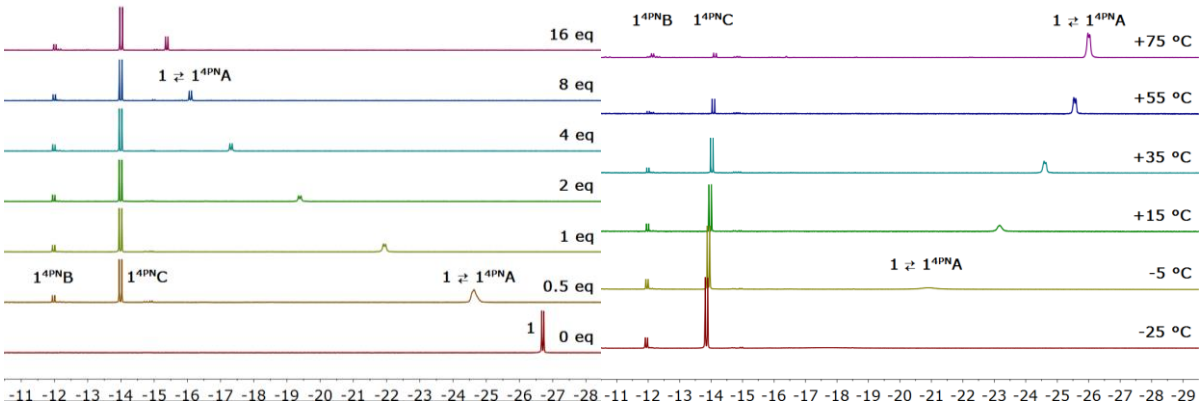

Figure 22: Ru-H region of the ^{1}H-NMR spectrum of 1 with varying equivalents of 4-pentenenitrile at 25 °C in toluene-d_8 (left), and with 1 equivalent of 4-pentenenitrile at varying temperatures in toluene-d_8 (right).

$$[\mathbf{1}] = \frac{-K_1([4PN]_0-[\mathbf{1}]_0)-1\pm\sqrt{(K_1([4PN]_0-[\mathbf{1}]_0+1)^2-4K_1([\mathbf{1}B]+[\mathbf{1}C]-[\mathbf{1}]_0)}}{2K_1} \quad (2)$$

$$[\mathbf{1}A] = \frac{-\left([\mathbf{1}]_0-2[\mathbf{1}B]-2[\mathbf{1}C]+[4PN]_0+\frac{1}{K_1}\right)\pm\sqrt{([\mathbf{1}]_0-2[\mathbf{1}B]-2[\mathbf{1}C]+[4PN]_0+\frac{1}{K_1})^2-4([\mathbf{1}]_0-[\mathbf{1}B]-[\mathbf{1}C])([4PN]_0-[\mathbf{1}B]-[\mathbf{1}C])}}{2} \quad (3)$$

1 and 4-pentenenitrile participating in equilibrium K_1 thus varies with varying amount of 4-pentenenitrile. The concentration of **1** and 4-pentenenitrile participating in equilibrium K_1 was deduced from the initial amount and the amount of $\mathbf{1}^{4PN}\mathbf{B}$ and $\mathbf{1}^{4PN}\mathbf{C}$ formed. Thordarsons fitting programme[36] was used to determine equilibrium constant K_1 as 41 M^{-1} (±20%). Using K_1, the concentrations of **1** and $\mathbf{1}^{4PN}\mathbf{A}$ in solution were determined using equations 2 and 3, and from this, K_2 was calculated as 0.5 M^{-1}. The derivation of equation 2 and 3 can be found in the appendix.

3.3.2 Temperature dependence

Variable-temperature NMR studies can give an insight into the temperature-dependent behaviour of a reaction, and therefore this experiment was also performed on the **1** + 4-pentenenitrile equilibria. Due to line broadening as well as a decrease in amount of $\mathbf{1}^{4PN}\mathbf{A}$, data at temperatures below -5 °C were not usable. At temperatures above 55 °C, decomposition is observed, and hence only the data between -5 °C and +55 °C were used to calculate the thermodynamics of these equilibria. Relative concentrations of **1**, $\mathbf{1}^{4PN}\mathbf{A}$, $\mathbf{1}^{4PN}\mathbf{B}$, and $\mathbf{1}^{4PN}\mathbf{C}$ were determined using the relative Ru-H integrals, as well as the observed chemical shift of $\mathbf{1} \rightleftarrows \mathbf{1}^{4PN}\mathbf{A}$. From this, the equilibrium constants at the variable temperatures were calculated, and a van 't Hoff plot (see Figure 23) afforded the corresponding enthalpy and entropy values shown in Table 5.

All three reactions are enthalpically favourable. The first two equilibria (K_1 and K_2) are entropically disfavoured. The formation of the nitrile adduct is influenced most by

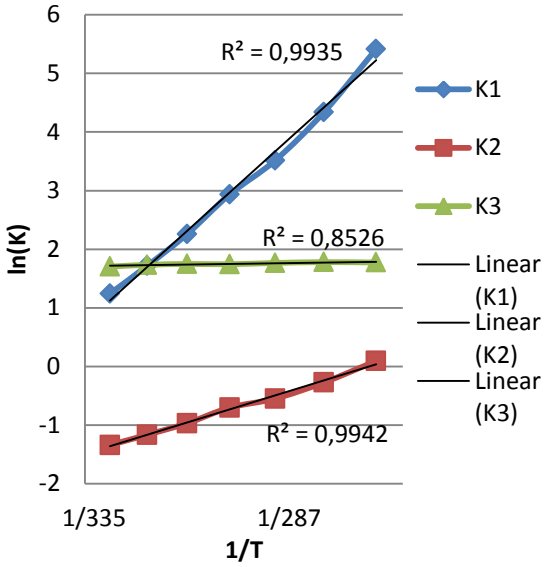

Figure 23: Van 't Hoff plot of equilibria K_1, K_2, and K_3. The corresponding values for ΔH and ΔS are given in Table 5.

	K_1	K_2	K_3	
ΔH	-50	-17	-0.82	kJ mol^{-1}
ΔS	-143	-63	12	J K^{-1} mol^{-1}

Table 5: Calculated values for ΔH and ΔS of equilibria K_1, K_2, and K_3.

entropy with ΔS = -143 J K^{-1} mol^{-1}, as was to be expected because this is an addition reaction where two molecules come together to form one. The formation of $\mathbf{1}^{4PN}\mathbf{B}$ is also entropically disfavoured, as this reaction too restricts the motion of the molecule.

As can be seen in the Van 't Hoff plot in Figure 23, the formation of the nitrile adduct $\mathbf{1}^{4PN}\mathbf{A}$ is favoured at all measured temperatures (ln(K) > 0), as is the third reaction, the formation of the deprotonated ketimine complex $\mathbf{1}^{4PN}\mathbf{C}$. For the second equilibrium (K_2) ln(K) < 0, and the reaction equilibrium will be more on the side of $\mathbf{1}^{4PN}\mathbf{A}$ than $\mathbf{1}^{4PN}\mathbf{B}$. Indeed, in solution, only a small amount of $\mathbf{1}^{4PN}\mathbf{B}$ is observed. In the case of acetonitrile, complex $\mathbf{1}^{AN}\mathbf{B}$ is not observed at all.

3.4 Reactivity of the formed imine

The oxa-Michael addition to 2- and 3-pentenenitrile catalysed by **1** is in fact a conjugate nucleophilic addition. For 2- and 3-pentenenitrile, only 1,4-addition was observed and no 1,2-addition. For the activated nitriles described here, 1,4-addition is generally not applicable, but 1,2-addition might result in interesting complexes. Another suggested mode of reaction is Diels-Alder type chemistry, and therefore cycloaddition using an activated acetylene was also attempted.

3.4.1 Nucleophilic addition

Complex $\mathbf{1}^{PN}$ undergoes oxa-Michael addition in its tautomeric form, the ketimido complex **A** in Figure 12 (page 10). However, no product formation was observed for cinnamonitrile or 4-pentenenitrile and isopropanol in the presence of **1**. This can be explained by the formation of complex $\mathbf{1}^{CN}$, where the ketimine is protonated. Addition of octanethiol to crotonitrile proceeds very rapidly in the presence of **1** and with a high yield (99%). Therefore, addition of octanethiol to $\mathbf{1}^{AN}$ and $\mathbf{1}^{CN}$ was attempted. Instead of the expected addition of octanethiol to the nitrile, addition of the thiol to **1** was observed, resulting in complex $\mathbf{1}^{SH}$, shown in Figure 24. The rearomatised complex $\mathbf{1}^{SH}$ was formed quantitatively and no addition to acetonitrile was observed. Addition of other nucleophiles such as diethylamine and triethylsilane did not yield any reaction, not even at elevated temperatures (50°C).

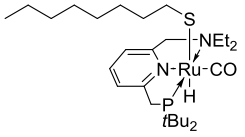

$\mathbf{1}^{SH}$

Figure 24: Replacement of acetonitrile by octanethiol yields $\mathbf{1}^{SH}$.

Addition of *o*-toluenesulfonamide was also attempted, as this was shown to add to the [Rh]-ketimine complex **4a**.[25] Addition of *o*-toluenesulfonamide to $\mathbf{1}^{CN}$ in thf gave an insoluble salt. X-ray crystallography showed it to be complex **5**, of which the molecular structure is shown in Figure 25. The bonds of the PNN ligand backbone are of similar lengths compared to complex $\mathbf{1}^{BC}$, while the C-N bond is significantly shorter (1.29 Å compared to 1.34 Å). This indicates a rearomatised pyridine backbone and a C=N double bond instead of a C-N single bond. The distance between the ketimine nitrogen (N3 in Figure 25) and the sulfonamide nitrogen (N4 in Figure 25) is relatively short: 2.97 Å. This indicates the positive charge of the ruthenium complex is situated mainly on N3. This indication of a four-coordinated nitrogen is supported by the observation of an imine proton at δ = 11.42 ppm in ^{1}H-NMR spectroscopy (CD_3CN).

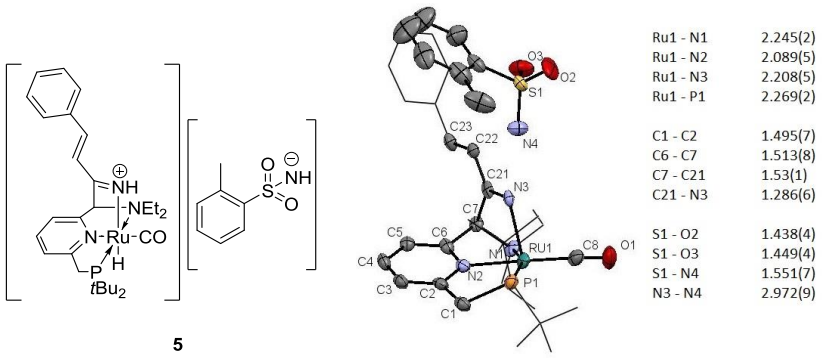

5

Figure 25: Molecular structure of compound 5. Selected bond lengths [Å] are given and thermal ellipsoids are set at 50% probability. The P^{t}Bu$_2$ and NEt$_2$ groups are drawn as wire-frame model and H-atoms are omitted for clarity.

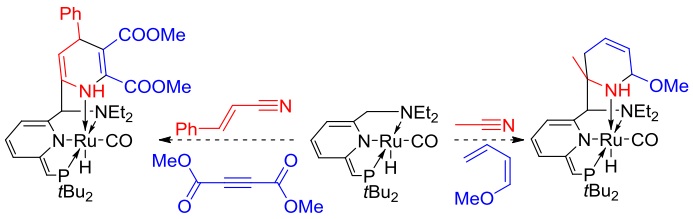

Figure 26: Attemted cycloaddition reactions, with proposed outcome (not realised).

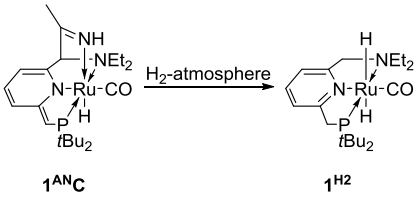

Figure 27: Formation of the dihydride complex 1^{H2} from 1^{AN}.

3.4.2 Cycloaddition

To further explore the possibilities of reactions with the ketimine moiety, cycloadditions were attempted, both with the ketimine as a diene and as a dienophile. The attempted reactions are shown in Figure 26. The reaction with 1-methoxy-1,3-butadiene did not proceed and dimethyl acetylenedicarboxylate reacts vigorously with complex **1** to form a paramagnetic species. A rapid colour change from red to blue, purple and brown resulted with an intensity loss in the ^{1}H-NMR spectrum. Less reactive acetylenes such as diphenyl acetylene might give some insight into the reaction.

3.4.3 Addition of H_2

Hydrogenation of nitriles by pincer complexes has been reported, as was described in the introduction (see Figure 4). Apart from this aliphatic [Fe]PNP complex, several cobalt-complexes were shown to hydrogenate nitriles to amines. A [Co]PNNH complex showed the best performances (92% yield using 2 mol% catalyst). The cobalt analogue of **1** also showed catalytic activity (84% yield of benzylamine using 4 mol% of catalyst), but this [Co]PNN complex also formed *N*-benzylidene-1-phenylmethanamine in 5% yield.[12]

Analogous to the [Co]PNN complex, the hydrogenation of acetonitrile by complex **1** was attempted. Unfortunately, this resulted in the dihydride complex $\mathbf{1}^{H2}$, and no amine-formation was observed. This is summarised in Figure 27. This dihydride complex $\mathbf{1}^{H2}$ was already reported before by Milstein and co-workers.[7]

3.4.4 Generation of ethylene

During the variable temperature NMR studies on **1** and 4-pentenenitrile, decomposition at higher temperatures was observed. This decomposed compound included a sharp

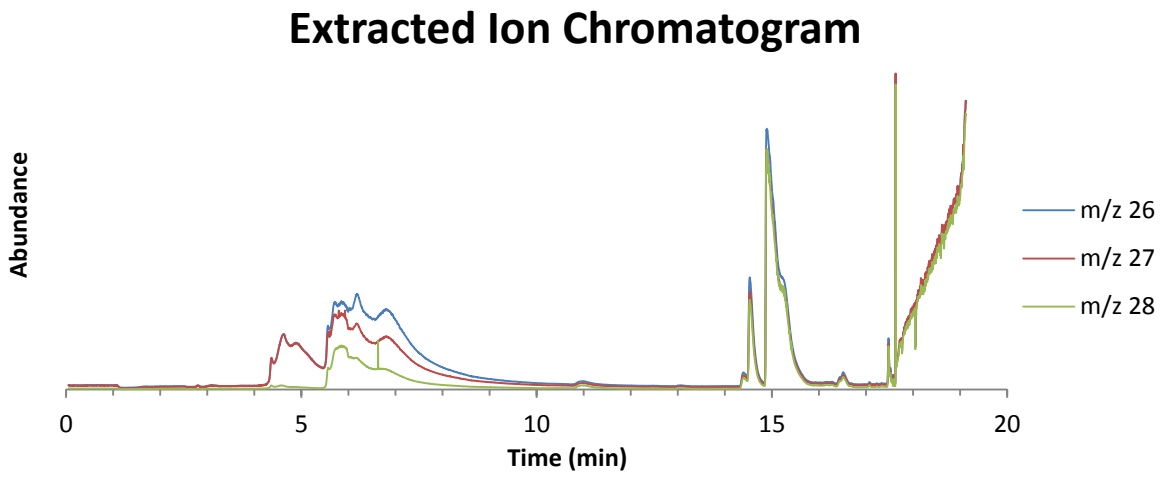

Figure 28: Extracted Ion Chromatogram. Using carbosieve-SIII, the headspace of the reaction was captured. This analyte was then analysed by GC-MS under a constant N_2-gas flow. Subtraction of this constant N_2-signal results in the above graph.

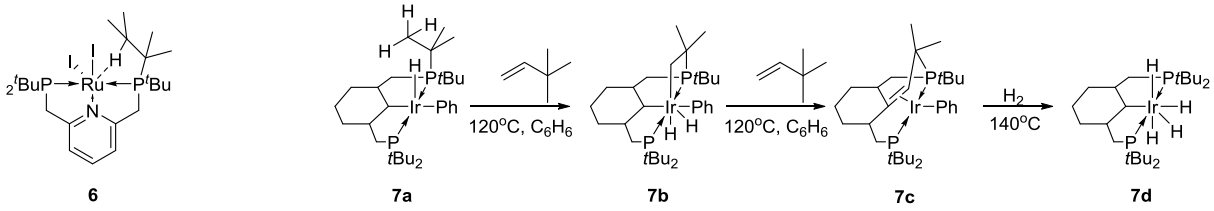

Figure 29: Ruthenium PNP complex 6 with agostic C-H bond interaction (left),[42] and activation of the P^{t}Bu$_2$ ligand side arm by iridium complex 7 (right).[43]

singlet resonance in the ^{1}H-NMR spectrum at δ = 5.24 ppm (in toluene-d$_8$), with a ^{13}C-NMR resonance at δ = 123.30 ppm. This is indicative of ethylene. The absence of any coupling pattern supports this hypothesis. Ethylene was also detected using gas-capturing and subsequent GC-MS analysis (see Figure 28).

Ethylene has a mass of 28 g/mol, the same as nitrogen gas. This complicates the detection of ethylene, but using a constant flow of nitrogen gas, which was then subtracted from the resulting spectrum resulted in the chromatogram in Figure 28. Between 4 and 10 minutes, an increase in intensity for ions with a mass of 26, 27 and 28 g/mol is observed. This is likely to be ethylene. The peaks above 10 minutes are likely to be a less volatile hydrocarbon such as toluene, which was used as a solvent. In the ^{1}H-NMR spectrum, a sharp singlet resonance at 0.80 ppm (in toluene-d$_8$) suggests additional formation of ethane, but this could not be confirmed by GC-MS. When 4-pentenenitrile was omitted and pure complex **1** was heated to 80°C for 30 minutes, no ethylene was observed. The nitrile is therefore needed for this reaction to occur.

The generation of ethylene is suggested to go via a cyclometallation pathway. Cyclometallation of the ligand side-arm has been reported before, mainly in iridium complexes.[37–41] For ruthenium complexes, cyclometallations are much rarer. Milstein *et al*. report an agostic ruthenium C-H bond interaction on the ^{t}BuP-ligand arm of [Ru]I$_2$PNP complex **6**. This is illustrated in Figure 29.[42] This interaction was, however, not followed by a C-H bond cleavage or C-Ru bond formation. Polukeev and Wendt, on the other hand, report C-C double bond formation using the iridium complex **7a**.[43] They report reversible double bond formation via C-H activation of the P^{t}Bu$_2$-side arm of the iridium complex **7a**. A schematic representation of the mechanism is given in Figure 29.

Upon heating of the Ir^{III}-complex **7a** in the presence of neohexene as a hydrogen acceptor, the Ir^{I}-complex **7c** is formed, which has a C=C bond formed between the Cα and a methyl of the ^{t}BuP-ligand arm. The proposed mechanism proceeds through intermediate **7b**, the result of oxidative addition of the ligand arm. The formation of **7c** proved to be reversible, and heating complex **7c** under a H$_2$-atmosphere resulted in the Ir^{V}-complex **7d**, via a Ir^{III} intermediate, as reported in *Chem. Sci.*, **2015**, 6, 2060-2067.[43]

Contrary to complex **7**, ligand activation by complex **1^{4PN}** is not reversible, as ethylene is liberated from the complex. The NEt$_2$-arm is suspected to be the ligand side-arm to be activated, as this is more likely to release ethylene. A suggested mechanism of this reaction is shown in Figure 30. The Ru^{II}⇄Ru^0 equilibrium in the first step has never been observed, but a similar complex was proposed as an intermediate in the catalytic water splitting by complex **1**.[44] A ligand C-H bond can then add oxidatively to the Ru^0 centre, resulting in complex **8a**. This complex could then eliminate ethylene, resulting in complex **8b**. This last reaction can be seen as a dehydroamination, as an amine and a hydride

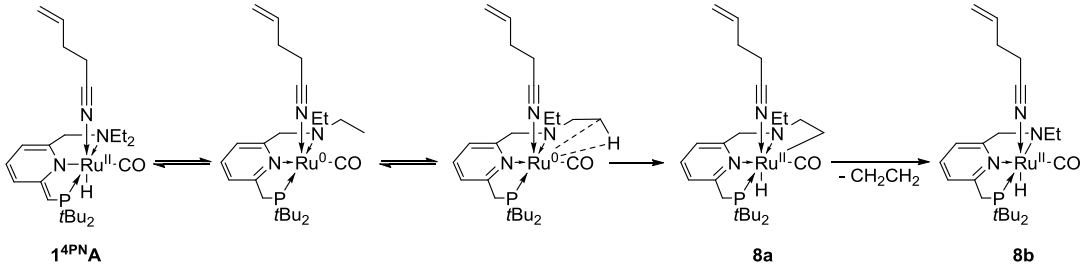

Figure 30: Suggested mechanism of ethylene release by 1^{4PN}.

are eliminated resulting in a double bond. However, the complexes resulting from ethylene generation could not be characterised, so the origin of the ethylene still needs to be explored.

In industry, ethylene can be generated by the cracking of hydrocarbons, from methanol or from ethanol.[45] Ethylene generated from bio-ethanol is used to make (partly) bio-based plastics, such polyethylene terephthalate used in bottles. Heterogeneous catalysts such as the zeolite material HZSM-5 are employed for this reaction. [46] The synthesis of ethylene from ethylamine has not been reported before.

3.4.4.1 Replacement of CO-ligand

If the generated ethylene indeed originates from the NEt_2-ligand, it would be nice to see if this also can be done catalytically, without decomposition of the complex. To perform a catalytic dehydroamination, an alkylamine source other than the ligand is needed. Therefore, replacement of the CO-ligand for a tertiary amine was attempted.

Trimethylamine *N*-oxide is known to oxidise CO-ligands on carbonyl complexes such as $Fe(CO)_3$ and $Ru_3(CO)_{12}$,[47] and the trimethylamine resulting from this reaction could then take this empty site on the ruthenium centre. Unfortunately, the reaction with trimethylamine *N*-oxide did not yield any observable changes in the ^{1}H-NMR spectrum. This led to the conclusion that no reaction took place, as a change in electron density on the ruthenium centre would definitely influence the chemical shift of the hydride. This lack of reactivity could also be due to the low solubility of trimethylamine *N*-oxide in benzene-d_6. The use of a different, more polar solvent such as thf-d_8 could increase solubility and thereby allow the reaction to happen.

Introduction of a trialkylamine ligand is not known in literature. The only reported example, the $Ru_2Cl_4(BINAP)_2(NEt_3)$ complex of Ikariya *et al.*[48] later turned out to be the diethylammonium salt $[Et_2NH_2][Ru_2Cl_5(BINAP)_2]$ instead.[49] It was observed that a related complex, [*n*-Bu_2NH][$Ru_2Cl_4(dppb)_2$], can be synthesised readily both from *n*-Bu_3N and *n*-Bu_2NH.[50] Presumably, the trialkylamine undergoes a dehydroamination reaction here, although the generation of an alkene was not reported.

Just as with complex **1**, this reaction only occurs once for every ruthenium complex. An anionic dimeric complex is generated, which is shown in Figure 31. The mechanism of this reaction is unknown, and thus it does not provide further insight into the dehydroamination reaction observed for complex $\mathbf{1^{4PN}}$.

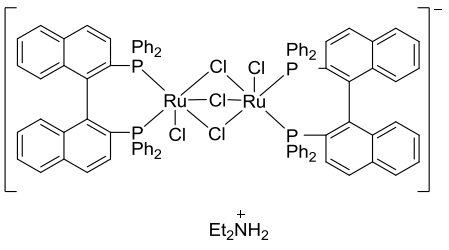

Figure 31: $[Et_2NH_2][Ru_2Cl_5(BINAP)_2]$ complex showing dealkylation (probably dehydroamination) during synthesis.[49]

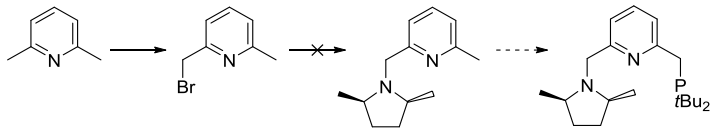

Figure 32: Attempted synthesis of a new chiral PNN ligand.

3.5 Asymmetric ligand synthesis

In order to carry out asymmetric oxa-Michael addition to unsaturated nitriles, the synthesis of a new PNN catalyst complex was attempted. This chiral ligand would favour oxa-Michael addition on one side only, and as such allow for enantioselective catalysis.

The ligand design and the attempted synthesis are shown in Figure 32. The purification of mono-brominated 2,6-lutidine succeeded by column chromatography followed by vacuum distillation. As some product was lost on the column, the yield could not be determined reliably. Unfortunately, the next step, replacement of the bromide by an amine was unsuccessful.

The attempted synthetic route is very similar to the described synthesis of the PNN ligand of complex **1**.[7] However, a different synthetic route could also be considered: introduction of a phosphine arm prior to an amine arm has been reported recently.[51,52] This suggested synthetic route is shown in Figure 33.

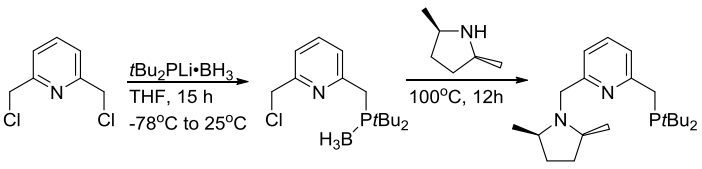

Figure 33: Suggested alternative synthetic route towards a new chiral PNN ligand.[51,52]

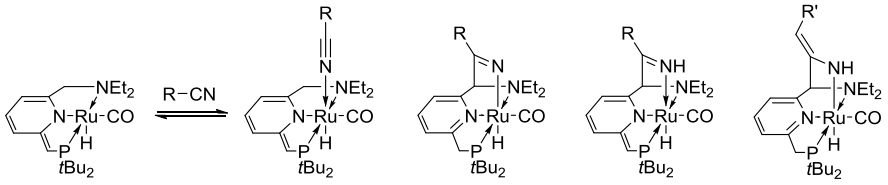

	1	1A	1B	1C	1D
4-pentenenitrile	43%		9%	48%	
Acetonitrile	51%			49%	
Benzonitrile	4%		20%	76%	
Benzyl cyanide					100%
Cinnamonitrile				100%	
2- or 3-pentenenitrile					100%

Table 6: Overview of the observed complexes reported in section 3.1 and earlier.[14] Percentages shown are observed ratios at room temperature and 1:1 stoichiometry of 1 and nitrile.

4 Conclusions

Different nitriles add to complex **1** to form a variety of different complexes. For some of the employed nitriles, such as 4-pentenenitrile and acetonitrile, multiple complexes are observed. The observed complexes and the ratios between the complexes in solution are shown in Table 6. The observation of different complexes in equilibrium (in the case of 4-pentenenitrile, acetonitrile and benzonitrile) implies that the energy difference between these complexes is small; there is no driving force towards the formation of a single complex. This observation is also supported by DFT calculations (see Table 4 on page 17), which also show the different complexes to be close in energy.

For 4-pentenenitrile, the observed equilibria were studied more thoroughly, and the calculated equilibrium constants at room temperature, as well as the calculated change in entropy and enthalpy are shown in Figure 34. In all cases, the first equilibrium (**1** ⇄ **1A**) is fast on the NMR timescale, implying that the energy barrier between the two complexes is rather low. This was however not calculated.

Nitrile coordinates to a free coordination site on the ruthenium centre. A negative entropy is expected, as two compounds come together to form one. Indeed, in the case of 4-pentenenitrile, the process is entropically disfavoured, however, the favourable enthalpic contribution is higher at room temperature (ΔG^{298K} = -7.4 kJ/mol). The second equilibrium, **1A** ⇄ **1B**, lies more towards **1A**, and complex **1B** is slightly higher in energy (ΔG^{298K} = 1.8 kJ/mol). The formation of **1C** from **1B** is favoured at any temperature. This is summarised in Figure 34.

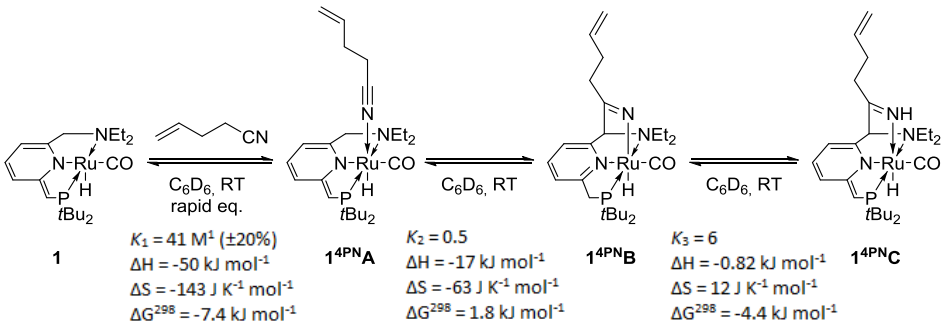

Figure 34: Reaction of 1 with 4-pentenenitrile. Calculated equilibrium constants at room temperature (K_1, K_2, and K_3) as well as the calculated ΔH, ΔS, and ΔG at 298K are shown for each equilibrium.

Complex **1^{4PN}B** is observed in minor quantities by ^{1}H-NMR, whereas **1^{AN}B** is not observed. This does not exclude **1^{AN}B** from being present in solution undetectably. DFT calculations suggest **1^{AN}C** is favoured over **1^{AN}B**, whereas it is the other way around for **1^{4PN}B**/**1^{4PN}C** and **1^{BN}B**/**1^{BN}C**. The calculations thus do not correspond to the experimental data. These calculations were performed in the gas phase. The effects that cause the calculations for **1^{4PN}** and **1^{BN}** to deviate from the experimental data will probably also affect complex **1^{AN}** in a similar way, suggesting that complex **1^{AN}C** is even more energetically favourable. This will cause the equilibrium **1^{AN}B** ⇄ **1^{AN}C** to shift more towards **1^{AN}C**, resulting in non-observable quantities of **1^{AN}B**. The formed equilibrium distribution is most probably at least partially influenced by the basicity of the formed ketimido-complex **1B**. This was tested using pentafluorobenzonitrile. Unfortunately, this reaction did not yield any characterisable results. Using different benzonitriles, both with electron-withdrawing and electron-donating groups, might give more insight into the formed complexes and equilibria.

The fact that the different complexes are close in energy could result in catalytic transformation of the substrate. The different stages in a catalytic cycle cannot differ too much in energy, as the reaction would get stuck in its most stable form and not proceed further. The oxa-Michael addition to 2- and 3-pentenenitrile uses the fact that the different complexes are close in energy. **1^{PN}D** is the only complex observed, but this has to isomerise to **1B** for the addition of an alcohol to occur. A **1D** analog is formed, which isomerises to a **1B** analog, liberates the product and regains complex **1**, which then can further react with a nitrile to repeat the cycle.

Cinnamonitrile and 4-pentenenitrile were not able to undergo such an oxa-Michael addition, as was to be expected. Addition to the double bond of cinnamonitrile breaks conjugation and this is therefore disfavoured. 4-pentenenitrile has to undergo an isomerisation to an internal alkene before oxa-Michael addition can occur. Although complex **1** is known to isomerise alkenes, isomerisation was not observed and oxa-Michael addition to 4-pentenenitrile did not take place.

The fact that all reactions are in equilibrium plays a crucial role in the addition of octanethiol. Oxa-Michael addition of octanethiol to crotonitrile was observed before.[18] In the case of acetonitrile or cinnamonitrile, the thiol does not react with the nitrile residue but instead reacts with free complex **1**, leading to the sole formation of complex **1^{SH}** in solution. Other addition reactions led to similar results, did not show a reaction at all or led to decomposition of the complexes. The reaction of *o*-toluenesulfonamide with **1^{CN}C** led to protonation of the complex and formation of the insoluble salt **5** (see Figure 35). Thus, the

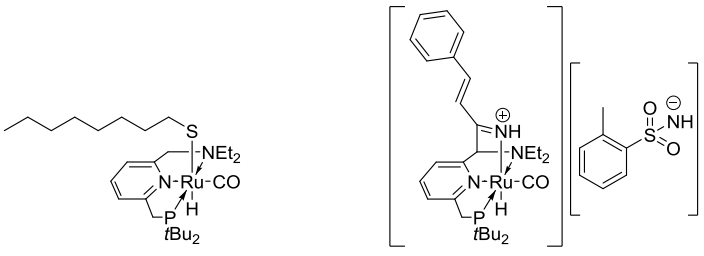

1^{SH} **5**

Figure 35: Complex 1^{SH} (left) is formed when complex 1^{AN} reacts with octanethiol, and complex 5 (right) when 1^{CN} reacts with *o*-toluenesulfonamide.

reactivity of the activated nitrile (complex) remains to be explored.

During the variable temperature NMR experiments on **1**^{4PN}, the generation of ethylene was observed at higher temperatures (>70°C). Ethylene can be synthesised from ethanol using a heterogeneous catalyst, but a synthesis from ethylamine has not been reported. Unfortunately, the resulting complex could not be characterised, and replacement of the CO ligand for triethylamine was unsuccessful.

All in all, the mode of nitrile activation by **1** has been further elucidated. Most nitriles form multiple complexes in solution, all of which are in equilibrium with one another. These equilibria show that the energy differences between the complexes are low. This was also confirmed by DFT calculations.

The reactivity of the activated nitriles remains unknown, as the attempts here to nucleophilic addition, cycloaddition or hydrogenation did not give the expected products.

The generation of ethylene from **1**^{4PN} at higher temperatures needs further exploration. Ruthenium-trialkylamine complexes have not been reported before, but the synthesis of such a compound should definitely be attempted. One strategy would be the synthesis of the complex from ligand, triethylamine and a CO-free ruthenium(II)-precursor.

5 Experimental

General considerations

*All reactions with metal-complexes were carried out under nitrogen atmosphere using standard glovebox, Schlenk, and vacuum-line techniques. Toluene, hexane and pentane (Aldrich, anhydrous, 99.8%) were passed over columns of Al_2O_3 (Fluka), BASF R3-11-supported Cu oxygen scavenger, and molecular sieves (Aldrich, 4 Å). THF (Aldrich, anhydrous, 99.8%) was dried by percolation over columns of Al_2O_3 (Fluka). Isopropanol , acetonitrile and dichloromethane were dried on CaH_2 and distilled prior to use. All solvents and reagents were degassed prior to use and stored under nitrogen. Compound **1** was obtained from Strem Chemicals or synthesised in situ from its chloride precursor (Strem Chemicals) following an adapted literature procedure.*[7] *NMR spectra were recorded on Varian Gemini 200, Varian 300, Varian 400, Agilent 400 or Varian Inova 500 spectrometers. The ^{1}H and ^{13}C NMR spectra were referenced internally using residual solvent resonances and reported in ppm relative to TMS (δ 0 ppm); J is reported in Hz. Gas chromatography measurements were performed on HP6890 series equipped with Rxi-5Sil column for GC/MS and HP5890 series II equipped with Rtx-1701 column for GC-MS/FID.*

Synthesis of $1^{CN}C$

In a J. Young NMR tube, a 1/1 mixture of **1** and cinnamonitrile was dissolved in benzene-d_6. After shaking for 15 min at RT, the reaction mixture was analysed by NMR spectroscopy.[26]

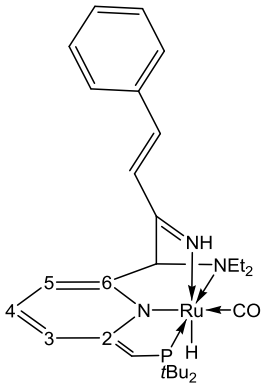

$1^{CN}C$

^{1}H NMR (500 MHz, C_6D_6): δ = 9.68 (s, 1H, C=N**H**), 7.12 – 7.01 (m, 5H, Ph), 6.81 (d, *J*=16.2, 1H, PhC**H**=CH), 6.54 (ddd, *J*=8.3, 6.3, 1.8, 1H, Py-H4), 6.38 (d, *J*=8.9, 1H, Py-H5), 5.93 (d, *J*=16.2, 1H, PhCH=C**H**), 5.71 (dd, *J*=6.4, 1.1, 1H, Py-H3), 4.54 (s, 1H, C**H**N$(CH_2CH_3)_2$), 3.77 (d, *J*=2.8, 1H, C**H**P$^{t}Bu_2$), 2.92 (dq, *J*=14.4, 7.2, 1H, N(**CH$_2$**$CH_3)_2$), 2.63 (m, 2H, N(**CH$_2$**$CH_3)_2$), 2.31 (dq, *J*=13.3, 7.1, 1H, N(**CH$_2$**$CH_3)_2$), 1.65 (d, *J*=13.0, 9H, P^{t}**Bu$_2$**), 1.37 (d, *J*=12.5, 9H, P^{t}**Bu$_2$**), 0.83 (t, *J*=7.0, 3H, N$(CH_2$**CH$_3$**$)_2$), 0.75 (t, *J*=7.1, 3H, N$(CH_2$**CH$_3$**$)_2$), -12.95 (d, *J*=32.2, 1H, Ru-H).

^{13}C NMR (126 MHz, C_6D_6): δ = 176.16 ((CH=CH)(CH)**C**=NH), 168.88 (d, *J* = 15.6, Py-C2), 151.43 (Py-C6), 139.47 (Ph**C**H=CH), 137.46 (Ph quaternary), 133.17 (Py-C4), 132.50 (Ph), 131.37 (Ph), 130.64 (Ph), 126.76 (PhCH=**C**H), 114.86 (d, *J* = 16.4, Py-C3), 101.24 (Py-C5), 75.46 (**C**HN$(CH_2CH_3)_2$), 69.07 (d, *J* = 54.3, **C**HP$^{t}Bu_2$), 51.12 (s, N(**C**H$_2$$CH_3)_2$), 48.55 (s, N(**C**H$_2$$CH_3)_2$), 40.49 (d, *J* = 15.8, P**C**$(CH_3)_3$), 38.71 (d, *J* = 33.9, P**C**$(CH_3)_3$), 33.37 (d, *J* = 3.3, PC(**C**H$_3$**)$_3$**), 32.75 (d, *J* = 5.3, PC(**C**H$_3$**)$_3$**), 12.86 and 12.17 (N$(CH_2$**C**H$_3)_2$).

^{31}P NMR (162 MHz, C_6D_6): δ = 105.68.

Synthesis of 1^{4PN}

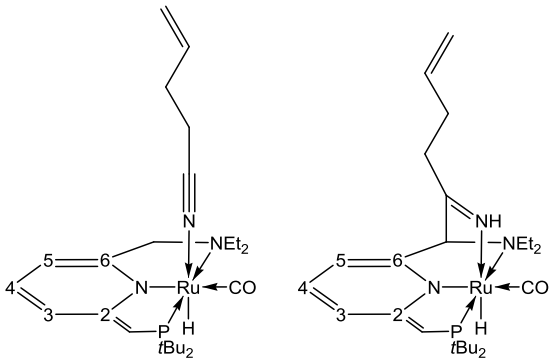

$1^{4PN}A$ $1^{4PN}B$

In a J. Young NMR tube, a 1/1 mixture of 1 and 4-pentenenitrile was dissolved in benzene-d6. After shaking for 15 min at RT, the reaction mixture was analysed by NMR spectroscopy.

$1^{4PN}A$:

^{1}H-NMR (400 MHz, C_6D_6): δ = 6.56-6.50 (m, Py-H4), 6.42 (d, *J* = 8.8, Py-H3), 5.36 (d, *J* = 6.5, Py-H5), 3.64 (d, *J* = 1.6, C**H**P), 3.29 (d, *J* = 13.8, C**H**HN), 3.04 (d, *J* = 13.8, CH**H**N), 2.67 – 2.51 (m, 3H, N(C**H**$_2$CH$_3$)$_2$), 2.35 (dq, 1H, N(CH$_2$CH$_3$)$_2$, *J* = 13.4, 7.2), 1.42 (dd, *J* = 13.9, 12.9, P^t**Bu$_2$**), 0.95 (t, *J* = 7.1, N**Et$_2$**), 0.75 (t, *J* = 7.2, N**Et$_2$**), -20.94 (d, *J* = 26.2, Ru-H).

^{13}C{^{1}H}-NMR (101 MHz, C_6D_6): δ = 207.49 (C≡O), 168.69 (d, *J* = 15.6, Py-C2), 156.46 (d, *J* = 2.5, Py-C6), 131.89 (d, *J* = 1.5, Py-C4), 119.36 (s, C≡N), 113.76 (d, *J* = 17.2, Py-C3), 96.59 (s, Py-C5), 65.02 (s, **C**H$_2$NEt$_2$), 64.94 (d, *J* = 54.2, **C**HP^{t}Bu$_2$), 54.70 (s, N(**C**H$_2$CH$_3$)$_2$), 50.97 (s, N(**C**H$_2$CH$_3$)$_2$), 37.97 (d, *J* = 22.2, P[**C**(CH$_3$)$_3$]$_2$), 35.70 (d, *J* = 29.7, P[**C**(CH$_3$)$_3$]$_2$), 30.05 (dd, *J* = 2.8, 4.2, P[C(**C**H$_3$)$_3$]$_2$), 11.28 (s, N(CH$_2$**C**H$_3$)$_2$), 9.99 (s, N(CH$_2$**C**H$_3$)$_2$).

^{31}P-{^{1}H}-NMR (162 MHz, C_6D_6): δ = 96.05 (d, *J* = 22.9).

$1^{4PN}C$:

^{1}H-NMR (400 MHz, C_6D_6): δ = 9.66 (s, C=N**H**), 6.56-6.50 (m, Py-H4), 6.35 (d, *J* = 8.8, Py-H3), 5.52 (d, *J* = 6.3, Py-H5), 3.73 (overlap of d, *J* = 1.6, C**H**P and C**H**N), 2.83 (dq, 1H, N(C**H**$_2$CH$_3$)$_2$, *J* = 14.4, 7.1), 2.67 – 2.51 (m, 1H, N(C**H**$_2$CH$_3$)$_2$), 2.48 (dq, 1H, N(CH$_2$CH$_3$)$_2$, *J* = 13.3, 7.1), 2.10 (dqd, 1H, N(CH$_2$CH$_3$)$_3$, *J* = 13.9, 6.8, 1.9), 1.61 (d, *J* = 13.0, P^t**Bu$_2$**), 1.33 (d, *J* = 12.3, P^t**Bu$_2$**), 0.80 (t, N(CH$_2$C**H$_3$**)$_2$, *J* = 7.1), 0.68 (t, N(CH$_2$C**H$_3$**)$_2$, *J* = 7.1), -13.88 (d, *J* = 21.6, Ru-H).

^{13}C{^{1}H}-NMR (101 MHz, C_6D_6): δ = 209.47 (d, *J* = 13.8, C≡O), 181.41 (s, **C**=NH), 166.54 (d, *J* = 15.4, Py-C2), 148.99 (d, *J* = 2.0, Py-C6), 130.57 (d, *J* = 1.4, Py-C4), 112.80 (d, *J* = 16.4, Py-C3), 98.75 (s, Py-C5), 77.24 (s, **C**HNEt$_2$), 66.85 (d, *J* = 54.3, **C**HP^{t}Bu$_2$), 48.58 (s, N(**C**H$_2$CH$_3$)$_2$), 46.22 (s, N(**C**H$_2$CH$_3$)$_2$), 38.17 (d, *J* = 15.9, P[**C**(CH$_3$)$_3$]$_2$), 36.34 (d, *J* = 34.0, P[**C**(CH$_3$)$_3$]$_2$), 31.01 (d, *J* = 3.2, P[C(**C**H$_3$)$_3$]$_2$), 30.43 (d, *J* = 5.5, P[C(**C**H$_3$)$_3$]$_2$), 10.55 (s, N(CH$_2$**C**H$_3$)$_2$), 9.59 (s, N(CH$_2$**C**H$_3$)$_2$).

^{31}P-{^{1}H}-NMR (162 MHz, C_6D_6): δ = 105.95 (s).

$1^{4PN}B$ (diagnostic signals):

^{1}H-NMR (400 MHz, C_6D_6): δ = -11.87 (d, *J* = 28.7, Ru-H).

^{31}P-NMR (162 MHz, C_6D_6): δ = 121.0 ppm (bs).

Synthesis of 1^{AN}

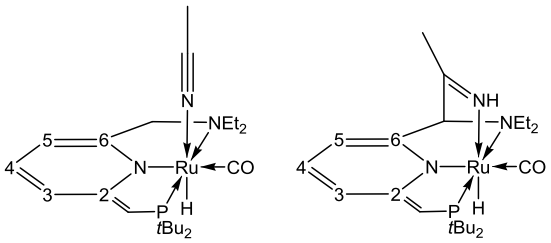

$1^{AN}A$ $1^{AN}B$

In a J. Young NMR tube, a 1/1 mixture of **1** and acetonitrile was dissolved in benzene-d$_6$. After shaking for 90 min at RT, the reaction mixture was analysed by NMR spectroscopy.

$1^{AN}A$:

^{1}H-NMR (400 MHz, C_6D_6): δ = 6.51 (td, 1H, Py-H4, *J* = 6.7, 1.8), 6.41 (d, 1H, Py-H3, *J* = 8.9), 5.29 (d, 1H, Py-H5, *J* = 6.3), 3.59 (d, 1H, CHP, *J* = 1.9), 3.34 (d, 1H, CHHN, *J* = 14.0), 2.78 (d, 1H, CHHN, *J* = 14.0), 2.67 – 2.39 (m, 3H, N(CH$_2$CH$_3$)$_2$), 2.20 (dqd, 1H, N(CHHCH$_3$)$_2$, *J* = 13.1, 7.3, 1.5), 1.38 (d, 9H, P(C(CH$_3$)$_3$)$_2$, *J* = 13.4), 1.37 (d, 9H, P(C(CH$_3$)$_3$)$_2$, *J* = 12.6), 0.89 (t, 3H, N(CH$_2$CH$_3$)$_2$, *J* = 7.1), 0.72 (t, 3H, N(CH$_2$CH$_3$)$_2$, *J* = 7.3), 0.60 (s, 3H, HN=CCH$_3$), -24.04 (bs, Ru-H).

^{13}C{^{1}H}-NMR (101 MHz, C_6D_6): δ = 0.27 (s, N≡C**C**H$_3$), 10.54 ((s, N(CH$_2$**C**H$_3$)$_2$), 11.33 (s, N(CH$_2$**C**H$_3$)$_2$), 29.60 (d, P(C(**C**H$_3$)$_3$)$_2$, *J* = 4.3), 29.63 (d, P(C(**C**H$_3$)$_3$)$_2$, *J* = 3.8), 35.51 (d,

P(**C**$(CH_3)_3)_2$, *J* = 28.3), 38.02 (d, P(**C**$(CH_3)_3)_2$, *J* = 24.2), 50.84 (s, N(**C**$H_2CH_3)_2$), 55.07 (s, N(**C**$H_2CH_3)_2$), 64.78 (d, Py**C**H_2NEt_2, *J* = 1.5), 65.14 (d, Py**C**HP^tBu_2, *J* = 54.2), 96.58 (s, Py-C5), 114.06 (d, Py-C3, *J* = 17.3), 116.70 (N≡**C**CH_3), 132.03 (d, Py-C4, *J* = 1.8), 156.71 (d, Py-C6, *J* = 2.6), 168.95 (d, Py-C2, 15.9), 207.12 (d, CO, *J* = 12.6).

^{31}P-{^{1}H}-NMR (162 MHz, C_6D_6): δ = 94.94 (s).

1^{AN}C:

^{1}H-NMR (400 MHz, C_6D_6): δ = 9.24 (s, 1H, C=NH), 6.53 (td, 1H, Py-H4, *J* = 6.7, 1.8), 6.39 (d, 1H, Py-H3, *J* = 8.9), 5.49 (d, 1H, Py-H5, *J* = 6.3), 3.73 (d, 1H, C**H**P, *J* = 2.7), 3.61 (s, 1H, C**H**N), 2.83 (dq, 1H, N(C**H**HC$H_3)_2$, *J* = 14.0, 7.2), 2.67 – 2.39 (m, 2H, NC**H**$_2$C$H_3)_2$), 2.06 (dqd, 1H, N(CH**H**C$H_3)_2$, *J* = 13.2, 7.0, 2.0), 1.61 (d, 9H, P(C(C**H**$_3)_3)_2$, *J* = 13.1), 1.32 (d, 9H, P(C(C**H**$_3)_3)_2$, *J* = 12.5), 1.18 (d, 3H, HN=CC**H**$_3$, *J* = 1.3), 0.75 (t, 3H, N(CH_2C**H**$_3)_2$, *J* = 7.2), 0.66 (t, 3H, N(CH_2C**H**$_3)_2$, *J* = 7.1), -13.95 (d, 1H, Ru-H, *J* = 32.4).

^{13}C{^{1}H}-NMR (101 MHz, C_6D_6): δ = 9.61 (s, N(CH_2**C**$H_3)_2$), 10.36 (s, N(CH_2**C**$H_3)_2$), 25.48 (s, N=C**C**H_3), 30.39 (d, P(C(**C**$H_3)_3)_2$, *J* = 5.5), 30.99 (d, P(C(**C**$H_3)_3)_2$, *J* = 3.3), 36.37 (d, P(**C**$(CH_3)_3)_2$, *J* = 33.9), 38.07 (d, P(**C**$(CH_3)_3)_2$, *J* = 15.7), 46.06 (s, N(**C**$H_2CH_3)_2$), 48.52 (s, N(**C**$H_2CH_3)_2$), 66.79 (d, Py**C**HP^tBu_2, *J* = 54.2), 77.10 (s, Py**C**HNEt_2), 98.59 (s, Py-C5), 112.88 (d, Py-C3, *J* = 16.5), 130.59 (d, Py-C4, *J* = 1.7), 148.82 (d, Py-C6, *J* = 2.0), 166.59 (d, Py-C2, *J* = 15.5), 179.06 (s, HN=**C**CH_3), 209.42 (d, CO, *J* = 13.8).

^{31}P-{^{1}H}-NMR (162 MHz, C_6D_6): δ = 106.00 (s).

Synthesis of 1^{BC}

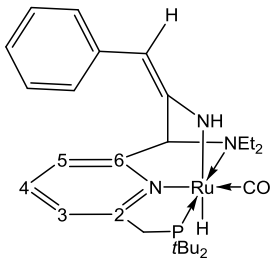

In a J. Young NMR tube, a 1/1 mixture of **1** and benzyl cyanide was dissolved in benzene-d_6. After shaking for 15 min at RT, the reaction mixture was analysed by NMR spectroscopy. A layer of hexane was added to the benzene-d_6 solution and red crystals were obtained.

^{1}H-NMR (400 MHz, C_6D_6): δ = 7.66 (d, 2H, $H_{Ar, ortho}$, *J* = 7.8), 7.35 (t, 2H, $H_{Ar, meta}$, *J* = 7.7), 6.95-6.79 (m, 3H, unresolved overlap $H_{Ar, para}$, Py-H4 and Py-H5), 6.42 (d, 1H, Py-H3, *J* = 7.5), 5.35 (s, 1H, Ph-C**H**=CNH), 5.10 (br s, 1H, Ph-CH=CN**H**), 4.13 (s, 1H, NC**H**-Py), 3.36 (q, 2H, N(C**H**$_2$C$H_3)_2$), *J* = 7.2), 2.87 (dd, 1H, PC**H**H-Py, *J* = 16.4, 7.7), 2.79 (dd, 1H, PCH**H**-Py, *J* = 16.4, 9.9), 2.40 (dq, 1H, N(C**H**HC$H_3)_2$), *J* = 13.2, 7.1), 2.19 (dqd, 1H, N(CH**H**C$H_3)_2$), *J* = 13.3, 6.8, 3.1), 1.25 (d, 9H, P^t**Bu$_2$**, *J* = 13.1), 0.94 (d, 9H, P^t**Bu$_2$**, *J* = 12.7), 0.94 (t, 3H, N(CH_2C**H**$_3)_2$), *J* = 7.2), 0.89 (t, 3H, N(CH_2C**H**$_3)_2$), *J* = 7.1), -11.98 (d, 1H, Ru-**H**, *J* = 28.7).

^{13}C-NMR (101 MHz, C_6D_6): δ = 209.43 (d, C≡O, *J* = 16.4), 160.91 (s, Py-C6), 159.71 (d, Py-C2, *J* = 3.9), 152.91 (s, PhCH=**C**NH), 144.53 (s, $C_{Ar, ipso}$), 136.51 (s, Py-C4), 128.80 (s, $C_{Ar, meta}$), 123.84 (s, $C_{Ar, ortho}$), 119.70 (s, $C_{Ar, para}$), 119.09 (s, Py-C5), 118.31 (d, Py-C3, *J* = 8.6), 89.42 (s, Ph**C**H=CNH), 82.29 (s, N**C**H-Py), 49.32 (s, N(**C**$H_2CH_3)_2$), 46.83 (s, N(**C**$H_2CH_3)_2$), 37.28 (d, Py-**C**H_2P, *J* = 10.6), 37.16 (d, P(**C**$(CH_3)_3)_2$, *J* = 20.6), 34.56 (d, P(**C**$(CH_3)_3)_2$, *J* = 23.3), 30.59 (d, P(C(**C**$H_3)_3)_2$, *J* = 3.3), 29.16 (d, P(C(**C**$H_3)_3)_2$, *J* = 4.9, 11.34 (s, N(CH_2**C**$H_3)_2$), 9.34 (s, N(CH_2**C**$H_3)_2$).

^{31}P-NMR (126 MHz, C_6D_6): δ = 120.73 (s).

Synthesis of 1^{BN}

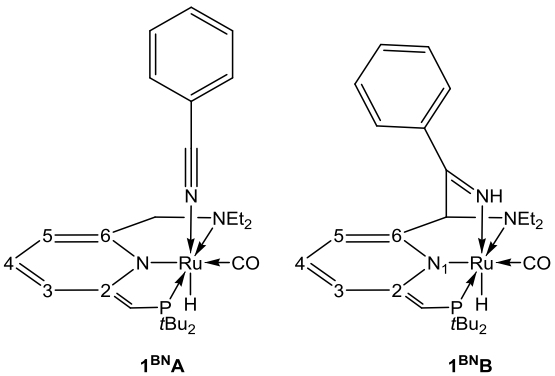

1^{BN}A **1^{BN}B**

In a J. Young NMR tube, a 1/1 mixture of **1** and benzonitrile was dissolved in benzene-d_6. The reaction mixture was analysed by ^{1}H-NMR after 5 min, 1 h, 1.75 h, 2.5 h and overnight, and by ^{13}C{^{1}H}-NMR, ^{31}P{^{1}H}-NMR, COSY, HSQC and HMBC overnight. **1^{BN}C** was observed as the major product. Species **1^{BN}A** had disappeared almost completely after 1 hour, and was therefore only characterised by ^{1}H-NMR. The existence of a third species.

Although this complex could not be fully characterised, it was suspected to be **1**^{BN}**B**.

1^{BN}**A:**
^{1}H-NMR (400 MHz, C_6D_6): δ = 6.93 (d, 2H, *J* = 7.6, $H_{Ar,\ ortho}$), 6.80 (d, 1H, *J* = 7.6, $H_{Ar,\ para}$), 6.63 (t, 2H, *J* = 7.6, $H_{Ar,meta}$), 6.55 (t, 1H, *J* = 7.6, Py-H4), 6.45 (d, 1H, *J* = 8.8, Py-H3), 5.36 (d, 1H, *J* = 6.3, Py-H5), 3.65 (bs, 1H, PyCHP^{t}Bu$_2$), 3.30 (d, 1H, *J* = 13.9, PyCHHNEt$_2$), 3.02 (d, 1H, *J* = 13.9, PyCHHNEt$_2$), 2.70 – 2.58 (m, 3H, N(CH$_2$CH$_3$)$_2$), 2.38 (dq, 1H, *J* = 13.8, 6.9, N(CH$_2$CH$_3$)$_2$), 1.43 (vt, 18H, *J* = 12.1, P(C(CH)$_3$)$_2$), 0.93 (t, 3H, *J* = 7.0, N(CH$_2$CH$_3$)$_2$), 0.73 (t, 3H, *J* = 7.2, N(CH$_2$CH$_3$)$_2$), -21.22 (s, 1H, Ru-H).
^{31}P-{^{1}H}-NMR (162 MHz, C_6D_6): δ = 95.35 (bs).

1^{BN}**C:**
^{1}H-NMR (400 MHz, C_6D_6): δ = 10.20 (s, 1H, C=NH), 7.01 – 6.88 (m, Ph and undefined signals), 6.48 (ddd, 1H, *J* = 8.9, 6.3, 1.8, Py-H4), 6.36 (d, 1H, *J* = 8.9, Py-H3), 5.61 (dd, 1H, *J* = 6.3, 0.9, Py-H5), 4.62 (s, 1H, PyCHNEt$_2$), 3.78 (d, 1H, *J* = 2.9, PyCHP^{t}Bu$_2$), 2.94 (dq, 1H, *J* = 14.0, 7.1, N(CH$_2$CH$_3$)$_2$), 2.70 (dqd, 1H, *J* = 20.9, 7.0, 1.6, N(CH$_2$CH$_3$)$_2$), 2.66 (dq, 1H, *J* = 13.6, 7.2, N(CH$_2$CH$_3$)$_2$), 2.30 (dqd, 1H, *J* = 13.2, 7.0, 2.0, N(CH$_2$CH$_3$)$_2$), 1.65 (d, 9H, *J* = 12.9, P(C(CH)$_3$)$_2$), 1.32 (d, 9H, *J* = 12.5, P(C(CH)$_3$)$_2$), 0.77 (t, 3H, *J* = 7.1, N(CH$_2$CH$_3$)$_2$), 0.75 (t, 3H, *J* = 7.1, N(CH$_2$CH$_3$)$_2$), -13.23 (d, 1H, *J* = 32.2, Ru-H).
^{13}C{^{1}H}-NMR (101 MHz, C_6D_6): δ = 209.42 (d, *J* = 13.6, C≡O), 176.46 (s, C=NH), 166.65 (d, *J* = 15.4, Py-C2), 148.69 (s, PyC6), 130.80 (d, *J* = 1.5, Py-C4), 112.86 (d, *J* = 16.4, Py-C3), 99.53 (s, Py-C5), 75.59 (s, CHNEt$_2$), 67.16 (d, *J* = 54.3, CHP^{t}Bu$_2$), 48.80 (s, N(CH$_2$CH$_3$)$_2$), 46.39 (s, N(CH$_2$CH$_3$)$_2$), 38.33 (d, *J* = 15.9, P(C(CH$_3$)$_3$)$_2$), 36.39 (d, *J* = 33.7, P(C(CH$_3$)$_3$)$_2$), 31.04 (d, *J* = 3.0, P(C(CH$_3$)$_3$)$_2$), 30.29 (d, *J* = 5.3, P(C(CH$_3$)$_3$)$_2$), 10.56 (s, N(CH$_2$CH$_3$)$_2$), 9.92 (s, N(CH$_2$CH$_3$)$_2$).
^{31}P-{^{1}H}-NMR (162 MHz, C_6D_6): δ = 105.97 (s).

1^{BN}**B** (diagnostic signals):
^{1}H-NMR (400 MHz, C_6D_6): δ = -10.02 (d, J = 25.3, Ru-H).
^{31}P-NMR (162 MHz, C_6D_6): δ = 120.87 ppm (d, J = 7.8).

Addition of octanethiol

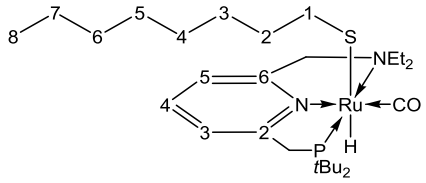

In a J. Young NMR tube, a 1/1 mixture of **1** and acetonitrile was dissolved in benzene-d_6. It was shaken for 1.5 hours, after which 1.4 eq. of octanethiol were added. The resulting complex was characterised by NMR.

^{1}H-NMR (400 MHz, C_6D_6): δ = 6.75 (1H, t, *J* = 7.7, Py-H4), 6.46 (1H, d, *J* = 7.8, Py-H3), 6.29 (1H, d, *J* = 7.7, Py-H5), 5.86 (1H, d, *J* = 14.2, PyC**H**HN), 3.79 (1H, dq, *J* = 12.9, 7.1, N(C**H**$_2$CH$_3$)$_2$), 3.67 (1H, dq, *J* = 13.0, 7.1, N(C**H**$_2$-CH$_3$)$_2$), 3.31 (1H, dt, *J* = 11.9, 7.3, SC**H**$_2$-(CH$_2$)$_6$CH$_3$), 3.23 (1H, dt, *J* = 11.9, 7.3, SC**H**$_2$-(CH$_2$)$_6$CH$_3$), 3.05 (1H, dd, *J* = 14.3, 2.3, Py-CH**H**N), 2.99 (1H, dd, *J* = 16.6, 9.3, PyC**H**HP), 2.74 (1H, dd, *J* = 16.6, 8.8, PyCH**H**P), 2.62 (1H, dq, *J* = 12.8, 6.7, N(C**H**$_2$CH$_3$)$_2$), 2.42 (1H, m, N(C**H**$_2$CH$_3$)$_2$), 2.19 (2H, q, *J* = 7.5, SCH$_2$C**H**$_2$-(CH$_2$)$_5$CH$_3$), 1.84 (2H, p, *J* = 7.5, S(CH$_2$)$_2$C**H**$_2$-(CH$_2$)$_4$CH$_3$), 1.50 (2H, m, S(CH$_2$)$_3$C**H**$_2$(CH$_2$)$_3$CH$_3$), 1.47 (9H, d, *J* = 13.2, P(C(C**H**$_3$)$_3$)$_2$), 1.38 (2H, m, S(CH$_2$)$_4$C**H**$_2$(CH$_2$)$_2$CH$_3$), 1.28 (13H, overlap of 2H S(CH$_2$)$_5$C**H**$_2$CH$_2$CH$_3$, 2H S(CH$_2$)$_6$C**H**$_2$CH$_3$, 9H, d, *J* = 12.7, P(C(C**H**$_3$)$_3$)$_2$), 1.01 (3H, t, *J* = 6.7, N(CH$_2$C**H**$_3$)$_2$), 0.97 (3H, t, *J* = 6.9, N(CH$_2$C**H**$_3$)$_2$), 0.87 (3H, t, *J* = 6.7, S(CH$_2$)$_7$C**H**$_3$), -10.67 (1H, d, *J* = 26.2, Ru-H).
^{13}C{^{1}H}-NMR (101 MHz, C_6D_6): δ = 210.58 (d, *J* = 16.4, CO), 161.40 (d, *J* = 4.1, Py-C2), 160.66 (d, *J* = 1.6, Py-C6), 135.32 (s, Py-C4), 119.27 (d, *J* = 9.3, Py-C3), 118.64 (s, Py-C5), 64.10 (s, Py**C**H$_2$N), 54.98 (s, N(**C**H$_2$CH$_3$)$_2$), 48.76 (s, N(**C**H$_2$CH$_3$)$_2$), 38.58 (d, *J* = 11.6, P(**C**(CH$_3$)$_3$)$_2$), 38.18 (d, *J* = 19.6, Py**C**H$_2$P), 37.91 (s, SCH$_2$**C**H$_2$(CH$_2$)$_5$CH$_3$), 35.71 (d, *J* = 24.5, P(**C**(CH$_3$)$_3$)$_2$), 33.37 (s, S**C**H$_2$(CH$_2$)$_6$CH$_3$), 32.47 (s, S(CH$_2$)$_6$**C**H$_2$CH$_3$), 30.81 (d, *J* = 3.1, P(C(**C**H$_3$)$_3$)$_2$), 30.39 (s, S(CH$_2$)$_2$**C**H$_2$(CH$_2$)$_4$CH$_3$), 30.34 (s, S(CH$_2$)$_3$**C**H$_2$(CH$_2$)$_3$CH$_3$), 30.11 (s, S(CH$_2$)$_4$**C**H$_2$-(CH$_2$)$_2$CH$_3$), 29.76 (d, *J* = 4.1, P(C(**C**H$_3$)$_3$)$_2$), 23.19 (s, S(CH$_2$)$_6$**C**H$_2$CH$_3$), 14.43 (s, S(CH$_2$)$_7$**C**H$_3$), 10.60 (s, N(CH$_2$**C**H$_3$)$_2$), 9.33 (s, N(CH$_2$**C**H$_3$)$_2$).
^{31}P-{^{1}H}-NMR (162 MHz, C_6D_6): δ = 109.49 (s).

Addition of *o*-toluenesulfonamide (Synthesis of 5)

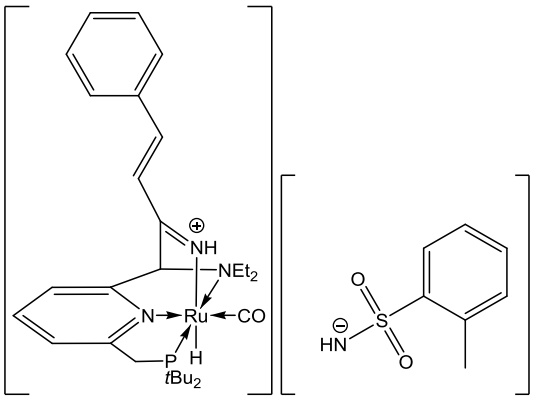

To a Schlenk flask were added 30.0 mg (0.066 mmol) of **1**, 16.70 µL (0.13 mmol) cinnamonitrile and 1.5 mL thf. The mixture was stirred and 11.4 mg (0.066 mmol) *o*-toluenesulfonamide was added. The mixture was stirred and a yellow powder precipitated in 64% yield. The resulting complex was characterised by NMR (CD_3CN and CD_2Cl_2) and recrystallised from CD_2Cl_2 and hexane.

^{1}H-NMR (400 MHz, CD_3CN): δ = 11.42 (bs, 1H, N**H**), 7.92 (d, 1H, *J* = 7.5, *o*-toluene), 7.87 (t, 1H, *J* = 7.7, Py-H4), 7.78 (d, 1H, *J* = 7.7, Py-H), 7.72 (d, 1H, *J* = 16.6, C**H**=CH), 7.70 – 7.67 (m, 2H, Ph), 7.49 (d, 1H, *J* = 7.8, Py-H), 7.48-7.44 (m, 3H, Ph), 7.19 (d, 1H, *J* = 16.5 Hz, CH=C**H**), 7.18-7.09 (m, 3H, *o*-toluene), 5.89 (d, 1H, *J* = 1.6, PyC**H**N), 3.66 (dd, 1H, *J* = 16.9, 10.6, PyC**H**HP), 3.43 (dd, 1H, *J* = 17.0, 7.9, PyCH**H**P), 3.09 – 2.80 (m, 2H, N(C**H$_2$**CH_3)$_2$), 2.69 (q, 2H, *J* = 6.9, N(C**H$_2$**CH_3)$_2$), 2.63 (s, 3H, toluene-C**H$_3$**), 1.39 (d, 9H, *J* = 13.7, P(C(C**H$_3$**)$_3$)$_2$), 1.15 (t, 3H, *J* = 7.1, N(CH_2C**H$_3$**)$_2$), 1.12 (t, 3H, *J* = 7.2, N(CH_2C**H$_3$**)$_2$), 1.00 (d, 9H, *J* = 13.2, P(C(C**H$_3$**)$_3$)$_2$), -12.29 (d, 1H, *J* = 29.4, Ru-H).
^{31}P-{^{1}H}-NMR (121 MHz, CD_3CN): δ = 117.80 (d, *J* = 14.8).

Addition of H_2

To a J. Young NMR tube 5.0 mg (0.010 mmol) of catalyst precursor **1a**, 2.4 mg (0.021 mmol) of potassium *tert*-butoxide and 0.54 µL (0.010 mmol) acetonitrile were dissolved in benzene-d_6. The NMR tube was charged with hydrogen gas at -196°C, which results in a H_2 pressure of approximately 4 bar at room temperature. The formed dihydride complex $\mathbf{1_{H2}}$ was characterised by ^{1}H and ^{31}P-NMR.

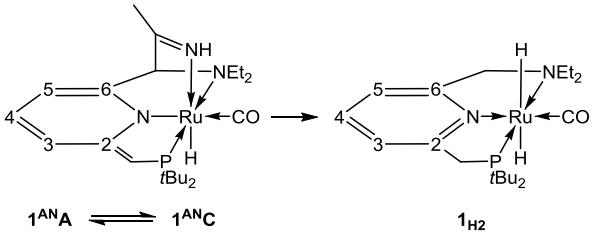

$\mathbf{1^{ANA}}$ ⇌ $\mathbf{1^{ANC}}$ $\mathbf{1_{H2}}$

^{1}H-NMR (400 MHz, C_6D_6): δ = 6.78 (t, 1H, *J* = 7.6, Py-H4), 6.49 (d, 1H, *J* = 7.8, Py-H) , 6.32 (d, 1H, *J* = 7.4, Py-H), 3.74 (s, 2H, PyC**H$_2$**N), 3.02 (d, 2H, *J* = 8.5, PyC**H$_2$**P), 2.95 (m, 2H, N(C**H$_2$**-CH_3)$_2$), 1.39 (d, 18H, *J* = 12.7, P(C(C**H$_3$**)$_3$)$_2$), 1.00 (t, 6H, *J* = 7.7, N(CH_2C**H$_3$**)$_2$), -4.19 (d, 2H, *J* = 17.0, Ru-H).
^{31}P-{^{1}H}-NMR (162 MHz, C_6D_6): δ = 123.99 (s).

Addition of H_2 to benzyl cyanide adduct $\mathbf{1^{BC}}$ results in mostly $\mathbf{1^{BC}}$ itself and little of the dihydride complex $\mathbf{1_{H2}}$, as was observed by ^{1}H-NMR.

Variable concentration NMR experiments with 1^{4PN}

To a J. Young NMR tube were added 9.0 mg (0.020 mmol) of **1** and 0.42 mL of toluene-d_8. A ^{1}H-NMR spectrum was recorded at 25°C. Subsequently, 4-pentenenitrile was added (1 µL, 0.010 mmol, 0.5 eq), and an NMR spectrum was again recorded. The amount of 4-pentenenitrile was now increased stepwise, and ^{1}H-NMR spectra were recorded at 1, 2, 4, 8, 16, 32, 64, and 114 equivalents of 4-pentenenitrile.

VT-NMR experiments with 1^{4PN}

To a J. Young NMR tube were added 9.0 mg (0.020 mmol) of **1**, 2.0 µL (0.020 mmol) 4-pentenenitrile and 0.62 mL toluene-d_8. ^{1}H-NMR and ^{31}P-NMR spectra were recorded at various temperatures (+25°C, -35°C, -25°C, -15°C, -5°C, +5°C, +15°C, +25°C, +35°C, +45°C, +55°C, +65°C, +75°C, +85°C, +25°C). Starting

from +75°C, formation of ethylene was observed. The tube was heated to 80°C for 2 hours, after which again ^{1}H-NMR and ^{31}P-NMR spectra were recorded.

Generation of ethylene

To a Schlenk flask were added 50.0 mg (0.102 mmol) catalyst precursor **1a**, 11.5 mg (0.102 mmol) potassium *tert*-butoxide, 10.2 µL (0.102 mmol) 4-pentenenitrile in 2.5 mL toluene. The system was equipped with a preheated glass rod containing carbosieve SIII. Under a constant N_2-flow, the mixture was heated to 80°C for 2 hours, after which the uptake on the carbosieve SIII was measured by GC-MS.

Control experiment generation of ethylene

In a J. Young NMR tube compound **1** was dissolved in toluene-d_8 and heated to 80°C for 30 minutes, after which the compound had decomposed without generation of ethylene.

Reactions with dimethyl acetylenedicarboxylate

To a J. Young tube was added a 1/1/1/1 mixture of catalyst precursor **1a**, potassium *tert*-butoxide, cinnamonitrile and dimethyl acetylenedicarboxylate. The reaction mixture turns blue first, but colour rapidly disappears. ^{1}H-NMR shows loss in signal intensity.

Addition of dimethyl acetylenedicarboxylate to a preformed mixture of 1/1/1 catalyst precursor **1a**, potassium *tert*-butoxide and cinnamonitrile shows comparable results.

Addition of dimethyl acetylenedicarboxylate to a preformed mixture of 1/1 catalyst precursor precursor **1a** and potassium *tert*-butoxide also shows similar results. The reaction mixture turns blue first and then changes to purple/brown, but only a loss in signal intensity is observed by ^{1}H-NMR.

Reaction with triethylsilane

To a J. Young NMR tube were added 5.0 mg (0.010 mmol) catalyst precursor **1a**, 1.2 mg (0.011 mmol) potassium *tert*-butoxide and 1.25 µL (0.01 mmol) cinnamonitrile in benzene-d_6. The mixture was shaken and 1.70 µL (0.011 mmol) thiethylsilane was added. The mixture was shaken and monitored over the weekend, but no significant change other than a loss of intensity was observed by ^{1}H-NMR.

Reaction with pentafluorobenzonitrile

In a J. Young NMR tube, a 1/1/1 mixture of **1a**, potassium *tert*-butoxide and pentafluoro-benzonitrile was dissolved in benzene-d_6. This resulted in a decrease in signal intensity in the ^{1}H-NMR spectrum and thus most probably the formation of either an insoluble or paramagnetic species. Attempts to crystallise from benzene failed.

Reaction with trimethylamine *N*-oxide

In a J. Young NMR tube, a 1/1 mixture of **1** and trimethylamine *N*-oxide was dissolved in benzene-d_6 in order to cleave the Ru-CO bond. Unfortunately, no change in ^{1}H-NMR spectrum was observed.

Synthesis of 2-bromomethyl-6-methylpyridine

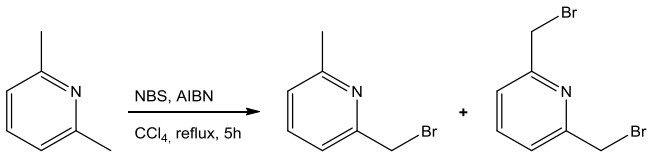

To a dry round-bottomed flask were added 5.359 g (50.0 mmol) 2,6-lutidine, 8.998 g (50.5 mmol) *N*-bromosuccinimide in 50 mL of CCl_4. The mixture was refluxed for 5 hours, during

which 140 mg of AIBN (azobisisobutyronitrile) was added every hour. The mixture was cooled to room temperature and stirred overnight, after which the mixture was filtrated and concentrated by rotary evaporation. The crude mixture of mono- and di-substituted lutidine was difficult to separate on column but 2-bromomethyl-6-methylpyridine could be isolated by vacuum distillation at 8.0 mbar and 100°C as a slightly pink solid.

2-bromomethyl-6-methylpyridine
^{1}H-NMR (300 MHz, $CDCl_3$): δ = 7.59 (t, 1H, *J* = 7.7, Py-H4), 7.26 (d, 1H, *J* = 7.6, Py-H3), 7.08 (d, 1H, *J* = 7.7, Py-H5), 4.53 (s, 2H, $PyCH_2Br$), 2.57 (s, 3H, $PyCH_3$).
2,6-bis(bromomethyl)pyridine
^{1}H-NMR (300 MHz, $CDCl_3$): δ = 7.71 (t, 1H, *J* = 7.7, Py-H4), 7.38 (d, 2H, *J* = 7.7, Py-H3), 4.54 (s, 4H, $PyCH_2Br$).

6 References

(1) Moulton, C. J.; Shaw, B. L. *J. Chem. Soc., Dalt. Trans.* **1976**, No. 11, 1020–1024.

(2) Koten, G. Van. *Top Organomet Chem* **2013**, *40*, 1.

(3) Göttker-Schnetmann, I.; White, P. S.; Brookhart, M. *Organometallics* **2004**, *23* (8), 1766–1776.

(4) Albrecht, M.; van Koten, G. *Angew. Chemie Int. Ed.* **2001**, *40* (20), 3750–3781.

(5) Trincado, M.; Grützmacher, H. In *Cooperative Catalysis*; Peters, R., Ed.; Wiley-VCH Verlag GmbH & Co. KGaA, 2015; pp 67–110.

(6) Bornschein, C.; Werkmeister, S.; Wendt, B.; Jiao, H.; Alberico, E.; Baumann, W.; Junge, H.; Junge, K.; Beller, M. *Nat. Commun.* **2014**, *5* (May), 4111.

(7) Zhang, J.; Leitus, G.; Ben-David, Y.; Milstein, D. *J. Am. Chem. Soc.* **2005**, *127*, 10840–10841.

(8) Haack, K.-J.; Hashiguchi, S.; Fujii, A.; Inoue, S.; Ikariya, T.; Noyori, R. *J. Am. Chem. Soc.* **1997**, *12* (3), 285–288.

(9) Maire, P.; Büttner, T.; Breher, F.; Le Floch, P.; Grützmacher, H. *Angew. Chemie Int. Ed.* **2005**, *44* (39), 6318–6323.

(10) Li, T.; Bergner, I.; Haque, F. N.; Iuliis, M. Z. D.; Song, D.; Morris, R. H. *Organometallics* **2007**, *26* (24), 5940–5949.

(11) Huff, C. A.; Kampf, J. W.; Sanford, M. S. *Organometallics* **2012**, *31* (13), 4643–4645.

(12) Mukherjee, A.; Srimani, D.; Chakraborty, S.; Ben-David, Y.; Milstein, D. *J. Am. Chem. Soc.* **2015**, *137* (28), 8888–8891.

(13) Gunanathan, C.; Milstein, D. *Chem. Rev.* **2014**, *114*, 12024–12087.

(14) Perdriau, S.; Chang, M.-C.; Otten, E.; Heeres, H. J.; de Vries, J. G. *Chem. - A Eur. J.* **2014**, *20* (47), 15434–15442.

(15) Keweloh, L.; Klöcker, H.; Würthwein, E.-U.; Uhl, W. *Angew. Chemie Int. Ed.* **2016**, *55* (9), 3212–3215.

(16) Vogt, M.; Nerush, A.; Iron, M. A.; Leitus, G.; Diskin-Posner, Y.; Shimon, L. J. W.; Ben-David, Y.; Milstein, D. *J. Am. Chem. Soc.* **2013**, *135* (45), 17004–17018.

(17) Zijlstra, D. S. Intermolecular oxa-Michael additions to unsaturated nitriles via a novel metal-ligand cooperative pathway, University of Groningen, 2015.

(18) Perdriau, S.; Zijlstra, D. S.; Heeres, H. J.; de Vries, J. G.; Otten, E. *Angew. Chemie Int. Ed.* **2015**, *54* (14), 4236–4240.

(19) Corbett, P. T.; Leclaire, J.; Vial, L.; West, K. R.; Wietor, J.-L.; Sanders, J. K. M.; Otto, S. *Chem. Rev.* **2006**, *106* (9), 3652–3711.

(20) Mindiola, D. J. *Angew. Chemie Int. Ed.* **2009**, *48* (34), 6198–6200.

(21) Katsuki, T. *Chem. Soc. Rev.* **2004**, *33* (7), 437–444.

(22) Yamada, S. *Coord. Chem. Rev.* **1999**, *190–192*, 537–555.

(23) Baleizão, C.; Garcia, H. *Chem. Rev.* **2006**, *106* (9), 3987–4043.

(24) Strecker, A. *Justus Liebigs Ann. Chem.* **1850**, *75* (1), 27–45.

(25) Tang, Z.; Otten, E.; Reek, J. N. H.; Vlugt, J. I. Van Der; Bruin, B. De. *Chem. Eur. J.* **2015**, *21*, 1–12.

(26) Perdriau, S. New catalytic reactions for the conversion of alkenes - From cashew nut shell liquid to unsaturated nitriles, University of Groningen, 2016.

(27) Eijsink, L. E.; Perdriau, S. C. P.; de Vries, J. G.; Otten, E. *Dalt. Trans.* **2016**, *45* (40), 16033–16039.

(28) Weigend, F.; Ahlrichs, R. *Phys. Chem. Chem. Phys.* **2005**, *7* (18), 3297–3305.

(29) Grimme, S.; Antony, J.; Ehrlich, S.; Krieg, H. *J. Chem. Phys.* **2010**, *132* (15).

(30) Levitt, M.; Perutz, M. F. *J. Mol. Biol.* **1988**, *201* (4), 751–754.

(31) Saggu, M.; Levinson, N. M.; Boxer, S. G. *J. Am. Chem. Soc.* **2012**, *134* (46), 18986–18997.

(32) Albertí, M.; Aguilar, A.; Lucas, J. M.; Pirani, F. *J. Phys. Chem. A* **2012**, *116* (22), 5480–5490.

(33) Masnovi, J.; Baker, R. J.; Towns, R. L. R.; Chen, Z. *J. Org. Chem.* **1991**, *56* (1), 176–179.

(34) Allerhand, A.; von Rague Schleyer, P. *J. Am. Chem. Soc.* **1963**, *85* (7), 866–870.

(35) Le Questel, J.-Y.; Berthelot, M.; Laurence, C. *J. Phys. Org. Chem.* **2000**, *13* (6), 347–358.

(36) Thordarson, P. *Chem. Soc. Rev.* **2011**, *40* (3), 1305–1323.

(37) Van, der Z. A. A. H.; Van, K. G.; Luijk, R.; Nordemann, R. A.; Spek, A. L. *Organometallics* **1988**, *7* (7), 1549–1556.

(38) Polukeev, A. V.; Kuklin, S. A.; Petrovskii, P. V.; Peregudov, A. S.; Dolgushin, F. M.; Ezernitskaya, M. G.; Koridze, A. A. *Russ. Chem. Bull.* **2010**, *59* (4), 745–749.

(39) Mohammad, H. A. Y.; Grimm, J. C.; Eichele, K.; Mack, H. G.; Speiser, B.; Novak, F.; Quintanilla, M. G.; Kaska, W. C.; Mayer, H. A. *Organometallics* **2002**, *21* (26), 5775–5784.

(40) Yamashita, M.; Moroe, Y.; Yano, T.; Nozaki, K. *Inorganica Chim. Acta* **2011**, *369* (1), 15–18.

(41) Esteruelas, M. A.; Oliván, M.; Vélez, A. *Inorg. Chem.* **2013**, *52* (9), 5339–5349.

(42) Zhang, J.; Gandelman, M.; Shimon, L. J. W.; Milstein, D. *Organometallics* **2008**, *27* (14), 3526–3533.

(43) Polukeev, A. V.; Marcos, R.; Ahlquist, M. S. G.; Wendt, O. F. *Chem. Sci.* **2015**, *6* (3), 2060–2067.

(44) Kohl, S. W.; Weiner, L.; Schwartsburd, L.; Konstantinovski, L.; Shimon, L. J. W.; Ben-David, Y.; Iron, M. A.; Milstein, D. *Science (80-.).* **2009**, *324* (5923), 74–77.

(45) Van Goethem, M. W. M.; Barendregt, S.; Grievink, J.; Moulijn, J. A.; Verheijen, P. J. T. *Ind. Eng. Chem. Res.* **2007**, *46* (12), 4045–4062.

(46) Ouyang, J.; Kong, F.; Su, G.; Hu, Y.; Song, Q. *Catal. Letters* **2009**, *132* (1–2), 64–74.

(47) Pearson, A. J.; Yamamoto, Y. In *Encyclopedia of Reagents for Organic Synthesis*; John

Wiley & Sons, Ltd: Chichester, UK, 2010; Vol. 1, pp 10–13.

(48) Ikariya, T.; Ishii, Y.; Kawano, H.; Arai, T.; Saburi, M.; Yoshikawa, S.; Akutagawa, S. *J. Chem. Soc., Chem. Commun.* **1985**, *12* (13), 922–924.

(49) DiMichele, L.; King, S. A.; Douglas, A. W. *Tetrahedron: Asymmetry* **2003**, *14* (22), 3427–3429.

(50) Joshi, A. M.; Thorburn, I. S.; Rettig, S. J.; James, B. R. *Inorganica Chim. Acta* **1992**, *198–200* (C), 283–296.

(51) Gargir, M.; Ben-David, Y.; Leitus, G.; Diskin-Posner, Y.; Shimon, L. J. W.; Milstein, D. *Organometallics* **2012**, *31* (17), 6207–6214.

(52) Fogler, E.; Garg, J. A.; Hu, P.; Leitus, G.; Shimon, L. J. W.; Milstein, D. *Chem. - A Eur. J.* **2014**, *20* (48), 15727–15731.

(53) Bordwell, F. G. *Acc. Chem. Res* **1988**, *21* (10), 456–463.

7 Appendix

7 Appendix

7.1 NMR spectra

7.1.1 1 + cinnamonitrile

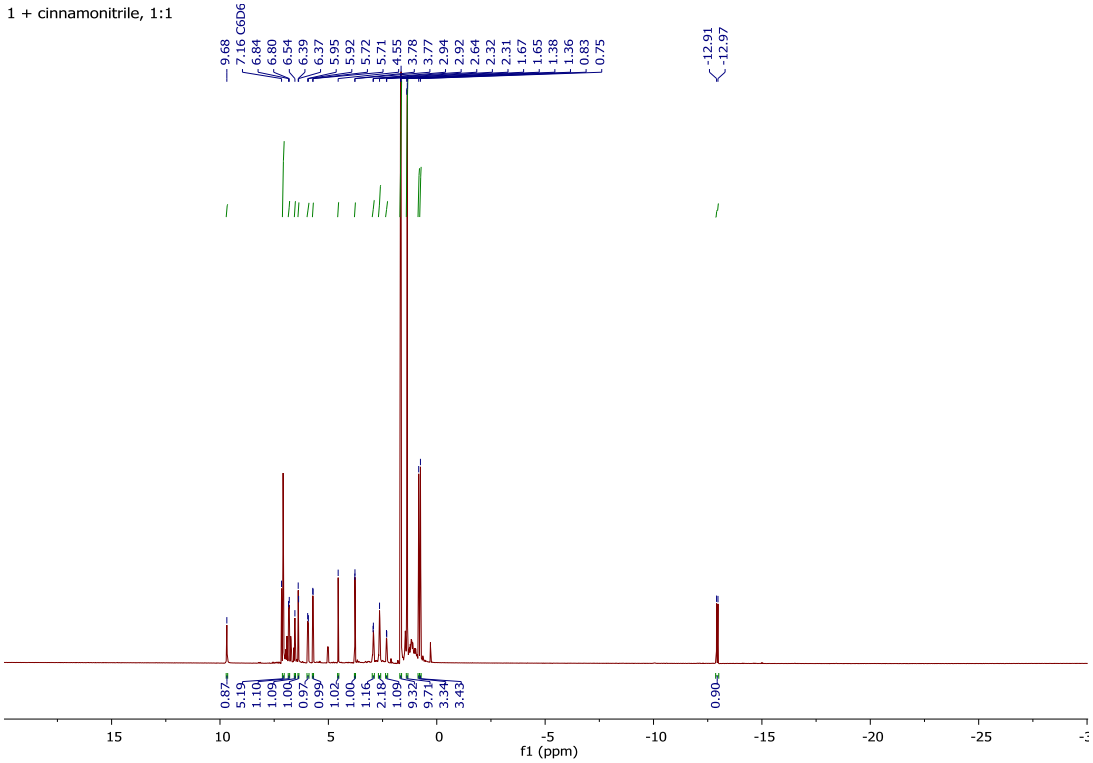

Figure 7.1-a: ^{1}H NMR spectrum of **1** + cinnamonitrile (**1^{CN}C**; full range)

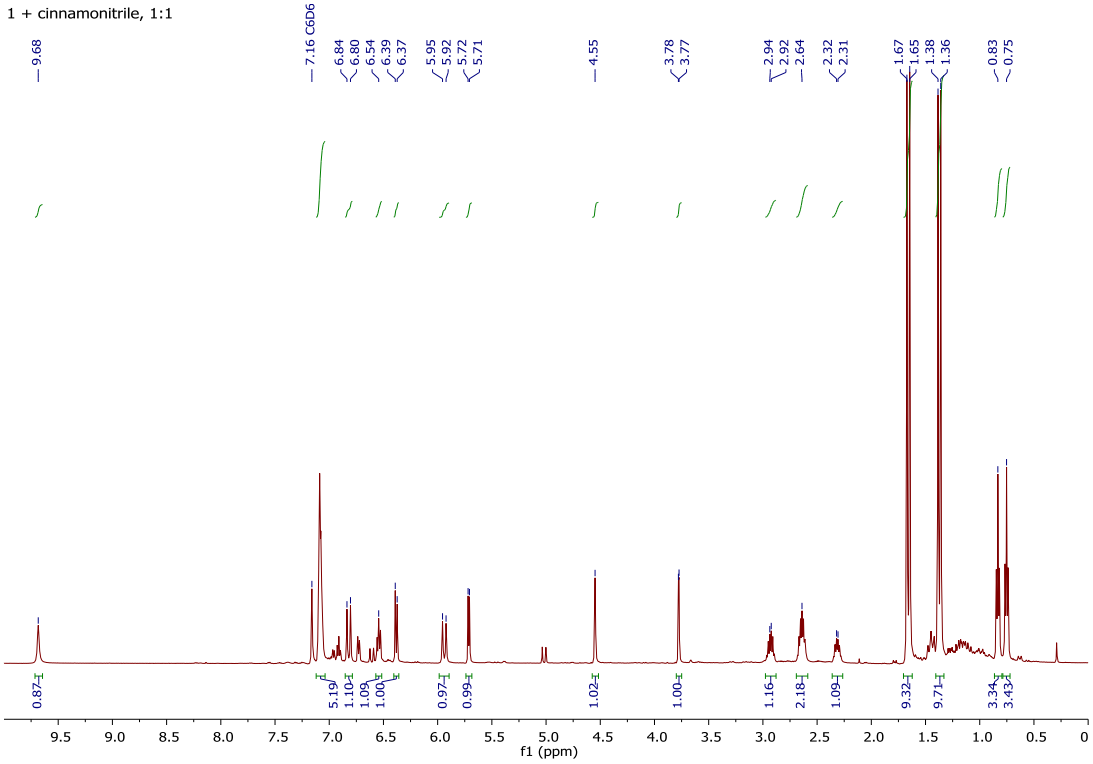

Figure 7.1-b: ^{1}H NMR spectrum of **1** + cinnamonitrile (**1^{CN}C**; between 0 and 10 ppm)

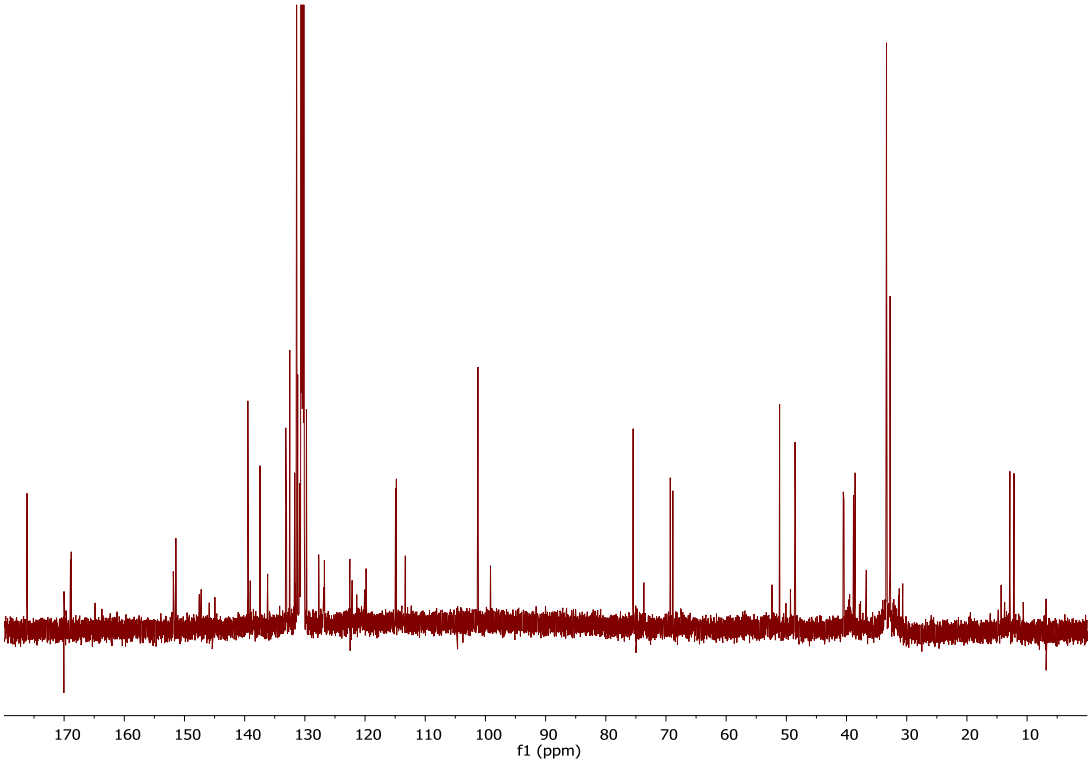

Figure 7.1-c: ^{13}C NMR spectrum of **1** + cinnamonitrile (**1**^{CN}**C**; decomposition starts to occur during acquisition of NMR data)

7.1.2 NMR spectra of 1 + 4-pentenenitrile

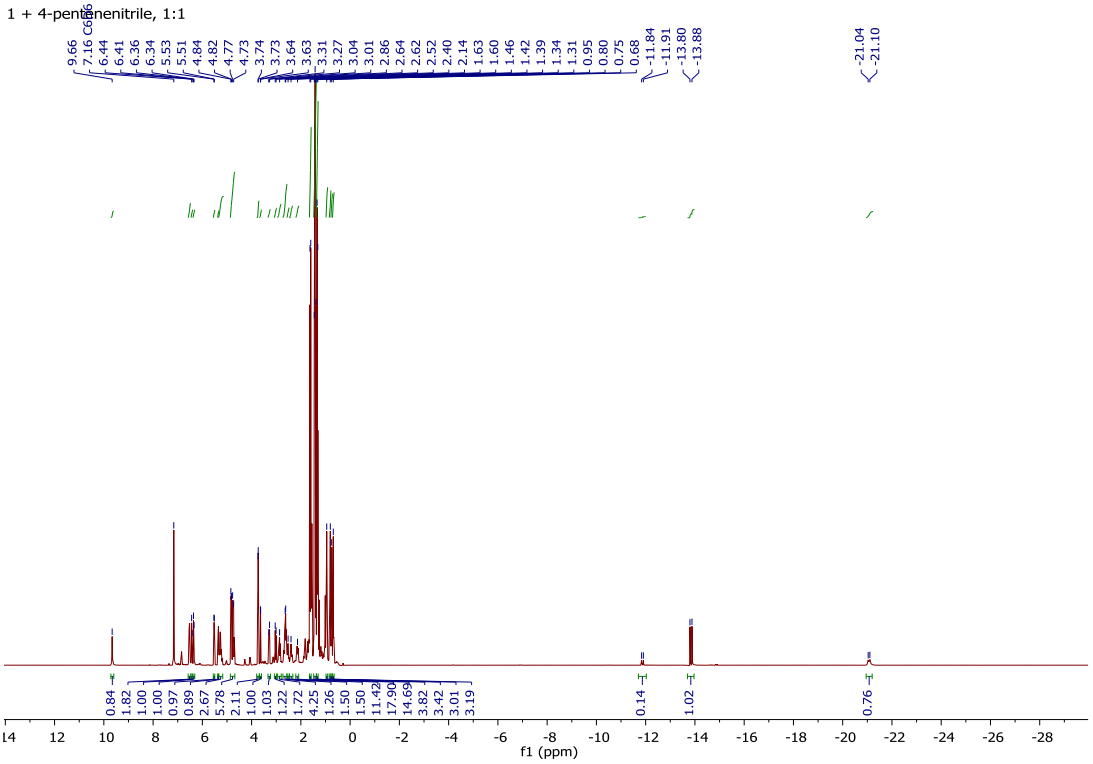

Figure 7.1-d: ^{1}H-NMR spectrum of **1 + 4-pentenenitrile ⇄ 1^{4PN}A ⇄ 1^{4PN}B ⇄ 1^{4PN}C** (full range)

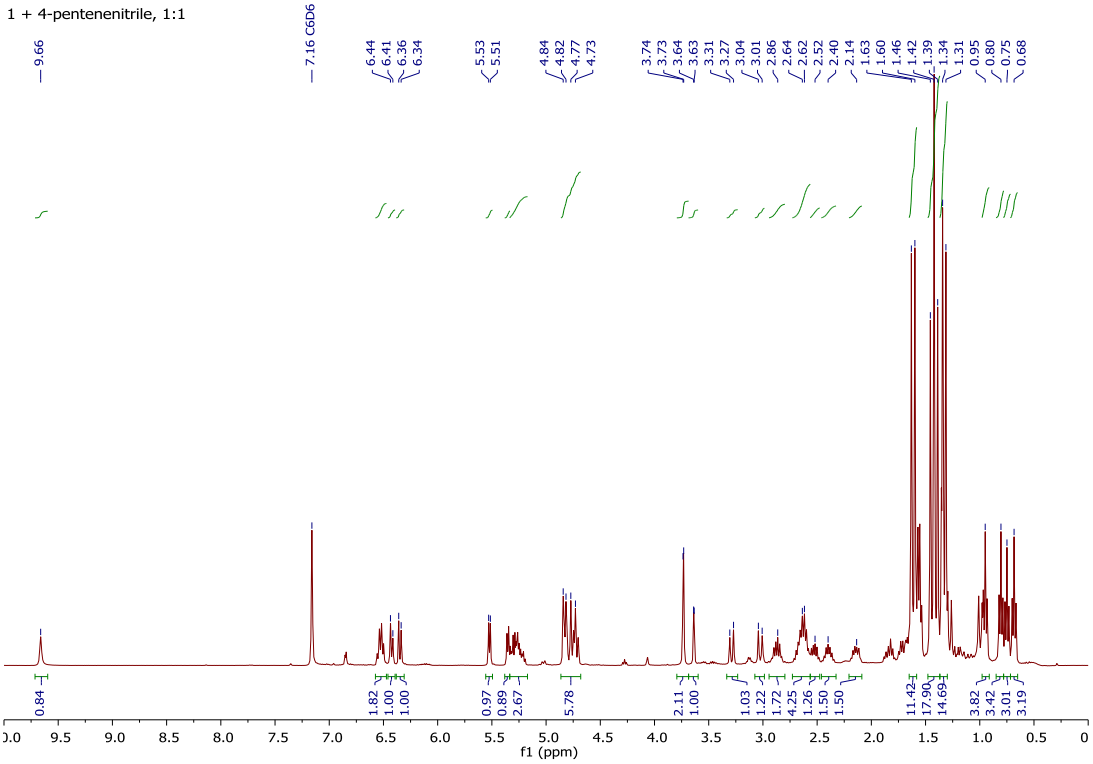

Figure 7.1-e: ^{1}H-NMR spectrum of **1 + 4-pentenenitrile ⇄ 1^{4PN}A ⇄ 1^{4PN}B ⇄ 1^{4PN}C** (between 0 and 10 ppm)

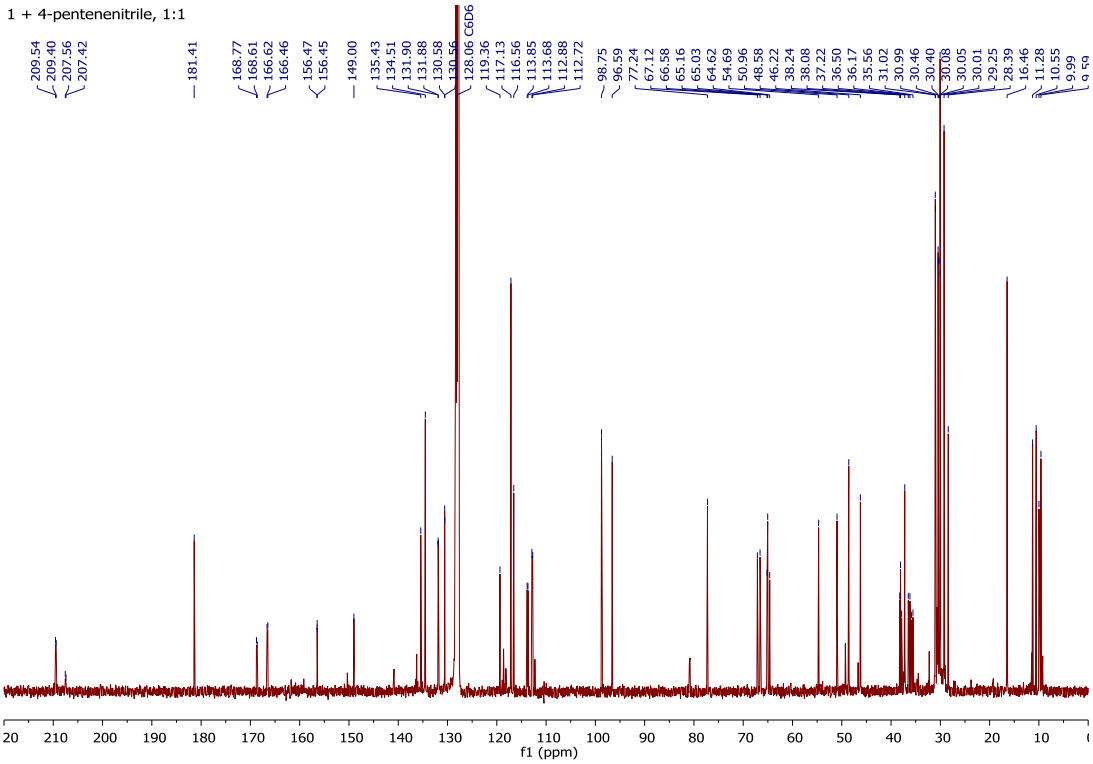

Figure 7.1-f: ^{13}C-NMR spectrum of **1 + 4-pentenenitrile ⇄ 1^{4PN}A ⇄ 1^{4PN}B ⇄ 1^{4PN}C**

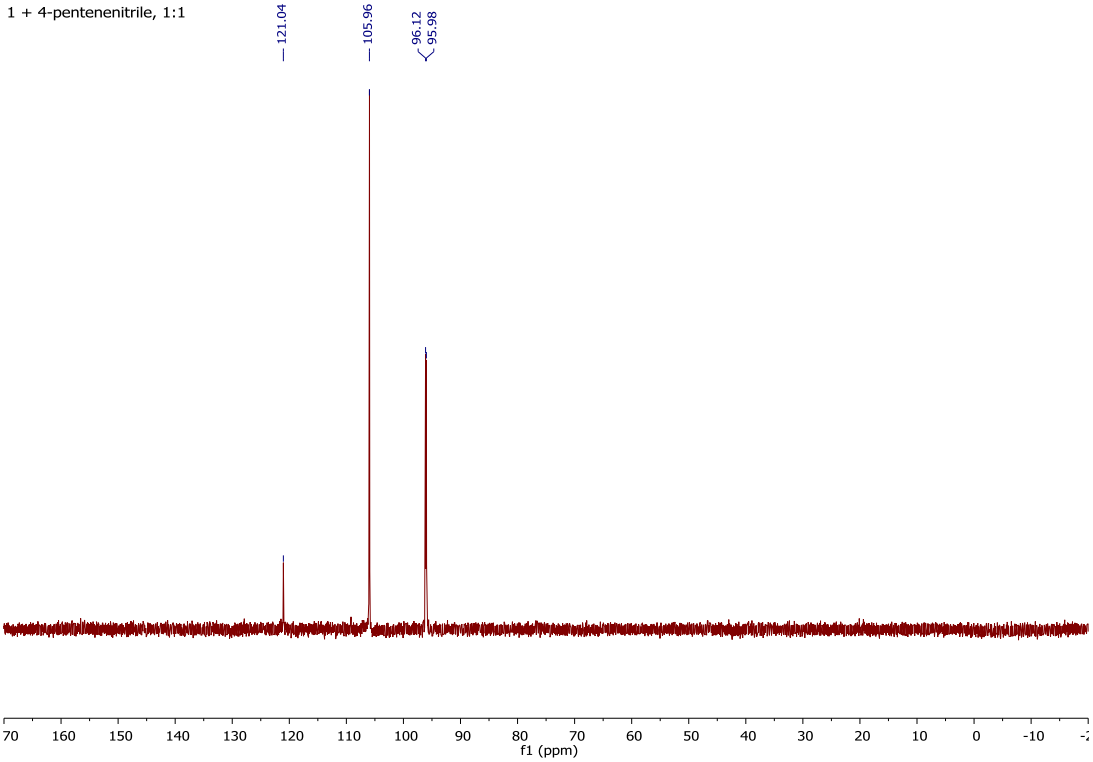

Figure 7.1-g: ^{31}P-NMR spectrum of **1 + 4-pentenenitrile ⇄ 1^{4PN}A ⇄ 1^{4PN}B ⇄ 1^{4PN}C**

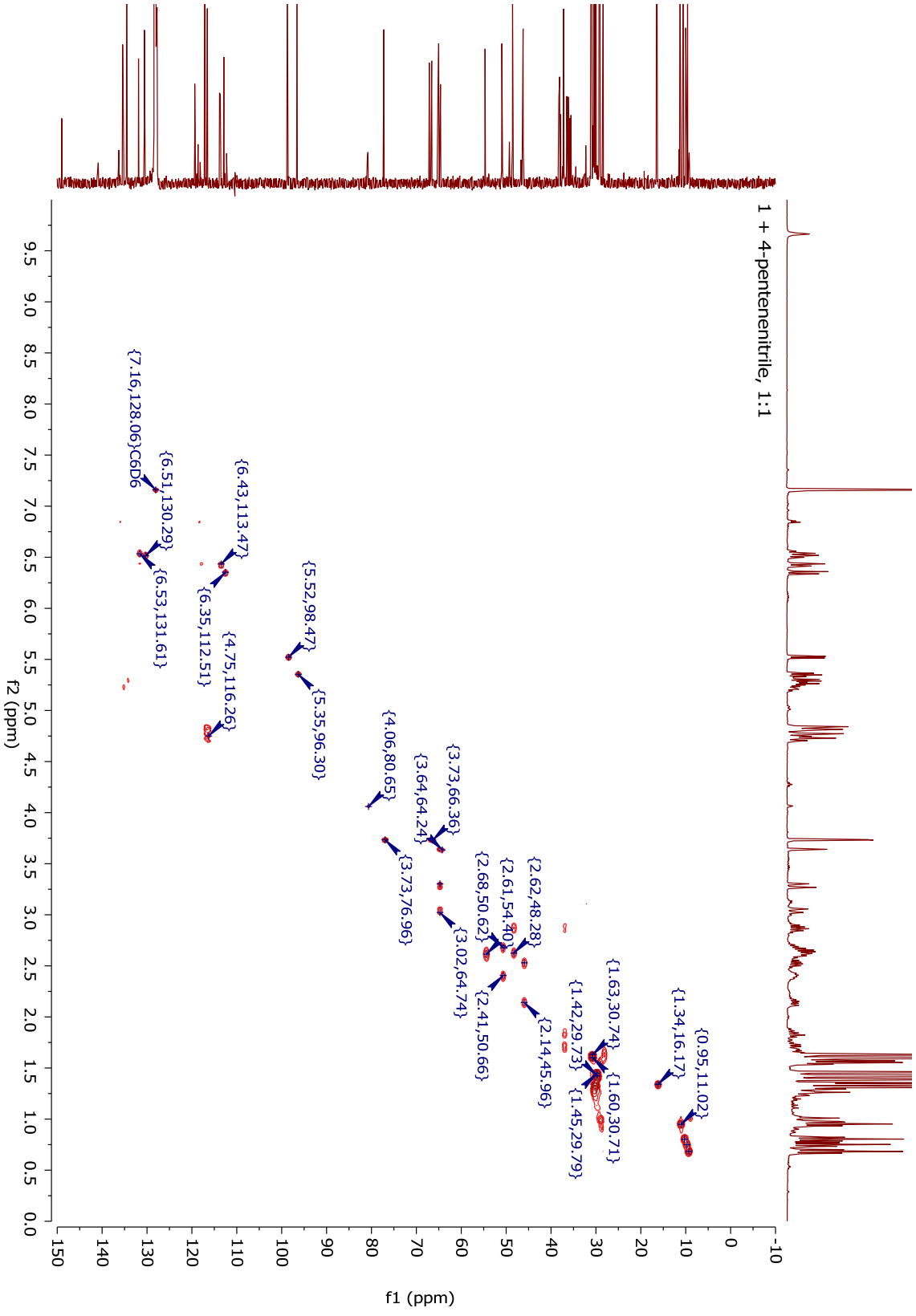

Figure 7.1-h: gHSQCAD-NMR spectrum of **1 + 4-pentenenitrile ⇄ 1^{4PN}A ⇄ 1^{4PN}B ⇄ 1^{4PN}C**

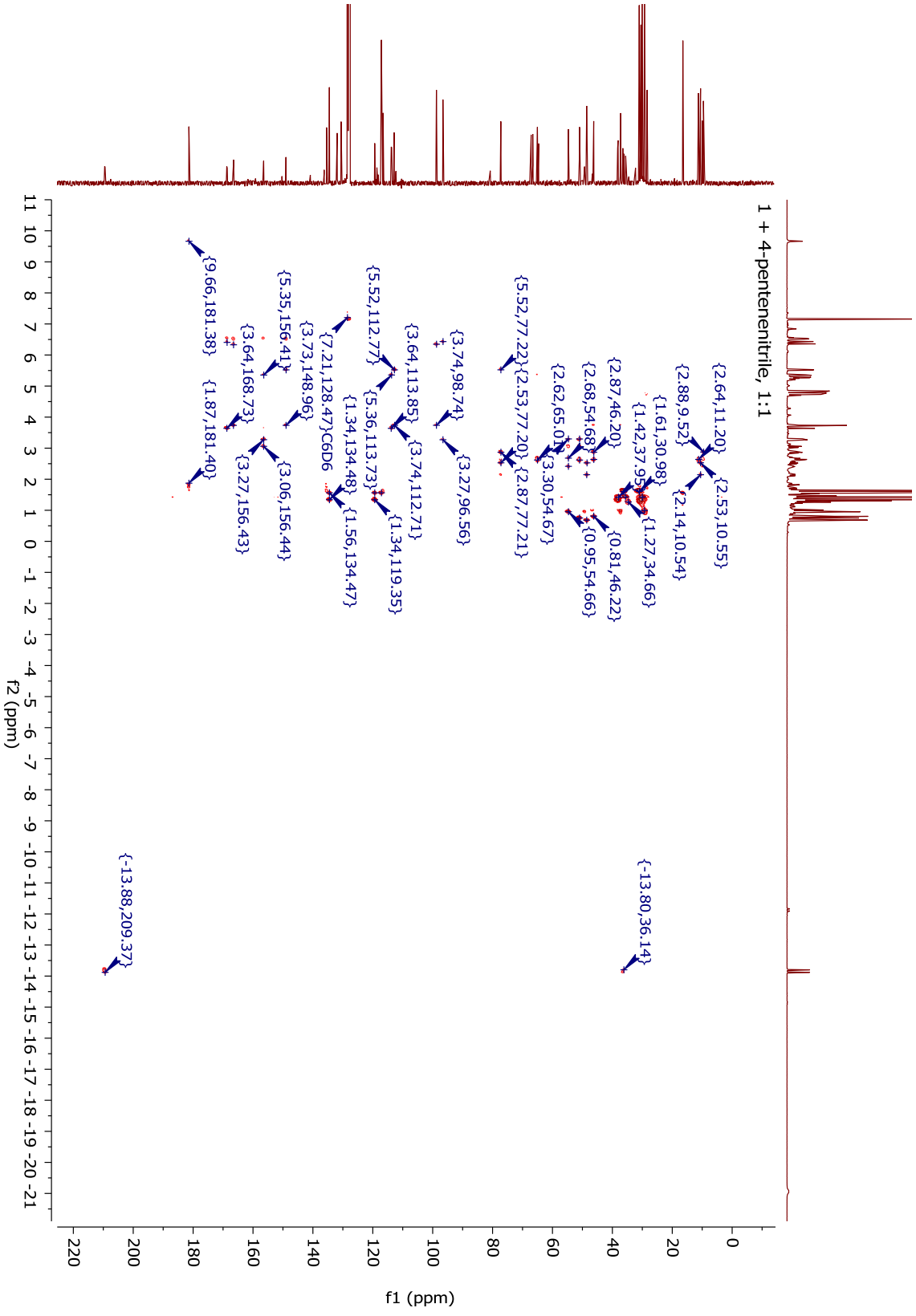

Figure 7.1-i: gHMBCAD-NMR spectrum of **1 + 4-pentenenitrile ⇄ 1^{4PN}A ⇄ 1^{4PN}B ⇄ 1^{4PN}C**

7.1.3 NMR spectra of 1 + acetonitrile

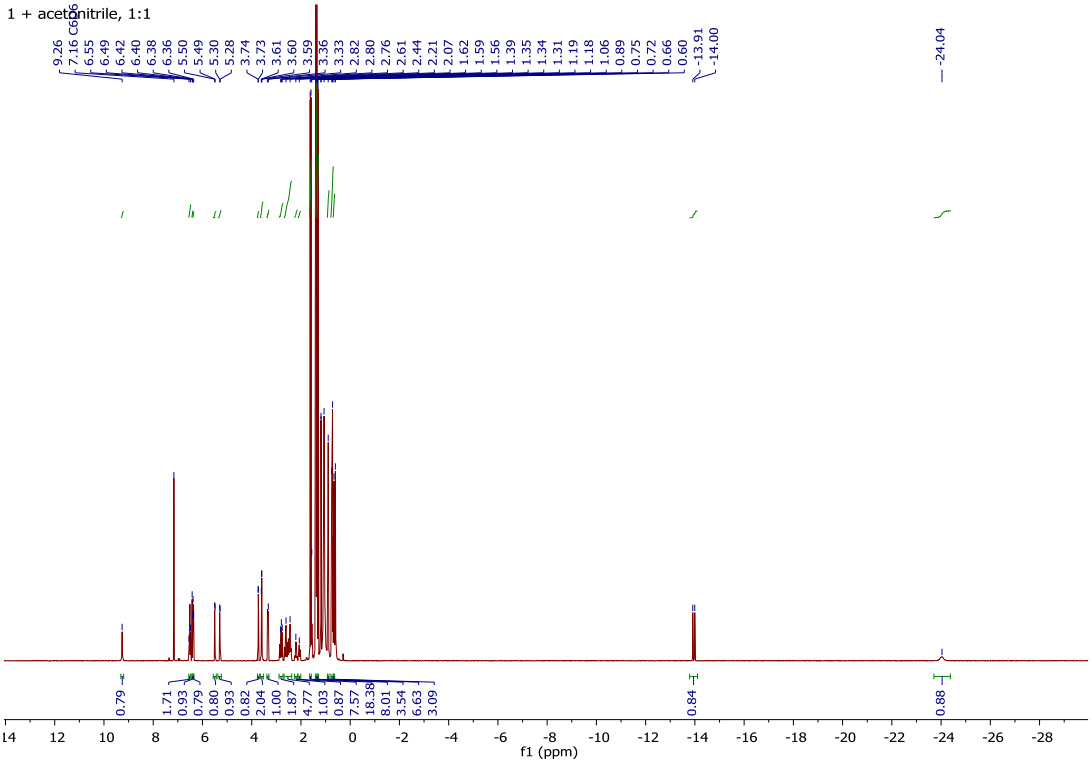

Figure 7.1-j: ^{1}H-NMR spectrum of **1 + acetonitrile ⇄ 1^{AN}A ⇄ 1^{AN}C** (full range)

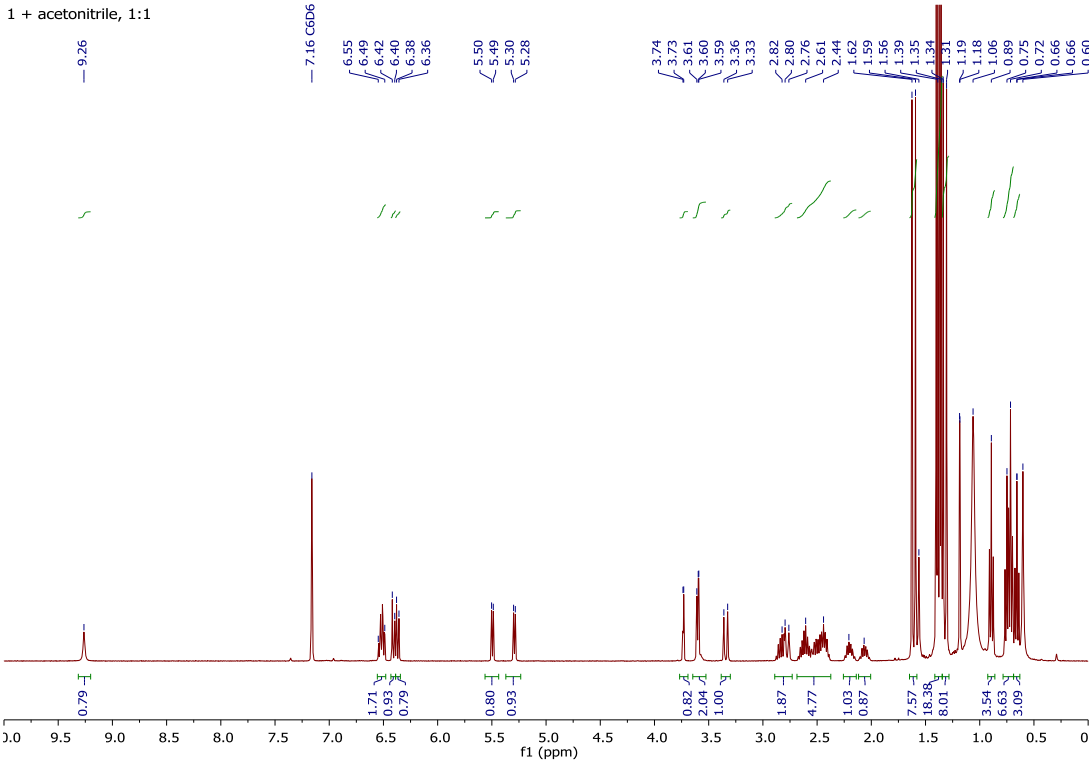

Figure 7.1-k: ^{1}H-NMR spectrum of **1 + acetonitrile ⇄ 1^{AN}A ⇄ 1^{AN}C** (between 0 and 10 ppm)

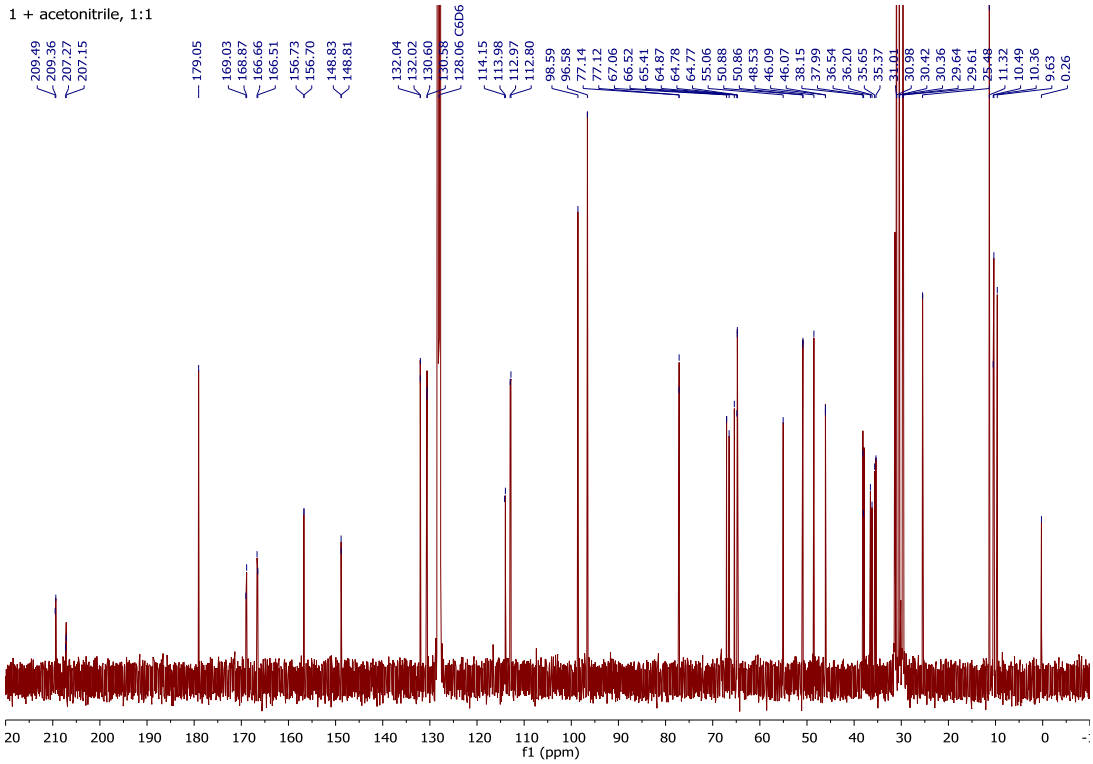

Figure 7.1-l: ^{13}C-NMR spectrum of **1 + acetonitrile ⇄ 1^{AN}A ⇄ 1^{AN}C**

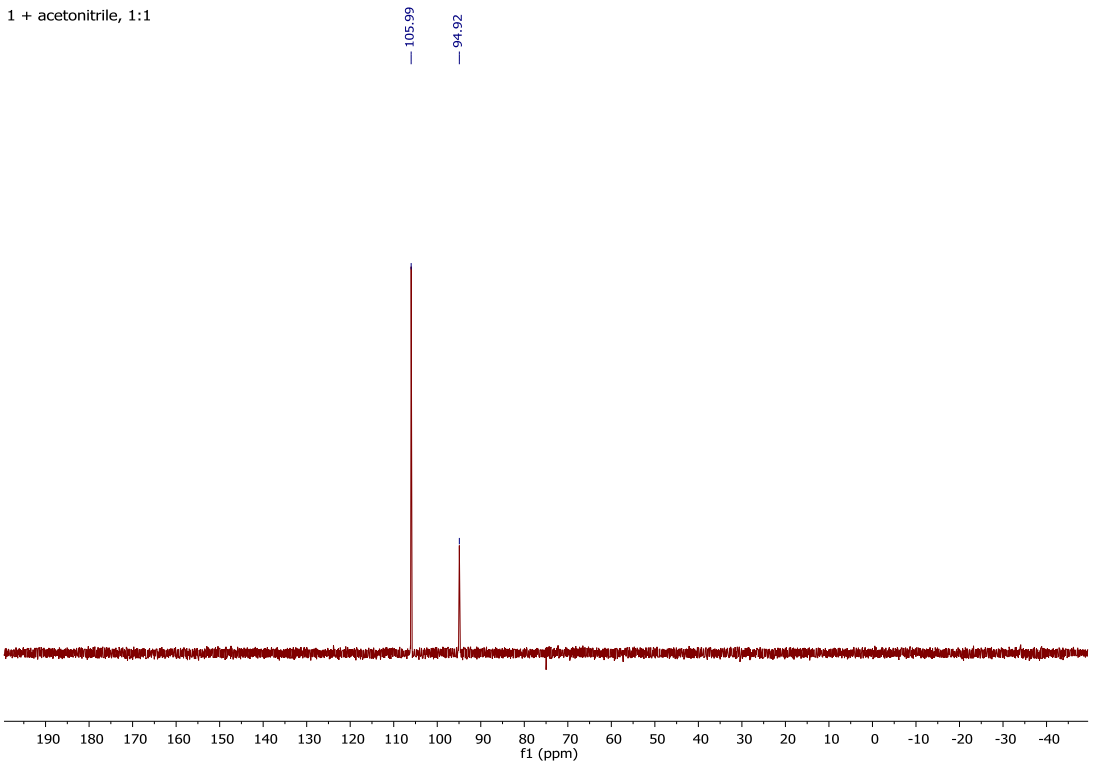

Figure 7.1-m: ^{31}P-NMR spectrum of **1 + acetonitrile ⇄ 1^{AN}A ⇄ 1^{AN}C**

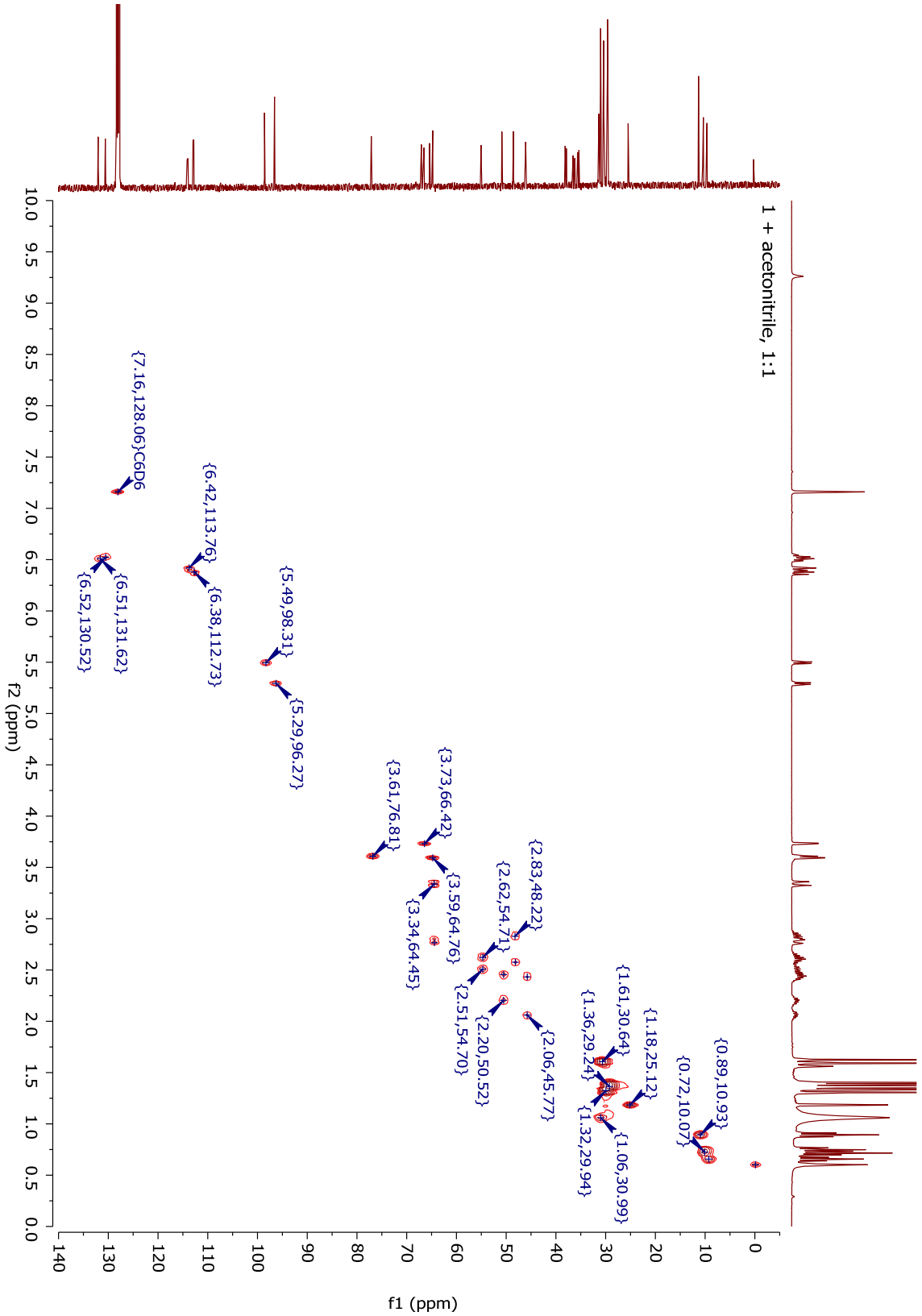

Figure 7.1-n: gHSQC-NMR spectrum of **1 + acetonitrile ⇄ 1^{AN}A ⇄ 1^{AN}C**

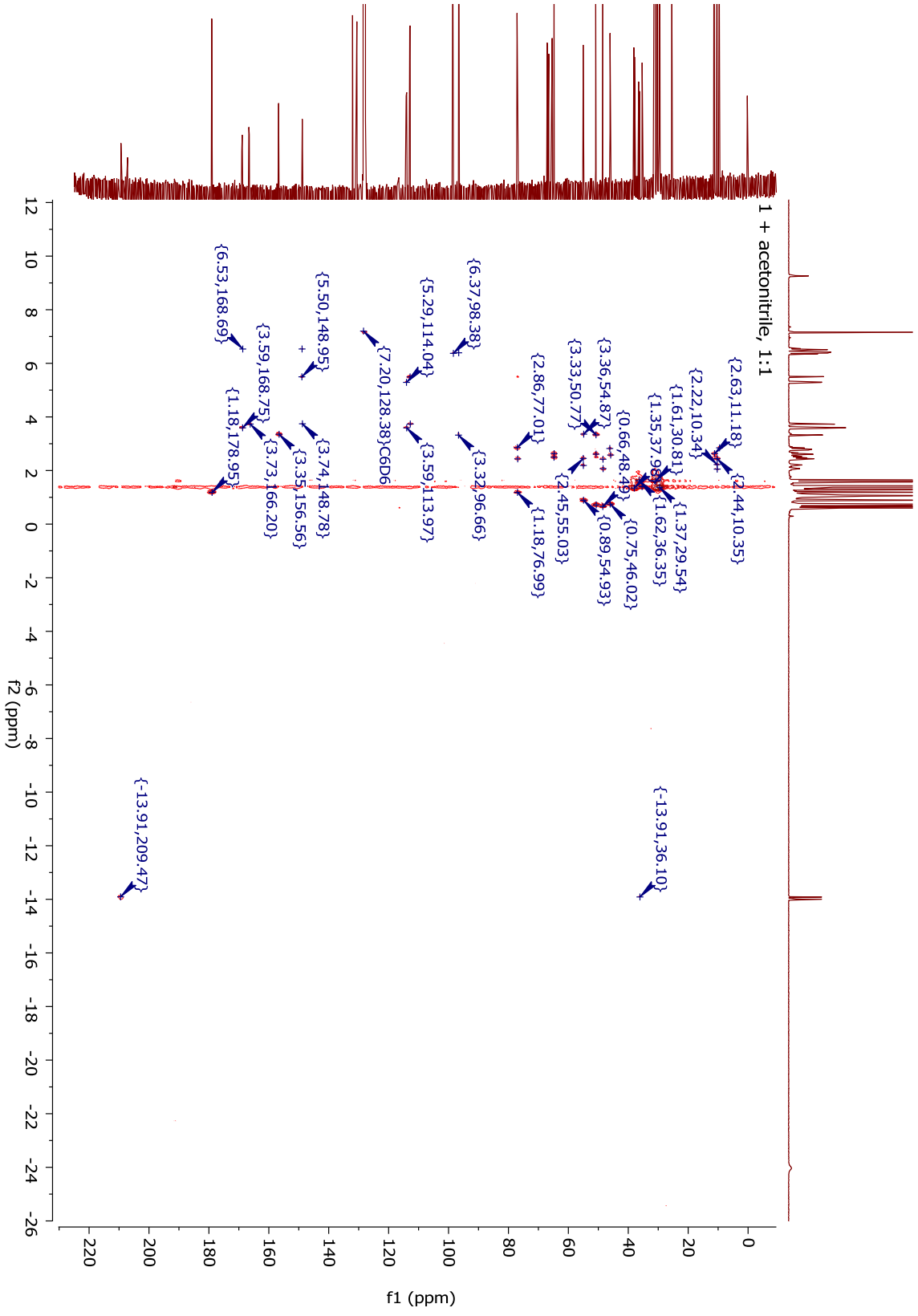

Figure 7.1-o: gHMBC-NMR spectrum of **1 + acetonitrile ⇄ 1^{AN}A ⇄ 1^{AN}C**

7.1.4 NMR spectra of 1 + benzonitrile

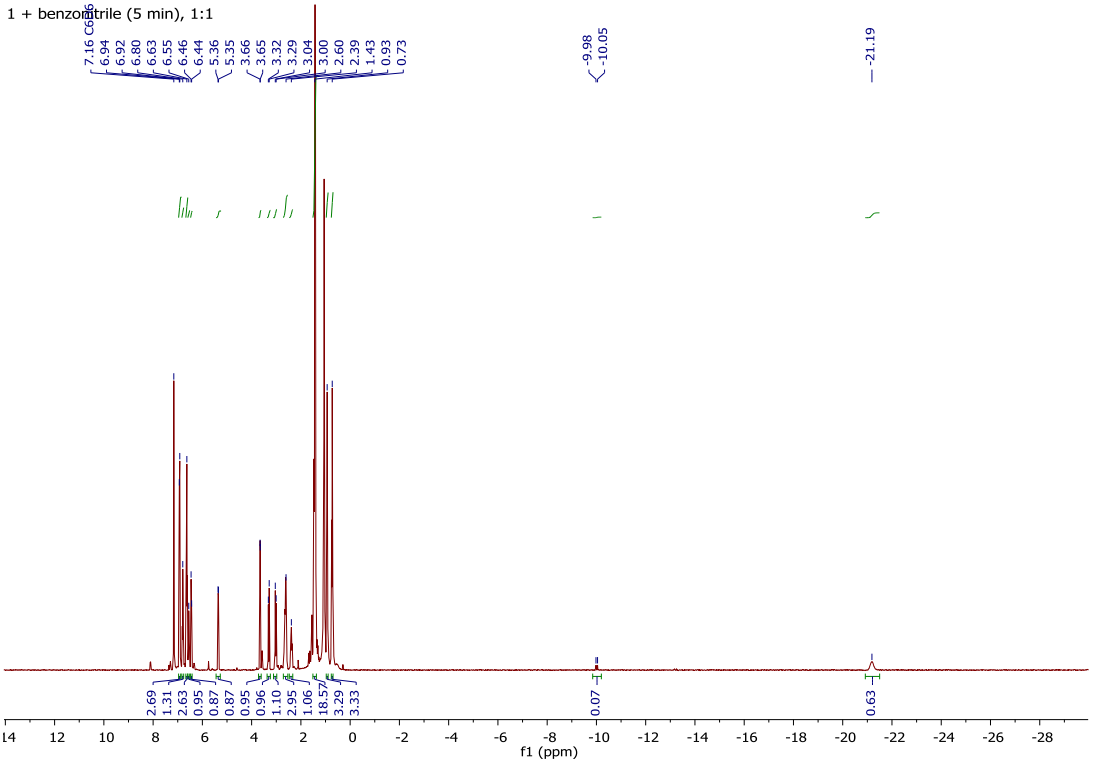

Figure 7.1-p: ^{1}H-NMR spectrum of **1 + benzonitrile ⇄ 1^{BN}A ⇄ 1^{BN}B** (after 5 minutes, full range)

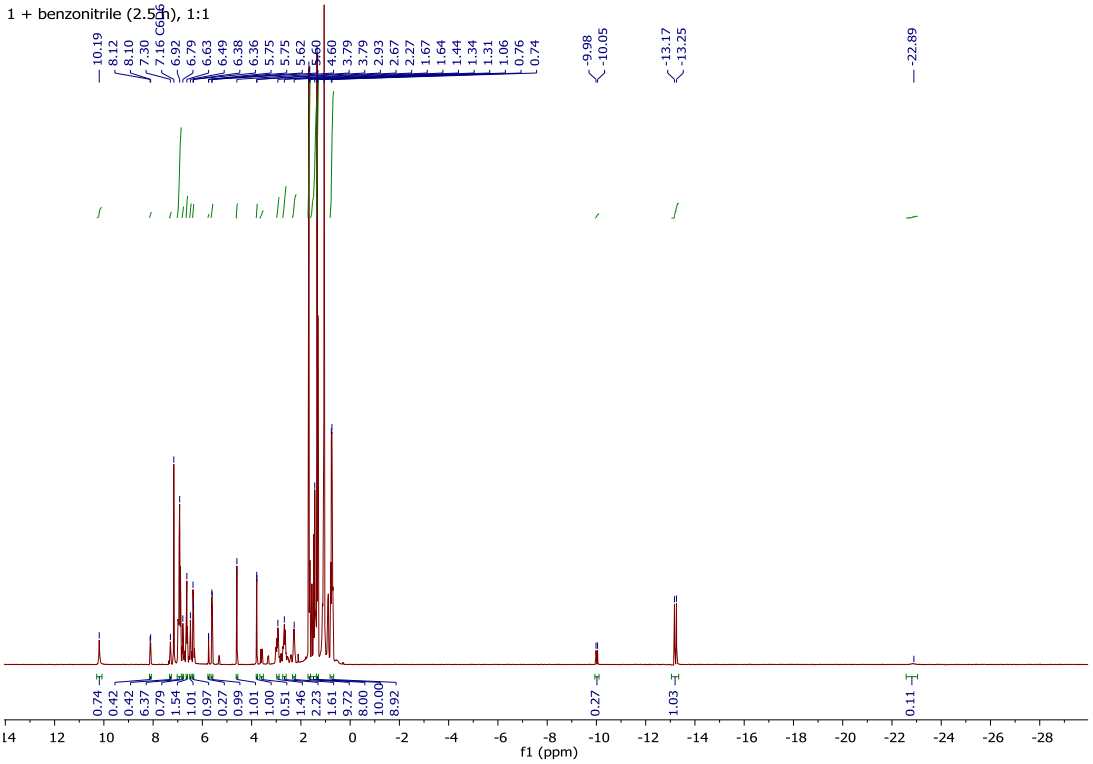

Figure 7.1-q: ^{1}H-NMR spectrum of **1^{BN}B + 1^{BN}C** (after 2.5 hours, full range)

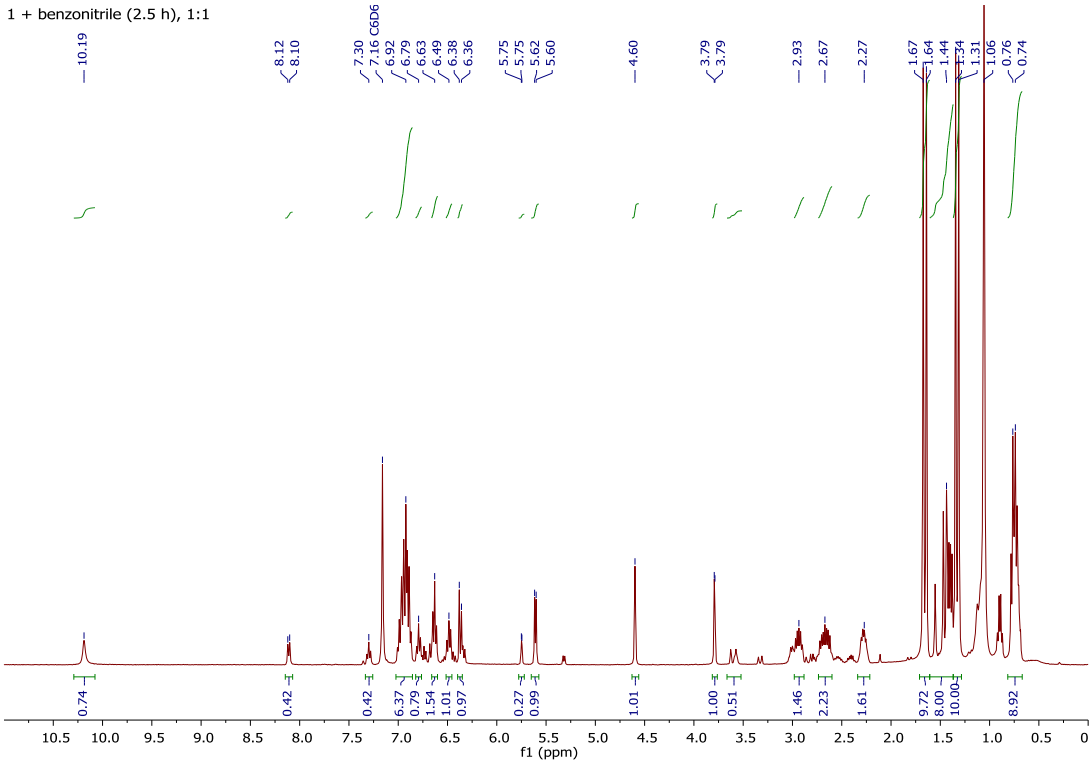

Figure 7.1-r: ^{1}H-NMR spectrum of **1^{BN}B + 1^{BN}C** (after 2.5 hours, between 0 and 11 ppm)

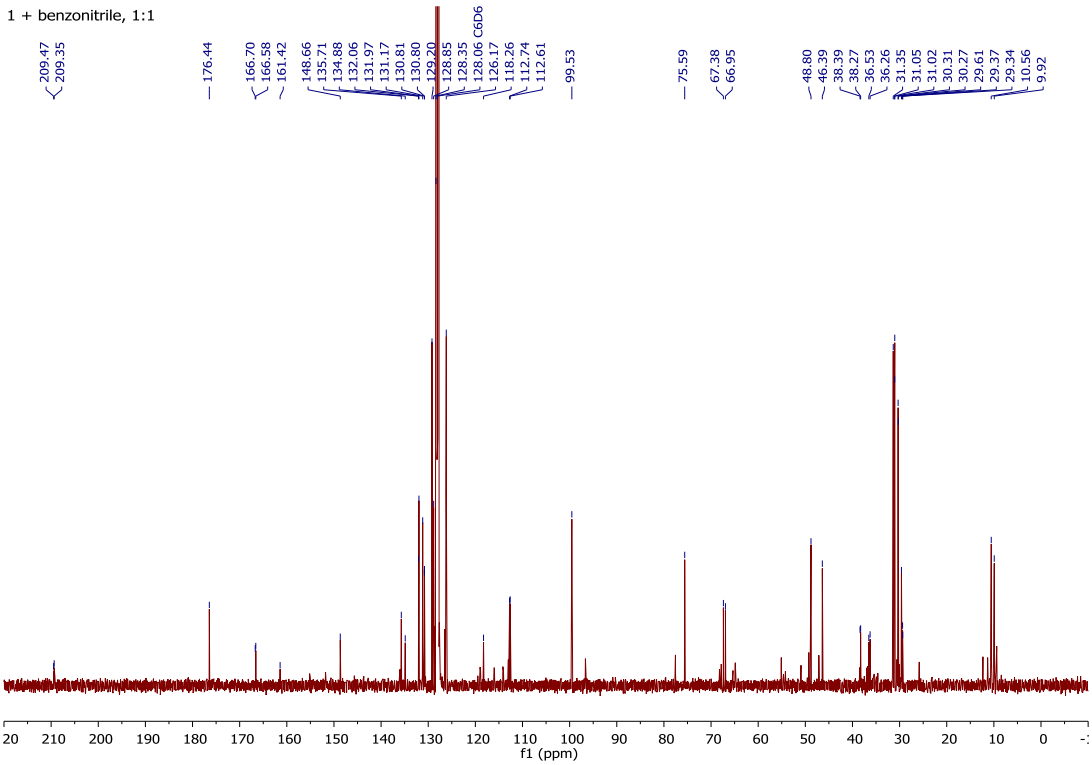

Figure 7.1-s: ^{13}C-NMR spectrum of **1^{BN}B + 1^{BN}C**

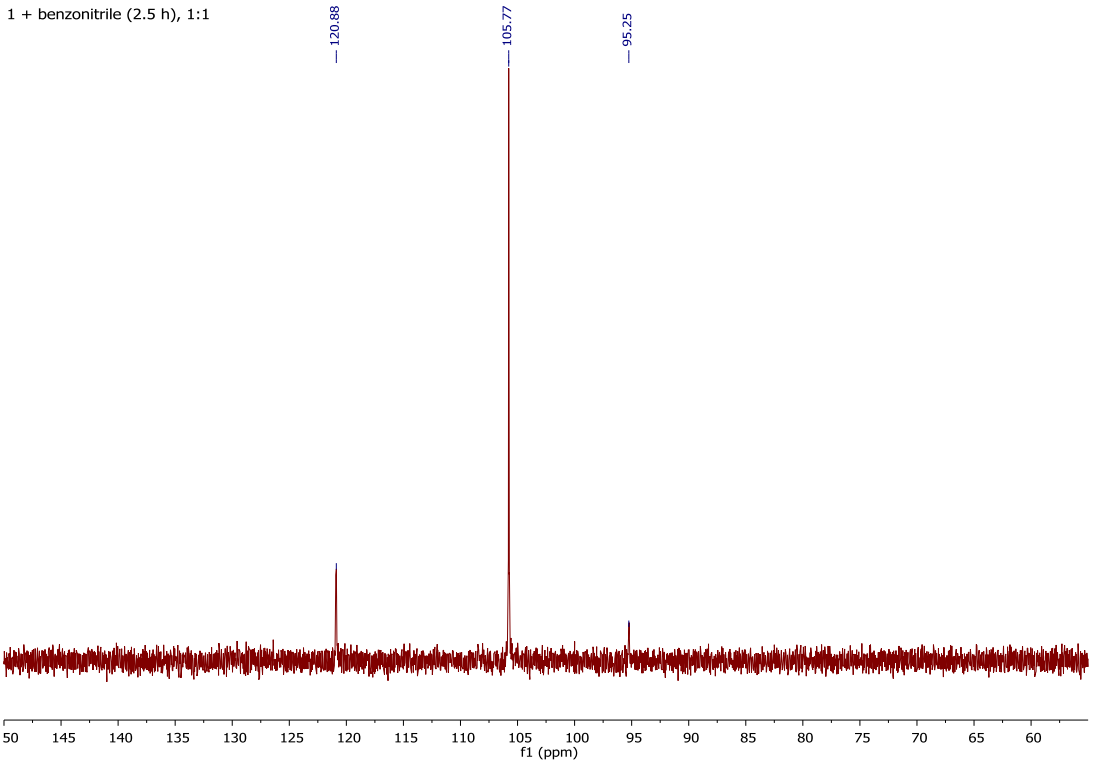

Figure 7.1-t: ^{31}P-NMR spectrum of **1^{BN}B + 1^{BN}C**

7.1.5 NMR spectra of 1 + benzyl cyanide

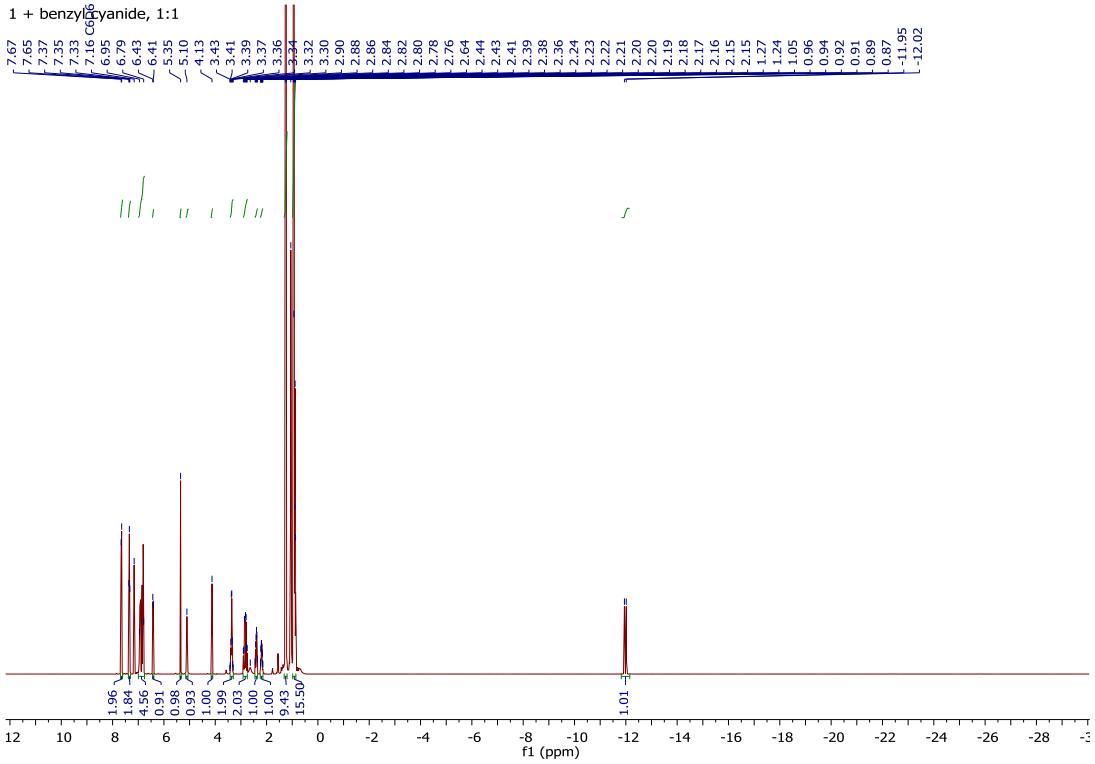

Figure 7.1-u: ^{1}H-NMR spectrum of **1^{BC}D** (full range)

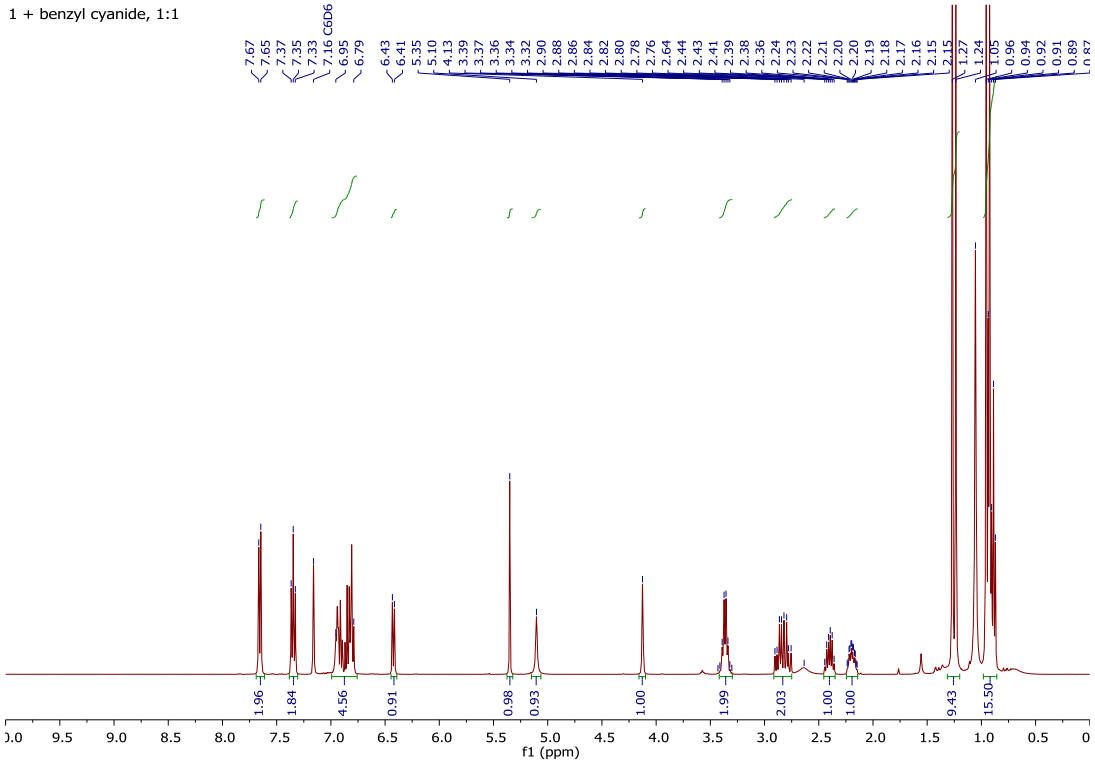

Figure 7.1-v: ^{1}H-NMR spectrum of **1^{BC}D** (between 0 and 10 ppm)

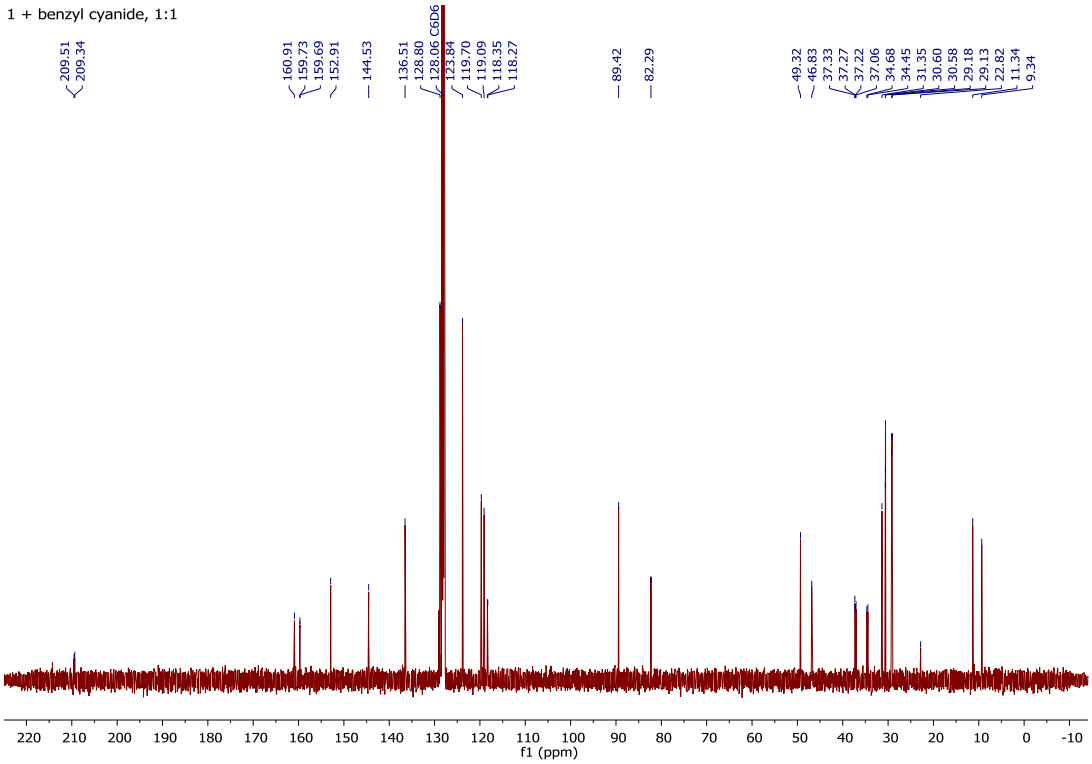

Figure 7.1-w: ^{13}C-NMR spectrum of **1^{BC}D**

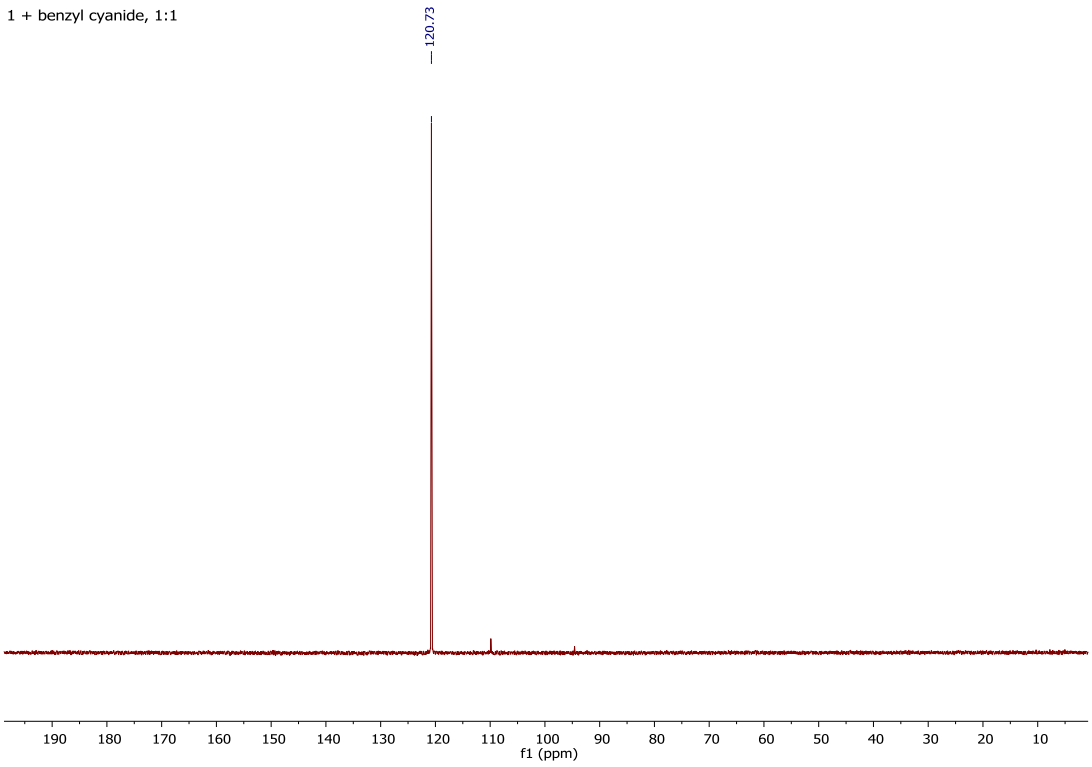

Figure 7.1-x: ^{31}P-NMR spectrum of **1^{BC}D**

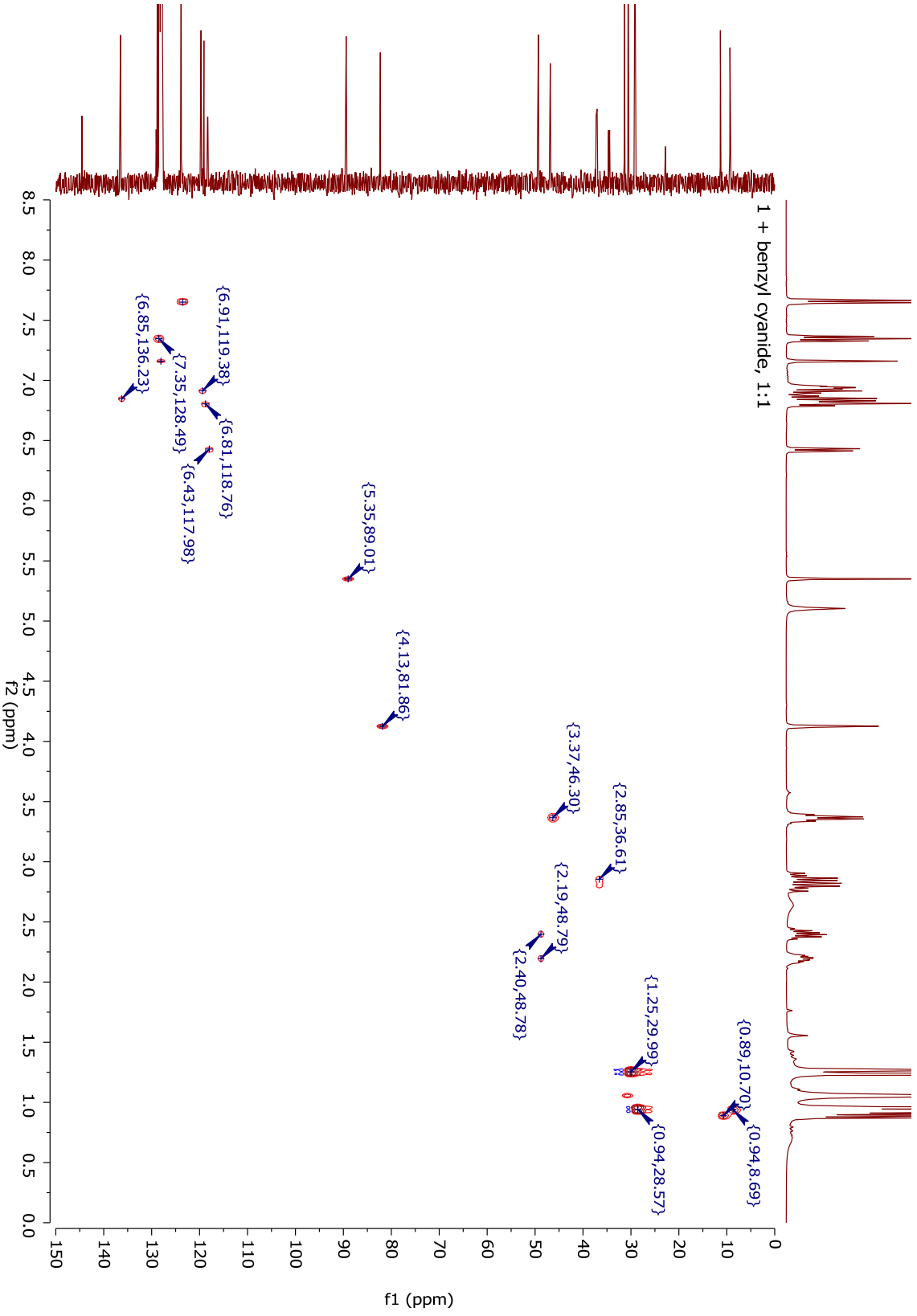

Figure 7.1-y: gHSQC-NMR spectrum of **1**^{BC}**D**

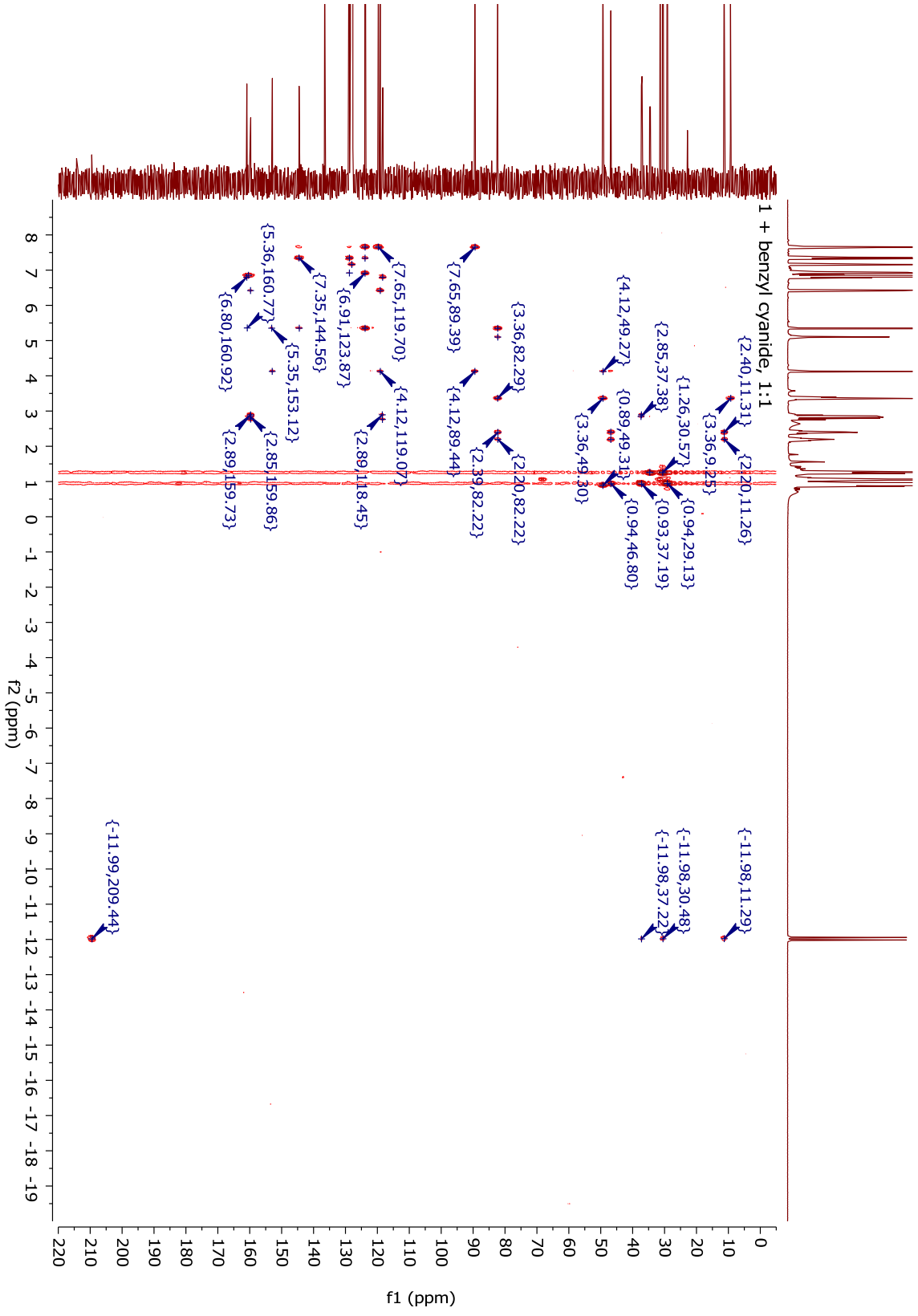

Figure 7.1-z: gHMBC-NMR spectrum of **1^{BC}D**

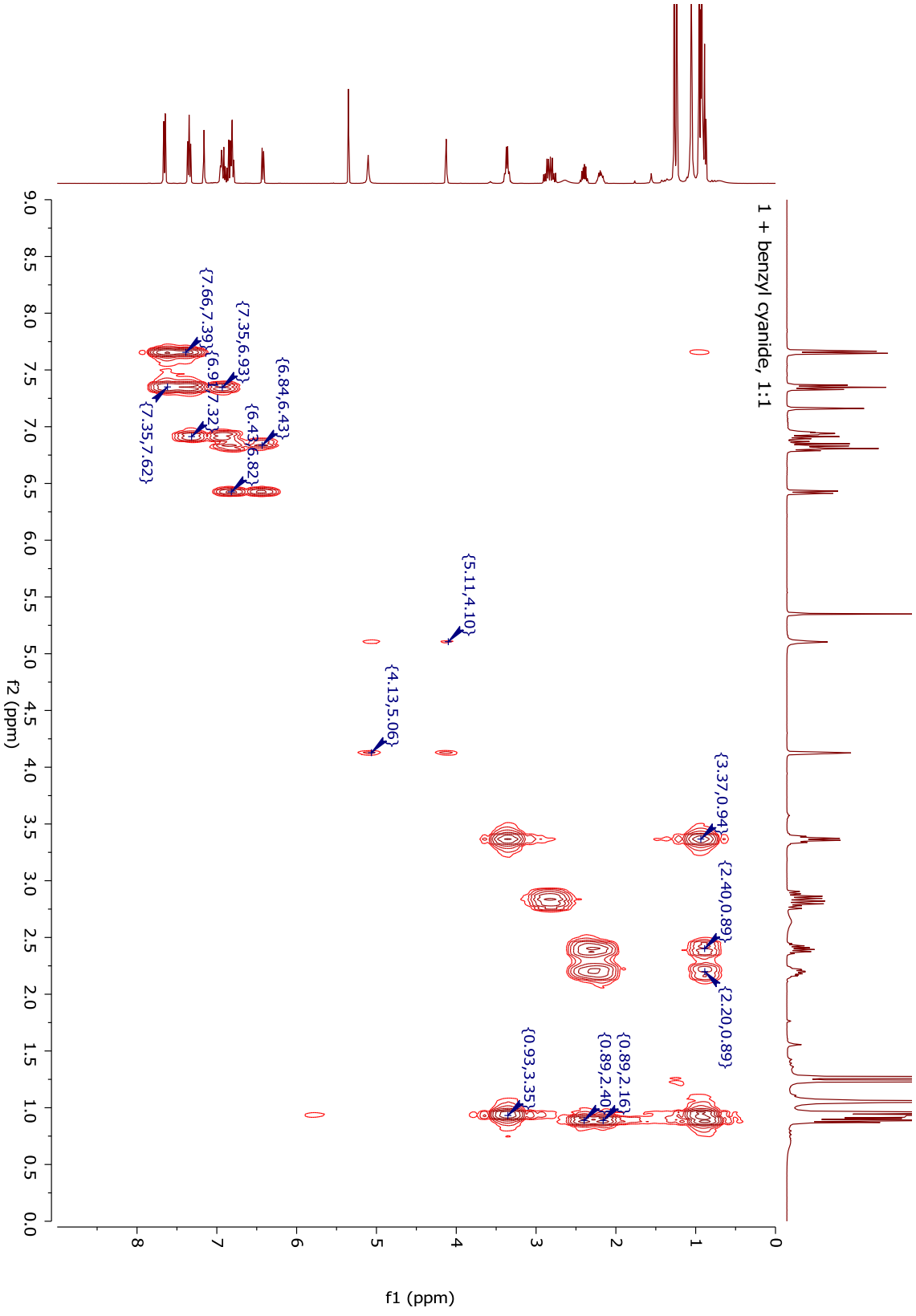

Figure 7.1-aa: DQFCOSY-NMR spectrum of **1^{BC}D**

7.1.6 NMR spectra of 1^{AN} + octanethiol (1^{SH})

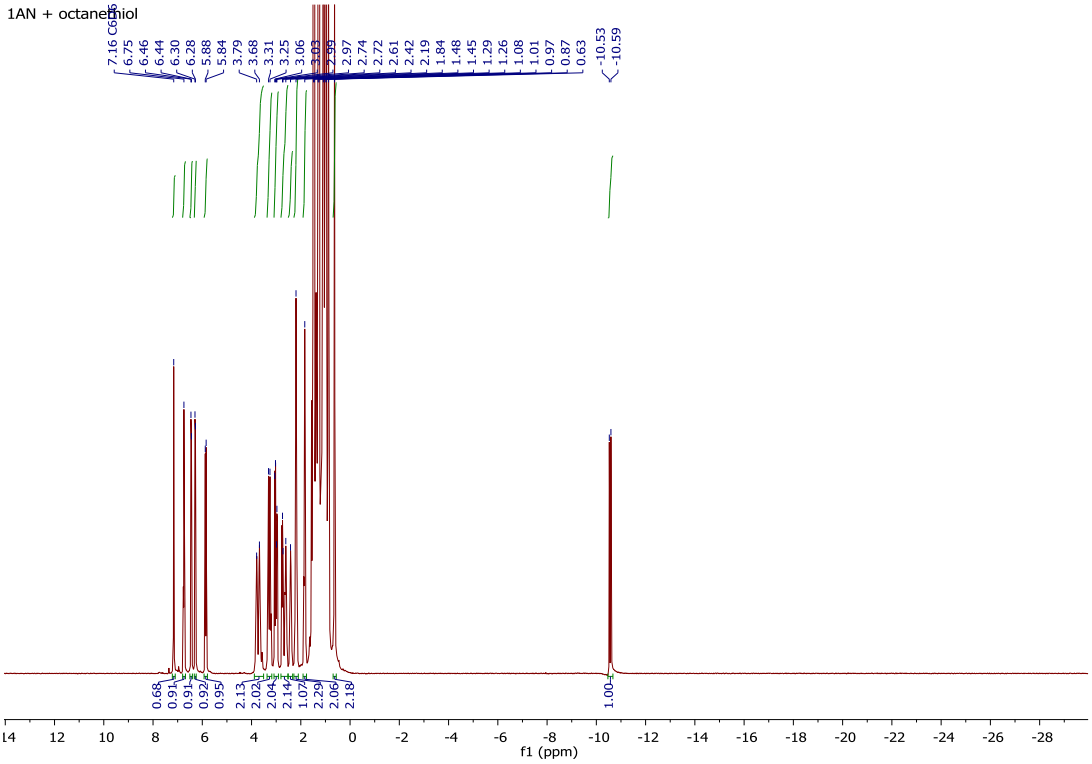

Figure 7.1-bb: ^{1}H-NMR spectrum of 1^{SH} (full range)

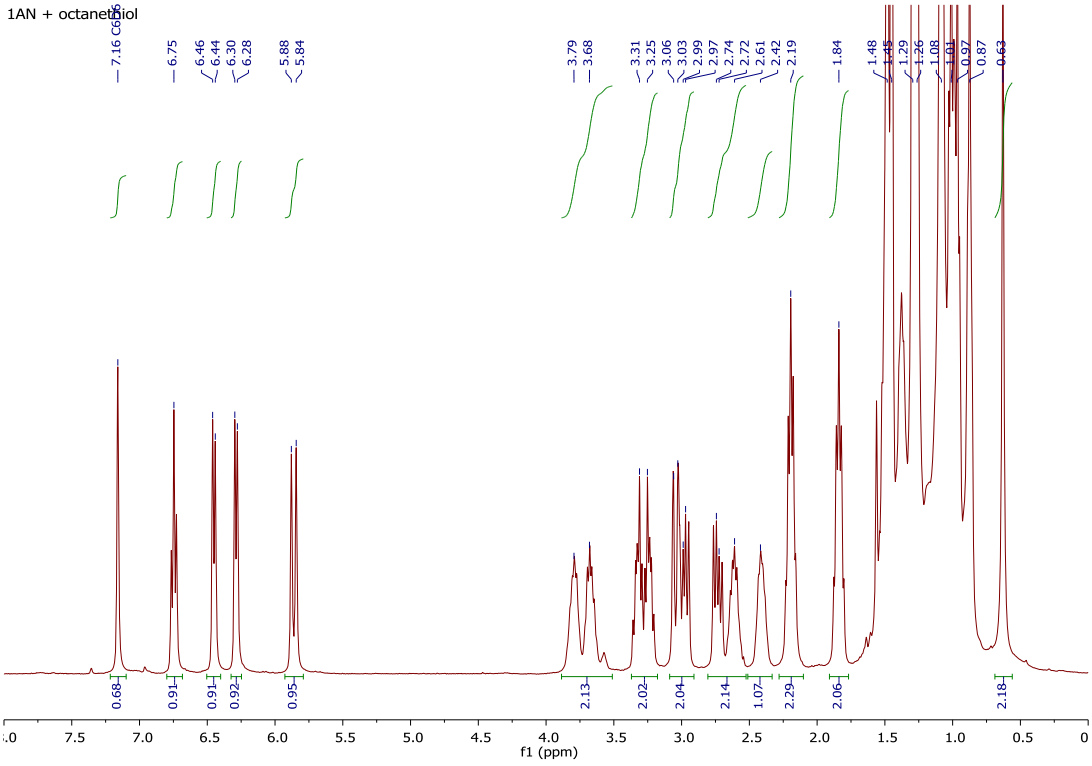

Figure 7.1-cc: ^{1}H-NMR spectrum of 1^{SH} (0 – 8 ppm)

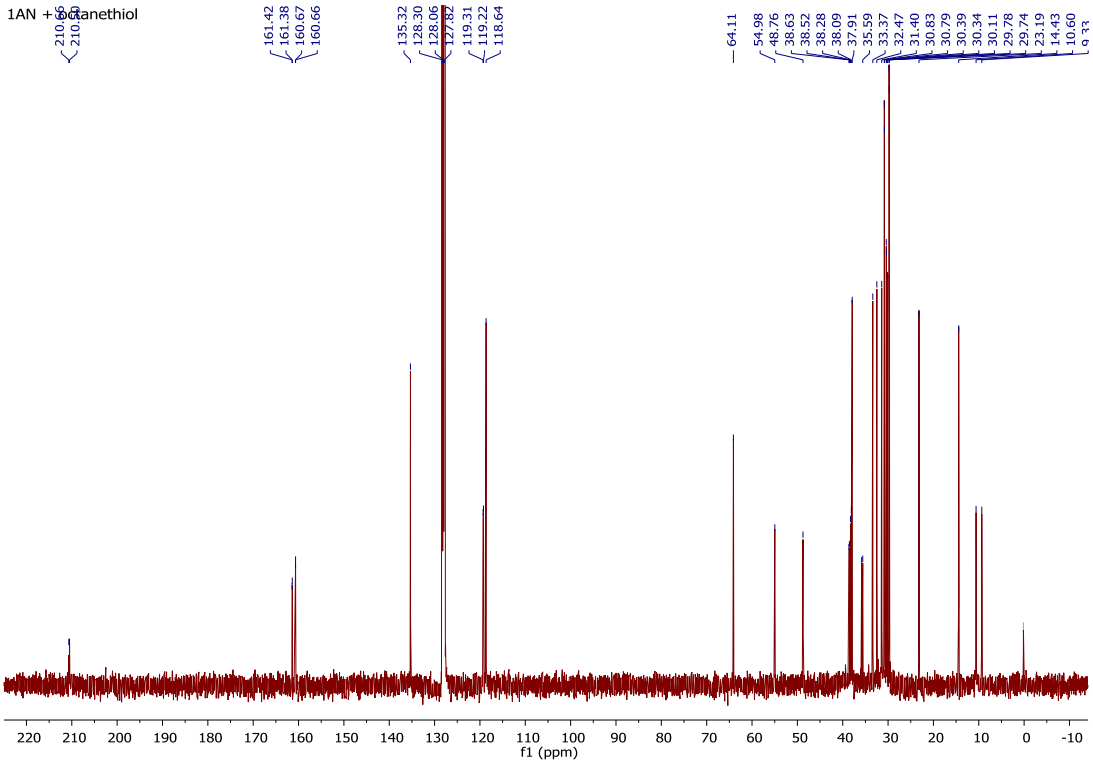

Figure 7.1-dd: ^{13}C-NMR spectrum of 1^{SH}

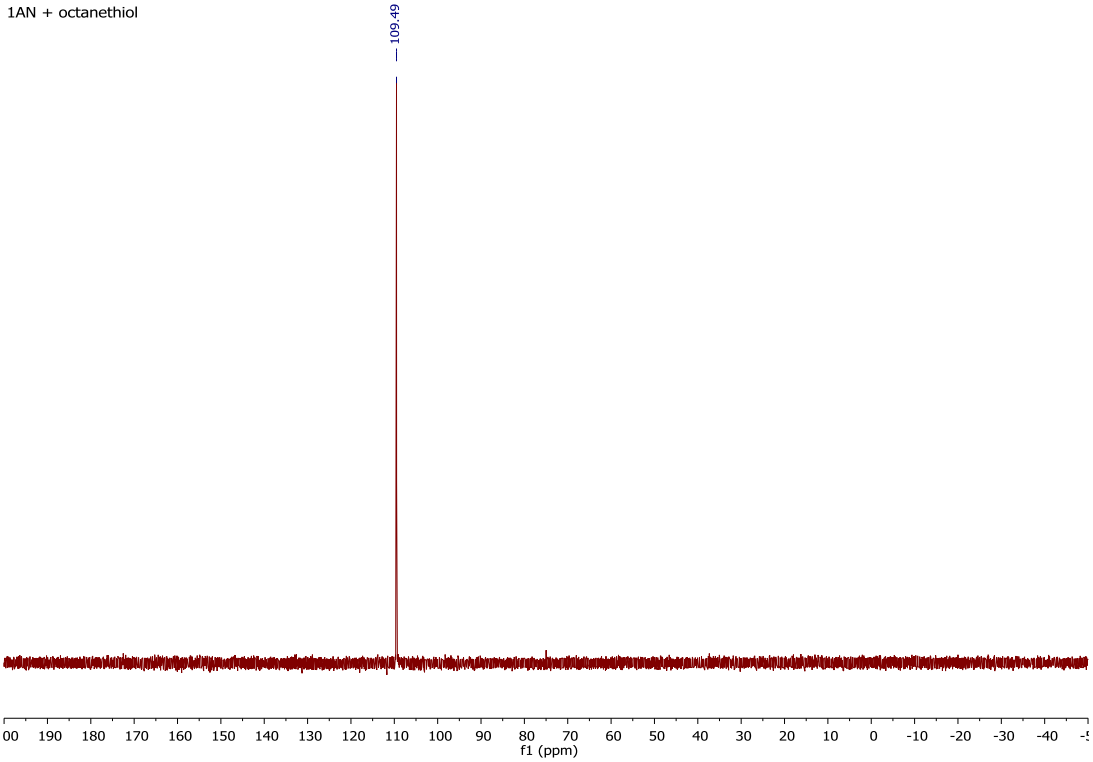

Figure 7.1-ee: ^{31}P-NMR spectrum of 1^{SH}

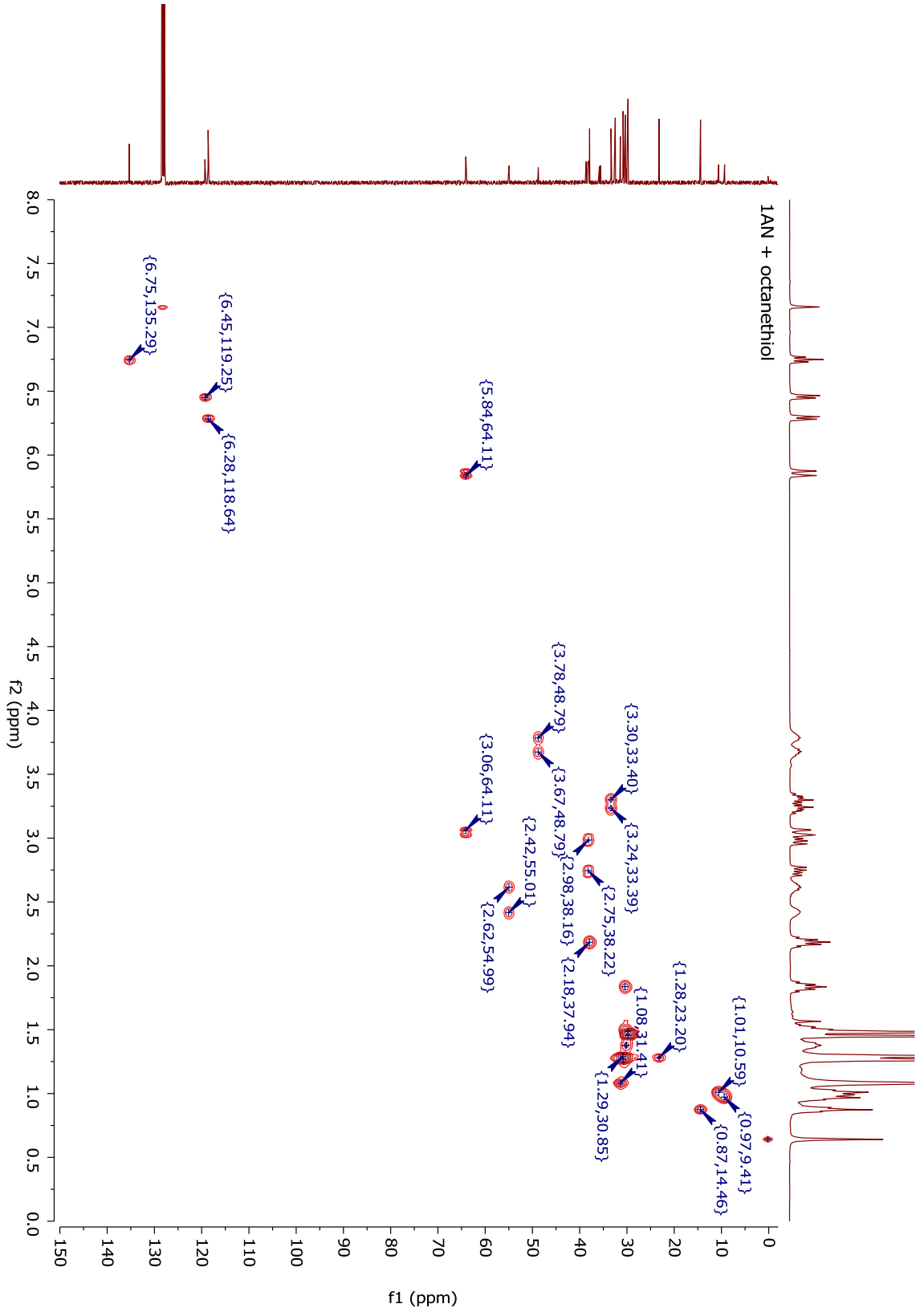

Figure 7.1-ff: gHSQC NMR spectrum of 1^{SH}

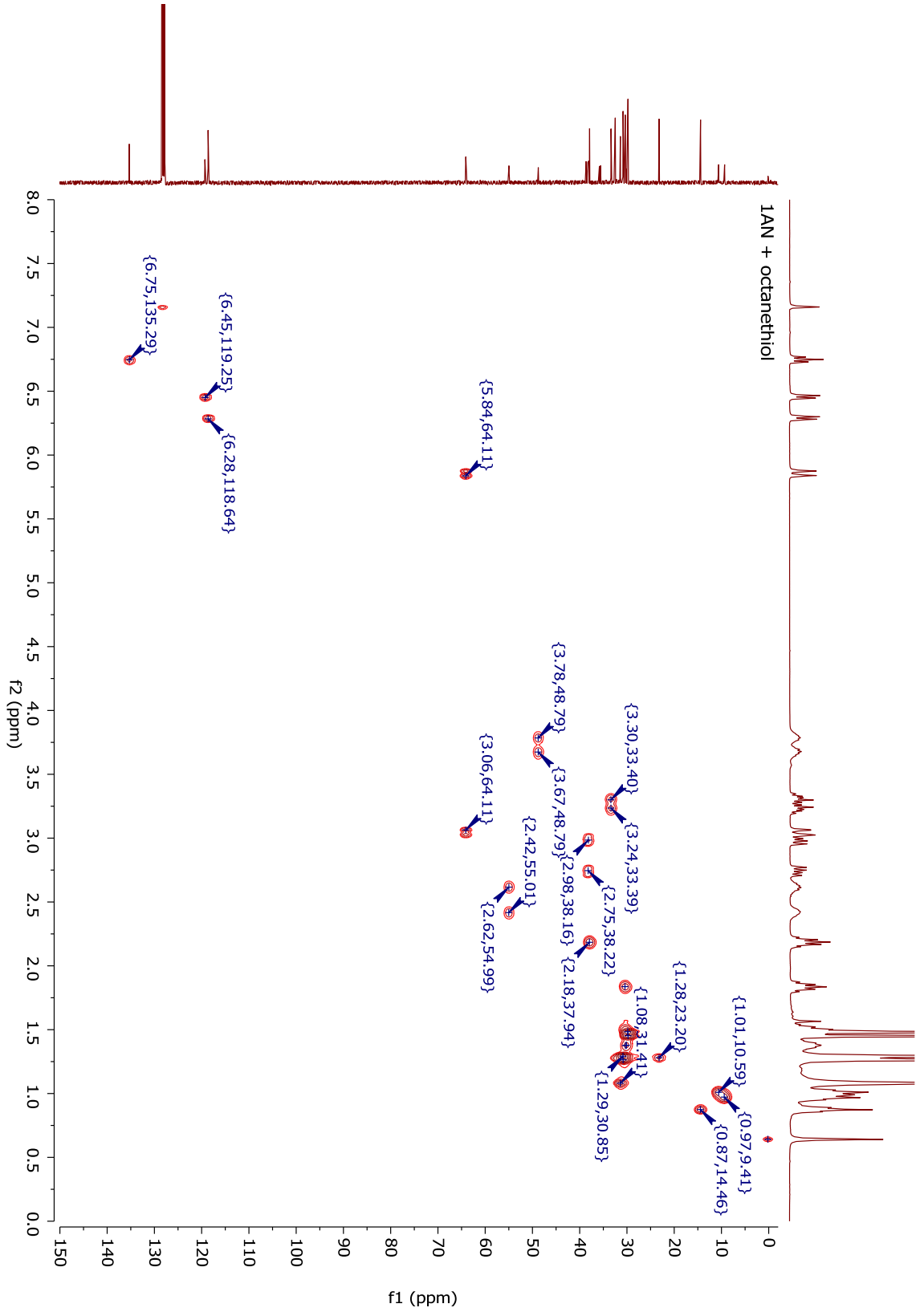

Figure 7.1-gg: gHMBC NMR spectrum of 1^{SH}

7.1.7 NMR spectra of 5

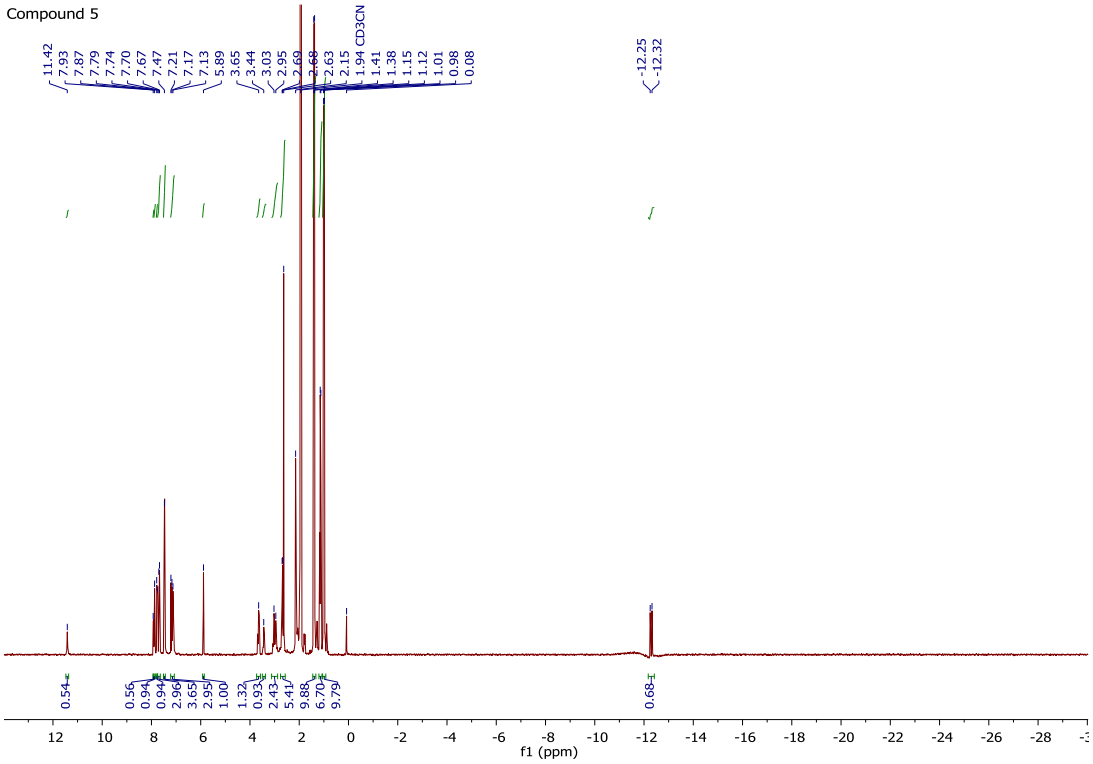

Figure 7.1-hh: ^{1}H-NMR spectrum of **5** (full range)

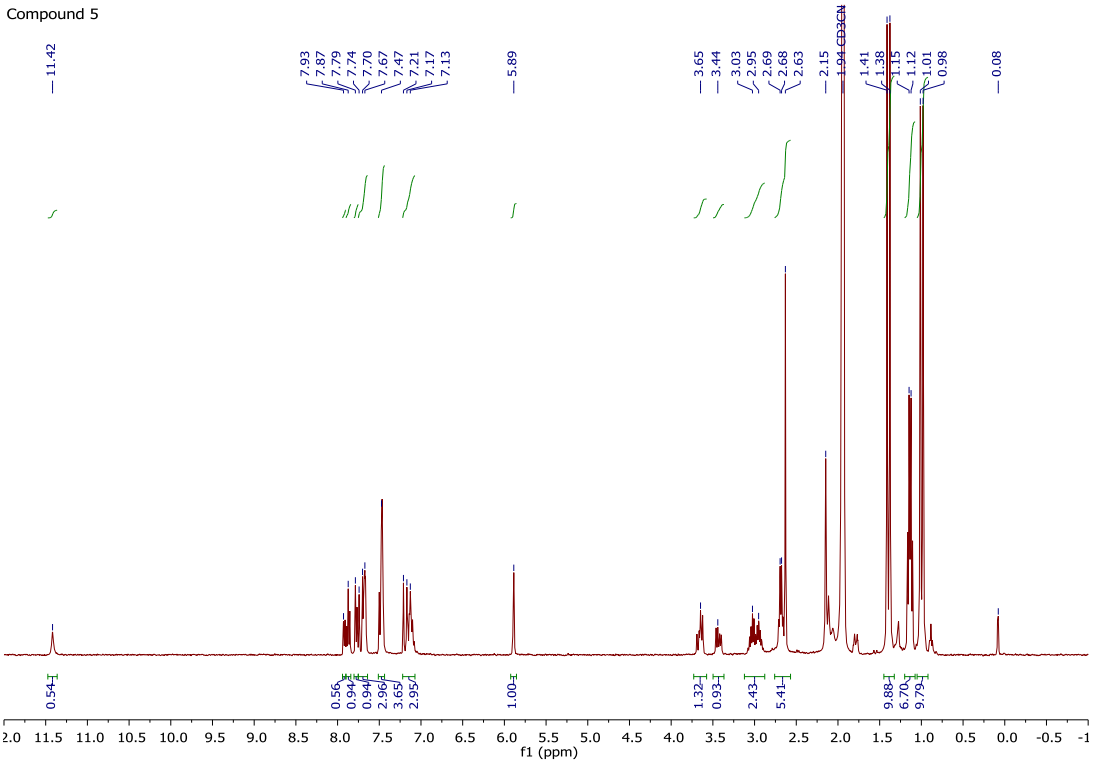

Figure 7.1-ii: ^{1}H-NMR spectrum of **5** (12 – -1 ppm)

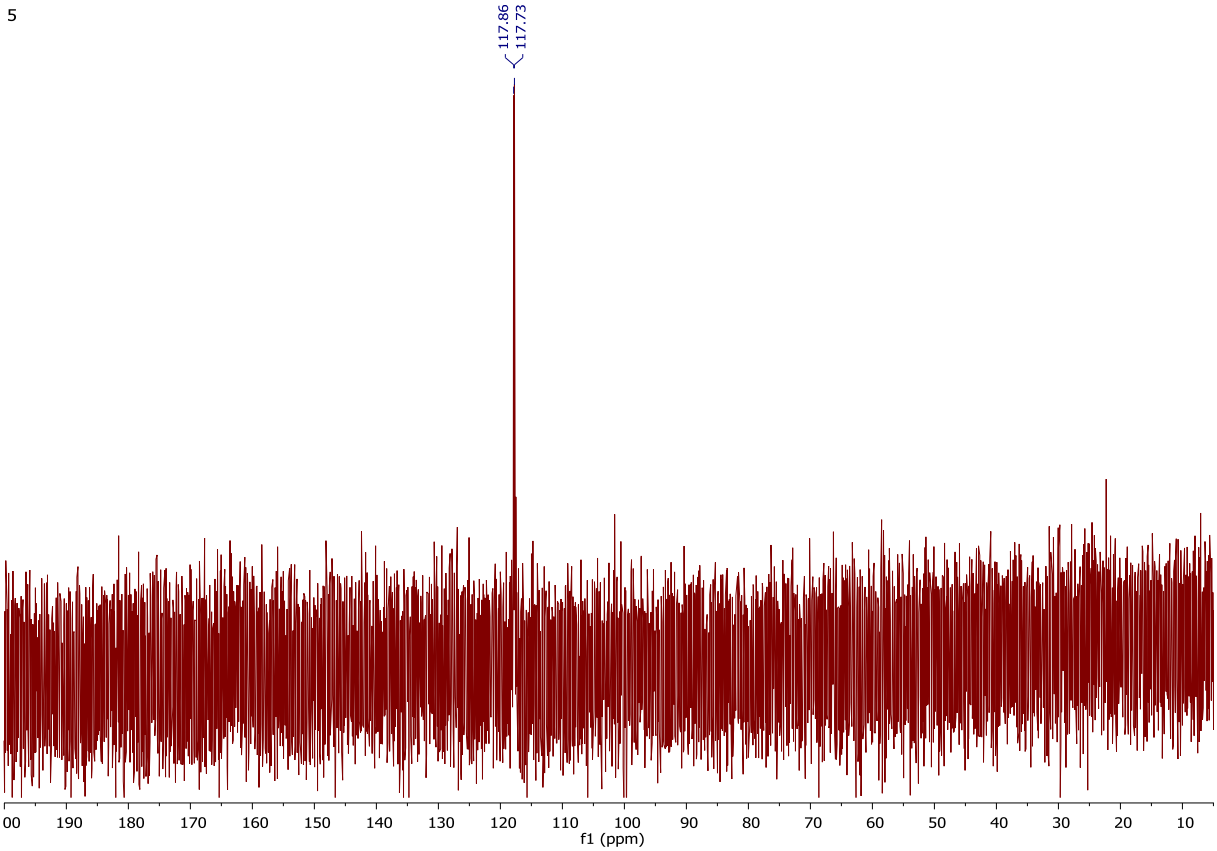

Figure 7.1-jj: ^{31}P-NMR spectrum of **5**

7.1.8 Generation of ethylene

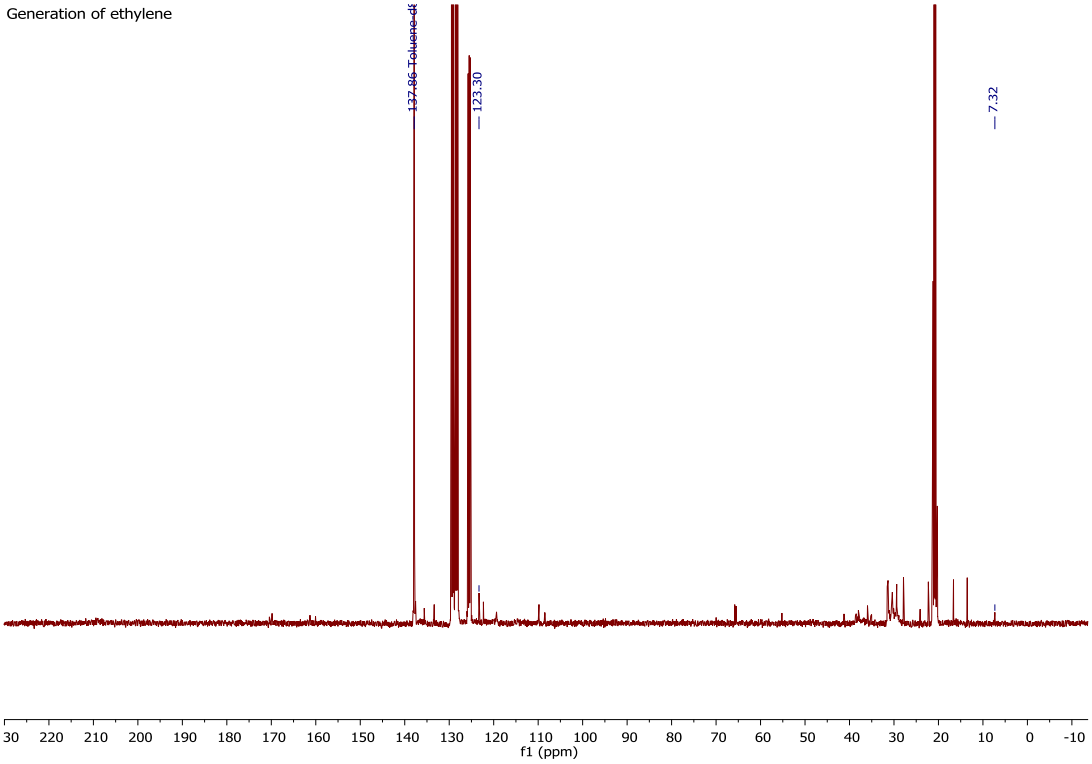

Figure 7.1-kk: ^{1}H-NMR spectrum of **1**^{4PN} at 70°C for a prolonged time

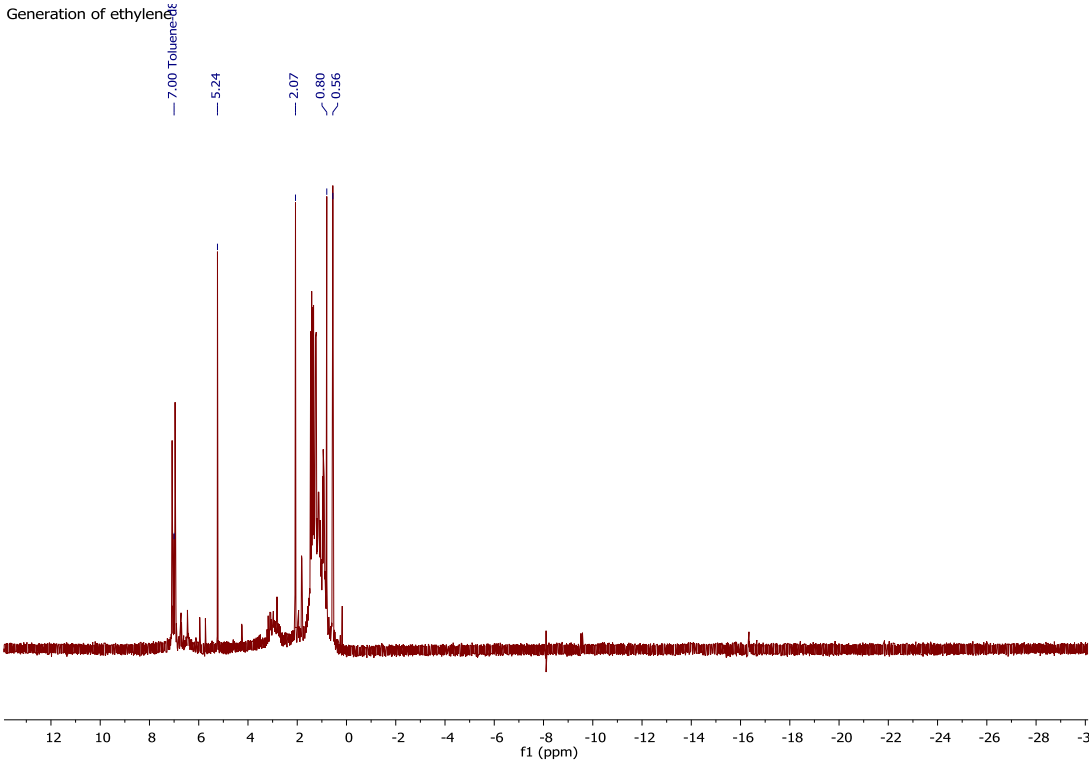

Figure 7.1-ll: ^{13}C-NMR spectrum of **1**^{PN} at 70°C for a prolonged time

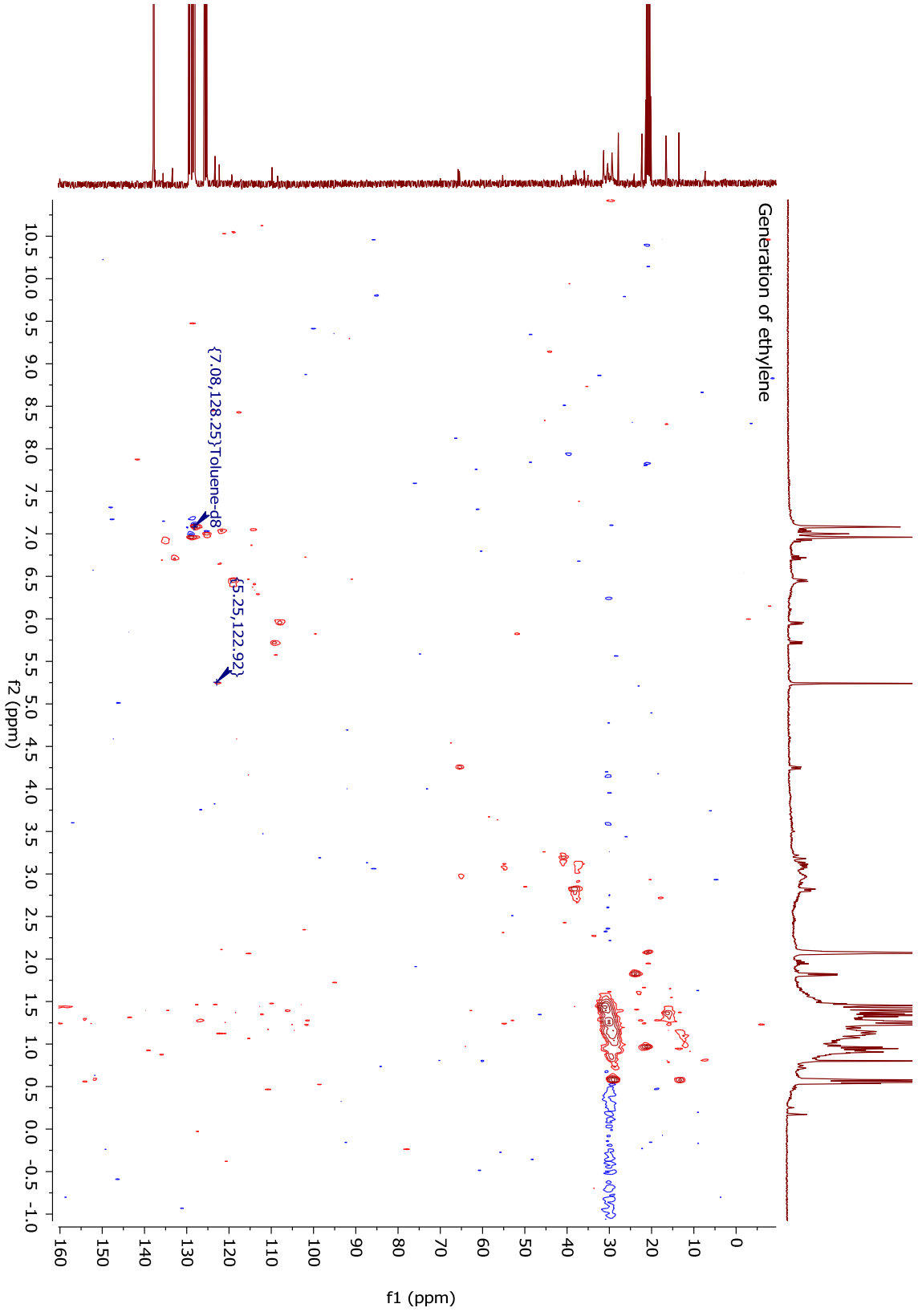

Figure 7.1-mm: gHSQC spectrum of **1**^{4PN}, after a prolonged time at 70°C

7.1.9 2-bromomethyl-6-methylpyridine

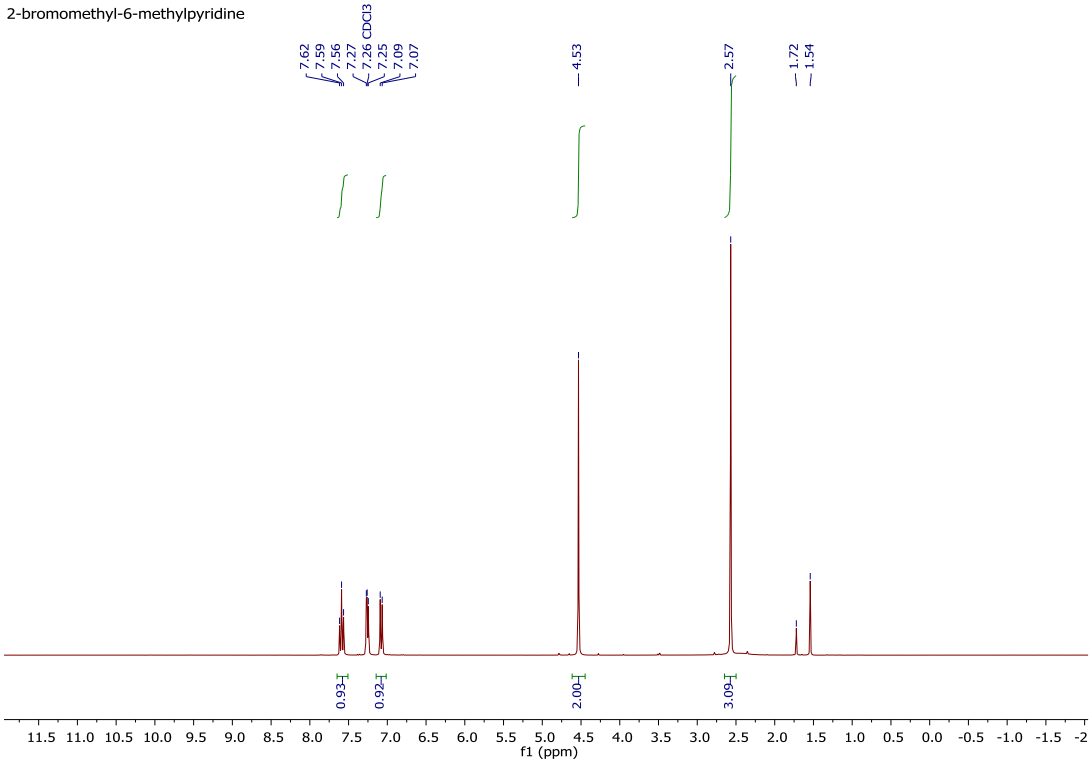

Figure 7.1-nn: ^{1}H-NMR spectrum of 2-bromomethyl-6-methylpyridine

7.2 Determination of the equilibrium constants

7.2.1 Thordarson Fitting Program

Using the Thordarson Fitting Program,(Thordarson, 2011) the equilibrium constant of the first equilibrium (K_1, $\mathbf{1} \rightleftarrows \mathbf{1}^{4PN}\mathbf{A}$) was calculated. The amount of **1** participating in this equilibrium was determined by subtracting the amount of $\mathbf{1}^{4PN}\mathbf{B}$ and $\mathbf{1}^{4PN}\mathbf{C}$ (determined by relative integrals) from the total added concentration. The same goes for the concentration of 4-pentenenitrile. Using the observed NMR shifts, the program calculates the related equilibrium constant.

Conc. 1	Conc. 4PN	Ru-H	Calc. Ru-H	Diff.	CHP	Calc. CHP	Diff.
0,047231	**0**	-26,70	-26,700	0,000	3,377	3,377	0,000
0,03181	**0,008413**	-24,63	-25,107	0,477	3,481	3,407	0,074
0,021971	**0,022296**	-21,94	-22,507	0,567	3,516	3,457	0,059
0,017063	**0,064497**	-19,39	-18,908	-0,482	3,546	3,526	0,020
0,01455	**0,154887**	-17,32	-16,977	-0,343	3,567	3,563	0,004
0,013433	**0,334486**	-16,09	-16,114	0,024	3,567	3,579	-0,012
0,012398	**0,675775**	-15,38	-15,716	0,336	3,548	3,587	-0,039

Conc. 1	Conc. 4PN	NEt_{2_1}	Calc. NEt_{2_1}	Diff.	NEt_{2_2}	Calc. NEt_{2_2}	Diff.
0,047231	**0**	0,72	0,720	0,000	0,87	0,870	0,000
0,03181	**0,008413**	0,75	0,741	0,009	0,90	0,897	0,003
0,021971	**0,022296**	0,78	0,776	0,004	0,95	0,942	0,008
0,017063	**0,064497**	0,81	0,823	-0,013	0,99	1,003	-0,013
0,01455	**0,154887**	0,84	0,849	-0,009	1,03	1,036	-0,006
0,013433	**0,334486**	0,86	0,860	0,000	1,05	1,051	-0,001
0,012398	**0,675775**	0,88	0,866	0,014	1,07	1,058	0,012

Table 7.2-1: Observed ^{1}H-NMR shifts for different added amounts of 4-pentenenitrile, as well as their shift calculated using the Thordarson Fitting Program and the difference between the observed and calculated shift.

sum of squares (ss)	Standard error (SEy)			covariance of fit
1,024859	0,21109			0,003073
Results for Ka	Results for other fitted parameters			
41,03052	11,38681	0,217715	0,150873	0,194663
%confidence interval on parameters (from asymptotic error):				
18,84685	3,26454	113,0859	163,1671	126,4711

Table 7.2-2: Outcome of the Thordarson Fitting Program, including result for K_1 and confidence interval.

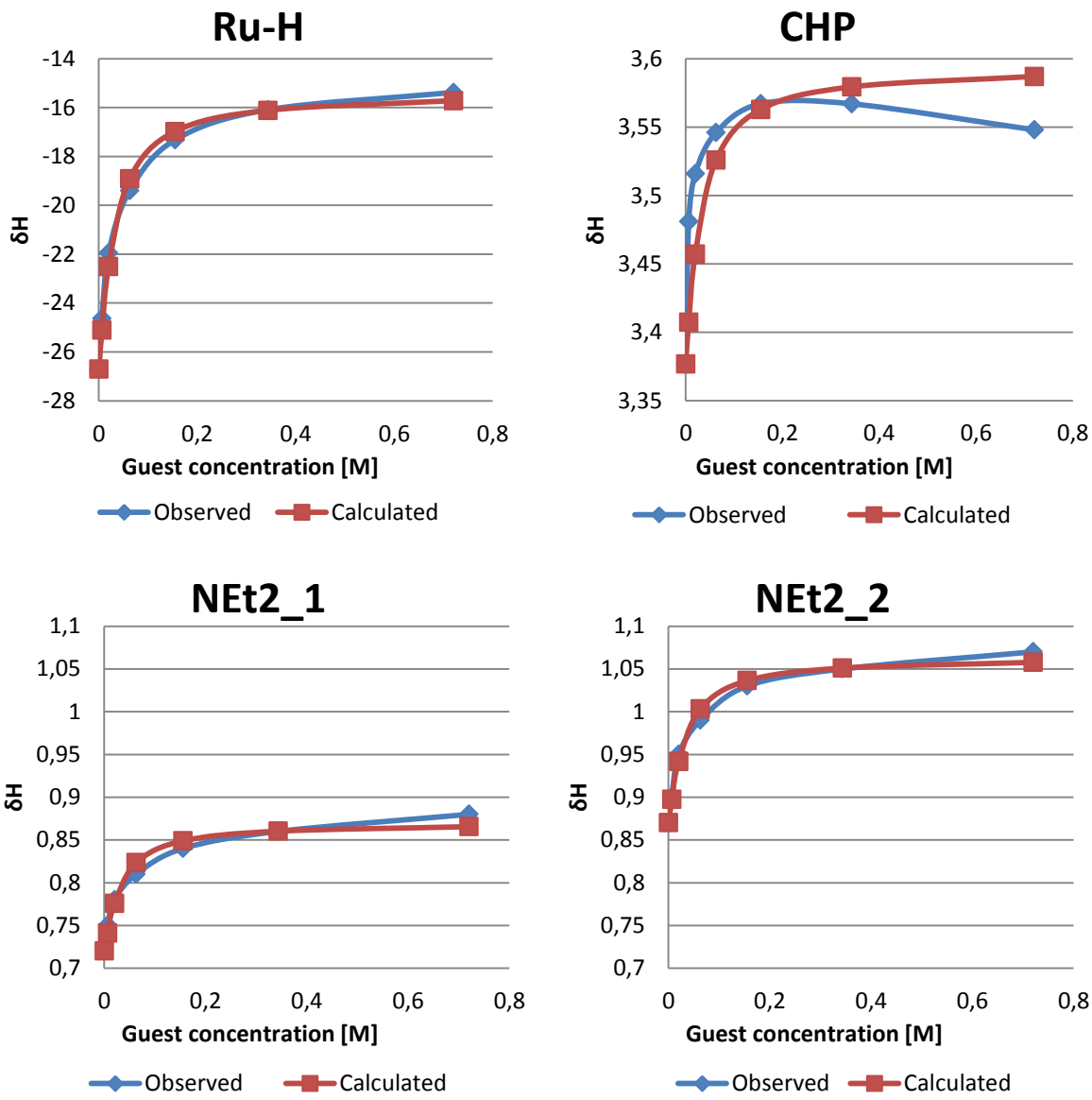

Figure 7.2-a: Observed and calculated shifts for the protons taken into consideration for the calculation of the equilibrium.

conc. 4PN (total)	area $1^{4PN}A$	delta 1A (Ru-H)	area $1^{4PN}B$	delta 1B (Ru-H)	area $1^{4PN}C$	delta 1C (Ru-H)
0	100	-26,7				
0,023615	63,65	-24,63	5,89	-11,98	30,46	-13,99
0,047231	42,42	-21,94	9,07	-11,98	48,51	-13,99
0,094461	33,21	-19,39	9,62	-11,98	57,17	-13,99
0,188923	28,27	-17,32	10,49	-11,99	61,24	-13,99
0,377845	26,53	-16,09	10,54	-12,00	62,93	-14,00
0,755691	25,40	-15,38	10,25	-12,02	64,35	-14,01

Table 7.2-3: Observed chemical shift and integrated area of given peaks.

7.2.2 Determination of K_2 and K_3

$$K_1 = \frac{[1A]}{[1][4PN]}$$
$$[1]_0 = [1] + [1A] + [1B] + [1C]$$
$$[1A] = [1]_0 - [1] - [1B] - [1C]$$
$$[1A] = [1]_1 - [1], with\ [1]_1 = [1]_0 - [1B] - [1C]$$

$$[4PN]_0 = [4PN] + [1A] + [1B] + [1C]$$
$$[4PN] = [4PN]_0 - [1A] - [1B] - [1C]$$
$$[4PN] = [4PN]_0 - [1]_0 + [1] + [1B] + [1C] - [1B] - [1C]$$
$$[4PN] = [4PN]_1 + [1], with\ [4PN]_1 = [4PN]_0 - [1]_0$$

$$[1A] = K_1 * [1] * [4PN]$$
$$[1]_1 - [\mathbf{1}] = K_1 * [\mathbf{1}] * ([4PN]_1 + [\mathbf{1}])$$
$$K_1 * [\mathbf{1}]^2 + (K_1 * [4PN]_1 + 1) * [\mathbf{1}] - [1]_1 = 0$$
$$[\mathbf{1}] = \frac{-b \pm \sqrt{b^2 - 4ac}}{2a}$$
$$with\ a = K_1; b = K_1 * ([4PN]_0 - [1]_0) + 1; c = [1B] + [1C] - [1]_0$$

$$[4PN] = [4PN]_0 - [1A] - [1B] - [1C]$$
$$[4PN] = [4PN]_2 - [1A], with\ [4PN]_2 = [4PN]_0 - [1B] - [1C]$$
$$[1A] = K_1 * [1] * [4PN]$$
$$[1] = [1]_1 - [1A]$$
$$[\mathbf{1A}] = K_1 * ([1]_1 - [\mathbf{1A}]) * ([4PN]_2 - [\mathbf{1A}]$$
$$[\mathbf{1A}] = K_1 * \left([\mathbf{1A}]^2 - [1]_1 * [\mathbf{1A}] - [4PN]_2 * [\mathbf{1A}] + [1]_1 * [4PN]_2\right)$$
$$[\mathbf{1A}]^2 - \left([1]_1 + [4PN]_2 + \frac{1}{K_1}\right) * [\mathbf{1A}] + [1]_1 * [4PN]_2 = 0$$
$$[\mathbf{1A}] = \frac{-b \pm \sqrt{b^2 - 4ac}}{2a}$$
$$with\ a = 1; b = [1]_0 - 2[1B] - 2[1C] + [4PN]_0 + \frac{1}{K_1};$$
$$c = ([1]_0 - [1B] - [1C])([4PN]_0 - [1B] - [1C])$$

[4PN] (total)	[1 ⇄ 1^{4PN}A]	[1^{4PN}B]	[1^{4PN}C]	[4PN] (free)	[1]	[1^{4PN}A]	[1^{4PN}B]/[1^{4PN}A]	[1^{4PN}C]/[1^{4PN}B]
0,0000	0,0472	0,0000	0,0000	0,0000	0,0472	0,0000		
0,0236	0,0301	0,0028	0,0144	0,0064	0,0267	0,0034	0,825	5,17
0,0472	0,0200	0,0043	0,0229	0,0200	0,0130	0,0070	0,613	5,35
0,0945	0,0157	0,0045	0,0270	0,0629	0,0050	0,0107	0,425	5,94
0,1889	0,0134	0,0050	0,0289	0,1550	0,0019	0,0114	0,434	5,84
0,3778	0,0125	0,0050	0,0297	0,3431	0,0009	0,0117	0,426	5,97
0,7557	0,0120	0,0048	0,0304	0,7205	0,0004	0,0116	0,417	6,28
							K_2 = 0,524	K_3 = 5,76

Table 7.2-4: Calculated concentrations of all species present in solution, as well as equilibrium constant.

7.2.3 Van 't Hoff plots

T (°C)	T (K)	∫(1/1A)	δ(obs)	∫(1B)	δ(1B)	∫(1C)	δ(1C)	[1]	[1A]	[1B]	[1C]
-5	268	21,18	-20,92	11,43	-11,96	67,39	-13,91	0,0043	0,0042	0,0046	0,0270
5	278	33,06	-22,19	9,66	-11,97	57,27	-13,94	0,0082	0,0051	0,0039	0,0229
15	288	45,68	-23,17	7,93	-11,98	46,38	-13,97	0,0128	0,0055	0,0032	0,0186
25	298	55,49	-23,87	6,62	-11,99	37,89	-14,00	0,0169	0,0053	0,0026	0,0152
35	308	68,69	-24,61	4,64	-11,99	26,67	-14,02	0,0226	0,0049	0,0019	0,0107
45	318	78,47	-25,15	3,23	-12,00	18,30	-14,05	0,0272	0,0041	0,0013	0,0073
55	328	85,84	-25,56	2,18	-12,00	11,98	-14,07	0,0310	0,0033	0,0009	0,0048

1/T (1/K)	K1	K2	K3	ln(K1)	ln(K2)	ln(K3)
0,00373	224,92156	1,09706	5,89589	5,41575	0,09263	1,77426
0,00360	76,42634	0,76103	5,92857	4,33633	-0,27308	1,77978
0,00347	33,58828	0,57772	5,84868	3,51418	-0,54867	1,76622
0,00336	18,82868	0,49533	5,72356	2,93538	-0,70253	1,74459
0,00325	9,57803	0,37977	5,74784	2,25947	-0,96820	1,74882
0,00314	5,57706	0,31204	5,66563	1,71866	-1,16464	1,73442
0,00305	3,46547	0,26176	5,49541	1,24285	-1,34034	1,70391

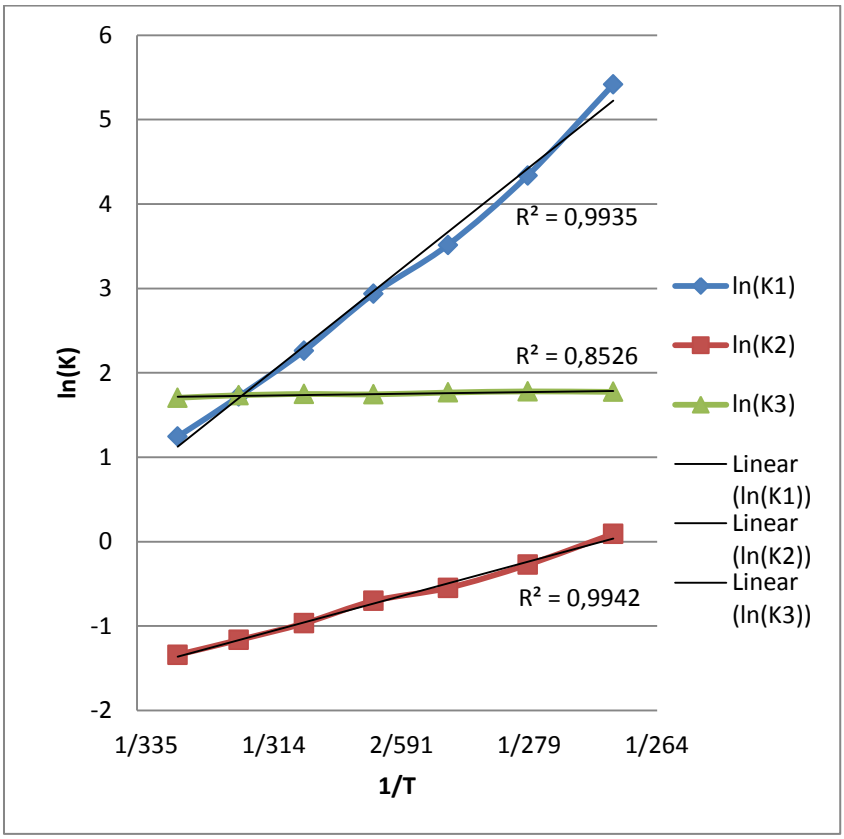

7.3 GC-MS measurements on ethylene